The Thesis Committee for Ryan Stuart Lester
Certifies that this is the approved version of the following Thesis:

Development of a Cryogenic Tracer Irradiation Facility

APPROVED BY
SUPERVISING COMMITTEE:

Derek Haas, Supervisor

William Charlton

Development of a Cryogenic Tracer Irradiation Facility

by

Ryan Stuart Lester

Thesis

Presented to the Faculty of the Graduate School of

The University of Texas at Austin

in Partial Fulfillment

of the Requirements

for the Degree of

Master of Science in Engineering

The University of Texas at Austin

May 2021

Acknowledgements

I would first like to thank my advisor Dr. Derek Haas for originally hiring me on as an undergraduate researcher and ultimately taking me under his wing and providing me with the truly extraordinary experience in continuing my education here at the University of Texas at Austin. Without his continual guidance and input I would not be where I am today. I would also like to acknowledge Dr. Sheldon Landsberger for initially connecting me to Dr. Haas in the very beginning and his continual moral support throughout this journey. I would like to thank Dr. Charlton as well for his moral support and educational instruction in both the academic and real world. As well as his encouragement to explore my ambition while always staying focused on my thesis. I would then like to thank Dr. Joe Artnak for his ability to help me grow both as a scientist and a student, and ultimately for his friendship during this whole process. I will remember those long nights working on PGAA for BP3 for the rest of my career.

I would next like to thank the support staff at NETL: Larry, Jim, and Tracy. Without those three this project would have never been put together as quickly and efficiently as it was, and I would have never learned so much from the endless supply of knowledge from them all. A special thanks to Larry for being someone I could always count on no matter what the problem was, and his continuous mentoring and friendship through our early morning talks before work. The devotion of time and effort to this facility, by these three, is unmatched.

And finally, I must thank my family, because without them none of this would have ever been possible. And to my Papa, Dr. Sam Zamrik, thank you for your endless supply of love and support and the constant reminder that everything will work out in due time.

Abstract

Development of a Cryogenic Tracer Irradiation Facility

Ryan Stuart Lester, M.S.E.

The University of Texas at Austin, 2021

Supervisor: Derek Haas

The goal of this thesis is to provide instruction on the design, modeling, construction, and implementation of a cryogenic tracer irradiation facility that produces isotopically pure noble gas samples both efficiently and cost effectively. These samples will be used for various research purposes. This facility will be installed into Beam Port 1 (BP1) of The University of Texas at Austin's Nuclear Engineering Teaching Lab (NETL) TRIGA Mark II reactor core. This work builds on previous creation of noble gas activities of ^{127}Xe and ^{37}Ar on the order of $3.7x10^{10}$ Bq (1 Ci). These were produced through the activation of ^{126}Xe and ^{36}Ar, respectively, in the 3-Element facility which sat within the reactor core. This new facility offers means to produce these tracer gases in ways that are much safer and more cost-effective.

Methods developed include solidification of the respective gases to increase sample density, change of location, and new facility components. The most important aspect of the design is the changes made to increase sample density by way of cryogenically freezing the gases onto a condenser. Beam Port 1 was chosen because it is larger than the in-core facilities and provided a safer location than in the core itself in the event that the pressure safety limit was exceeded. To efficiently freeze these gases a condensing system was designed and built by Cryomech Inc. The condensing system is composed of an irradiation canister, heat exchanger, helium compressor and transfer lines, and gas transfer lines.

Table of Contents

List of Tables

List of Figures

Chapter 1: Introduction

This document explains the design, construction, and implementation of a cryogenic irradiation facility. The goal of this work was to create a working facility that could efficiently, safely, and cost-effectively produce radiotracers to be used in future experiments for radionuclide detection. Radiotracers, or radioactive tracers, are isotopes that have been made radioactive by way of neutron interrogation to then be used to help identify, observe, or follow behaviors of various physical, chemical, or biological processes. Radiotracers are used in the nuclear field in a variety of ways, but in this instance, we will be focusing on their use in understanding subsurface gas transport.

To produce these radiotracers, the University of Texas at Austin's TRIGA MARK II research reactor will be used. Within Beam Port 1 (BP1) of the reactor an irradiation canister will be inserted into up to a point that is located adjacent to the reactor core, and gas will be cryo-trapped into a condenser within this canister. At this point, the reactor will be brought to power, and the now-frozen gas will be bombarded with neutrons to achieve a specific level of activity. The gases of immediate interest to be produced in this experiment are ^{127}Xe and ^{37}Ar, signatures of nuclear explosions.

This new method will fundamentally change the way these gases are produced and markedly improve the efficiencies of previous experimental attempts to irradiate tracer gases. Because of this improvement in efficiency, more gas can be

produced for a larger number of experiments, thus increasing the number of experiments possible. Without this ability to easily produce tracer gases, experiments to help increase the detecting efficiency for underground nuclear explosions (UNEs) would be few and far between thus prolonging critical science from being understood.

Chapter 2: History of Radionuclides in the Nuclear World

Radionuclides or radioisotopes are atoms that have an excess nuclear energy causing them to be unstable. Radionuclides can be found in a variety of environments from basic laboratory experimentation, the medical field, and even in various geological endeavors. However, the most abundant source of radionuclides in the environment are found in the event of a radiological release from a nuclear detonation.

Under the Comprehensive Nuclear Test-Ban Treaty (CTBT), no country in the world would be allowed to detonate nuclear bombs for military or civil purposes after it goes into force. This prohibition has not, however, been fully enforced since eight nations have not ratified the treaty. In the event of an underground nuclear explosion carried out to avoid detection, scientists would study seismic activity as well as gaseous and particle dissemination through the ground.

One key aspect of the UNE verification regime resides in the ability to conduct an On-Site Inspection (OSI) to clarify whether a nuclear explosion has been carried out in violation of the treaty (Burnett 2012). This OSI will aim to gather enough data to help states determine if a nuclear explosion has been carried out in violation of the Treaty. Radionuclides present in an area are a key indicator that an UNE has occurred. One major step toward confirming the occurrence of a UNE involves capturing short-lived noble gas radio isotopes produced by an explosion. These isotopes are often referred to as the "smoking gun' for nuclear explosion detections (Carrigan 2016). Radionuclide signals from UNE's are strongly influenced by the hydrogeologic regime in the surrounding area. The containment provided by the geology will have a direct impact on the delay effects of detonation-produced

radiotracers reaching the surface and can potentially lengthen the period of detectability for these elements (Carrigan 2016).

To understand if a country is testing we must develop technology to measure differences in background levels and abnormalities from naturally occurring isotopes (Burnett 2014). Argon and xenon have been selected to be studied for underground transport experiments because isotopes of those elements are likely to be the most prevalent radionuclide signatures resulting from a nuclear explosion. Due to their short half-lives, the ambient background concentrations for those gas components are extremely low and the International Monitoring System (IMS) has developed the measurement sensitivity for the ^{133}Xe exceeding 1 mBq m^{-3} (Sun 2012). In addition to nuclear explosions, radioxenon is produced and may be released from civil events such as medical isotope production and ^{37}Ar is also produced in subsurface regimes due to cosmic-neutron interactions with the activation of calcium by n, alpha reactions (Sun 2012).

To better understand under what hydrogeological conditions Xe and Ar will rise to the surface with signals large enough for detection, transport mechanisms from UNEs must be studied (Sun 2012). Radioxenon collection and analysis is a standard technique used to monitor for evidence of a nuclear detonation, but over fifty days past the event the ^{37}Ar signatures should be stronger than the radioxenon signatures (Aalseth 2011). This was verified during "Project Gasbuggy" a 27-kt underground test. From this discovery, two methods for generating an ^{37}Ar sample were explored by Aalseth, et al.:

- 40Ca (n, alpha) where neutrons are supplied by a reactor
- Irradiation of natural argon with reactor neutrons

The goal of these experiments was to develop an ultra-low background proportional counter for the measurement of ^{37}Ar relevant to the Treaty's On-site inspection results. In this experiment, the irradiation of 1 cm^3 of high purity natural argon took place at the University of Texas at Austin's TRIGA reactor for 1.5h, resulting in an activity of 1.31 +- 0.13 kBq (Aalseth 2011).

Chapter 3: Theory

The University of Texas at Austin has developed methods to produce isotopically pure noble gas samples for detector calibrations, quality control on detection systems, and for environmental tracer studies. This study will look at changes to previous work to improve the experiment in an efficient and cost-effective manner.

Beam port 1 (BP1) is located tangentially to Nuclear Engineering Teaching Laboratory's (NETL) TRIGA Mark II reactor core. This beam port is the only beam port to cut across the reactor structure entirely, forming BP1 as well as beam port 5 (BP5), which are divided in the middle by a graphite block. For the following safety analysis, a cryogenic irradiation facility will be inserted inside the beam port, on the BP1 side, up to the graphite block. The facility will consist of a vacuum canister containing a cold head and condenser, followed by a 14-foot flexible liquid helium transfer line that will run the length of the beam port and out into the reactor bay.

3.1 Facility Description

NETL has both in-core facilities for various irradiations and beam port facilities for larger experiments. Neutron fluxes associated with these facilities cover a wide range of values within the core and in each beam port area, having been optimized for different experiments.

3.1.1 In-Core Irradiation Facilities

NETL's in-core facilities are primarily used for various sample activation analysis techniques. The advantages of using these facilities include a higher neutron flux at these locations compared to outside the reactor shielding and the ability to utilize the pneumatic transfer system installed within NETL for rapid sample transfer. Disadvantages associated with these locations often include geometry restrictions for sample sizes and safety constraints where samples could become too activated thus violating the technical specifications for the reactor. For in-core gas irradiations, the three primary facilities that were of interest were the 3-Element Irradiator, the 7-Element Irradiator, and the Central Thimble. Table 1 below shows the neutron flux associated with these facilities.

Table 1. In-Core Irradiation Facility Neutron Fluxes (Biegalski 2016)

Facility	**Thermal Neutron Flux**	**Total Neutron Flux**
3-Element Irradiator	4×10^{12} n cm^{-2} s^{-1} (950 kW)	2.8×10^{13} n cm^{-2} s^{-1} (950 kW)
7-Element Irradiator	4×10^{12} n cm^{-2} s^{-1} (950 kW)	1.4×10^{13} n cm^{-2} s^{-1} (950 kW)
Central Thimble	1×9^{13} n cm^{-2} s^{-1} (950 kW)	7.0×10^{13} n cm^{-2} s^{-1} (950 kW)

As seen in Table 1, the facility with the highest neutron flux is the Central Thimble, however for this experiment the highest neutron flux is not the ultimate goal, therefore all facilities must be examined for potential utilization.

3.1.2 3-Element Irradiator

The 3-Element facility is an irradiation location present within the first 3 rings of NETL's reactor core providing it with a high neutron flux. There are two versions of the Irradiation vessel, both made of 6061 Aluminum alloy, but one having a lead liner while the other a Cadmium liner thus creating two different experimental environments. For the prior gas irradiation experiments the irradiator having a lead liner was utilized such that the reactor can be operated at its maximum power of 950 kW (Biegalski 2015). The overall length from the bottom of the canister to the top of the threaded fitting at the top of the canister is 50.4 in (1.28 m) with the length of usable volume equaling 48.1 in (1.22m) thus creating a maximum usable internal volume of 1.4 liters, immediately forcing an experimental constraint for this facility.

On top of the canister sits a threaded cap for the top fitting containing two O-ring seals, a pressure relief valve, and a gas valve for loading or purging the contents. The seals that protect the canister form both expansion and compression pressure in the canister consist of both a radial seal and an end seal. This double seal design provides extra protection against water leakage into the canister as well as gas leakage out. The pressure relief valve is also set to burst at 25 PSI thus creating another safety measure while also putting another experimental constraint on pressurizing the canister within the core to remain within the technical specifications listed for the in-core facility. A diagram of the facility is provided below in Figure 1.

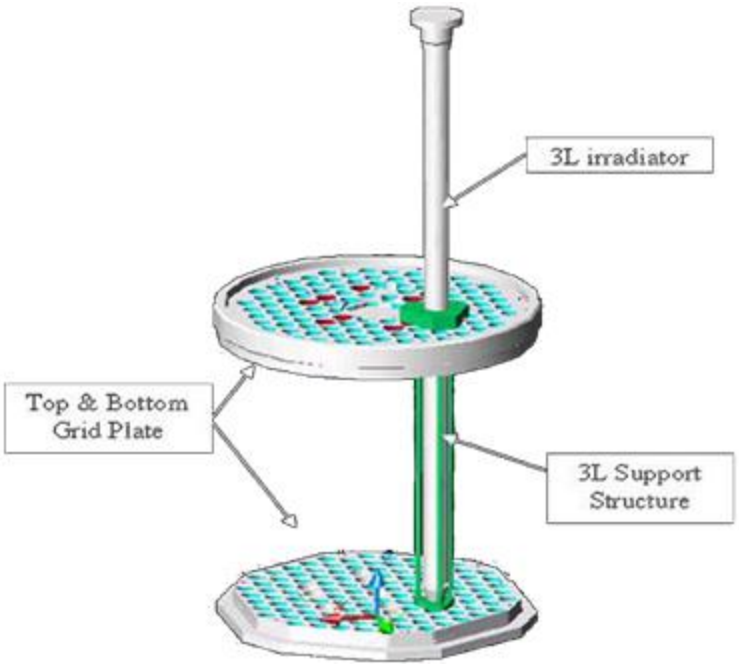

Figure 1. The 3-Element Irradiator (Biegalski, 2016)

3.1.3 7-Element Irradiator

The 7-Element irradiator is a large in-core facility used to in various neutron irradiation experiments. The implementation of this facility into the reactor core requires the removal of 7 reactor fuel pin elements, the central thimble, or somewhere in the outer three fuel rings of the core.

The 7-element irradiator canister is composed of 6061-T6 aluminum and contains a thick borated aluminum liner where the boron concentration is 4.5% by weight and is enriched to greater than 95% ^{10}B, which is the boron isotope that a large thermal region cross section that will then absorb a large amount of lower energy neutrons before they reach the inside of the canister. This design closely relates to the design of the cadmium-lined 3-Element Irradiator. The total height of the canister is also approximately 52 inches thus almost

matching the maximum usable volume of the 3-element facility. The main reason for this height extension is to limit the activation of some of the stainless-steel parts located on top of the canister.

3.1.4 Central Thimble

Lastly, the central thimble facility provides direct access to the reactor cores maximum neutron flux. This facility consists of an aluminum tube extending from the bottom of the reactor core to the top of the reactor pool. Samples would have to be placed inside of some canister and slid down the length of the central thimble to force the gas to stay within the confines of the core geometry. This then cuts back the volume of the central thimble to less than both the 3- and 7-element facilities as well as creating a new design hurdle for having to shield the shine coming from the central thimble up to the reactor deck.

3.2 Beam Port Facilities

In addition to the multiple in-core facilities NETL's core hosts, access to the core by way of horizontal neutron beam lines are created by 4 separate beam tubes that run through the reactor shielding structure. All beam tubes originate at the reactor core or in the reactor reflector with diameters of 6 inches. One tube passes the core tangentially and penetrates all the way through to the other side; this beam line is separated by a graphite block in the middle thus creating beam ports 1 and 5. A second tangential beam port starts in the reactor reflector oriented tangential to the reactor structure while the two remaining beam ports are oriented radially to the core and normal to the reactor shielding structure.

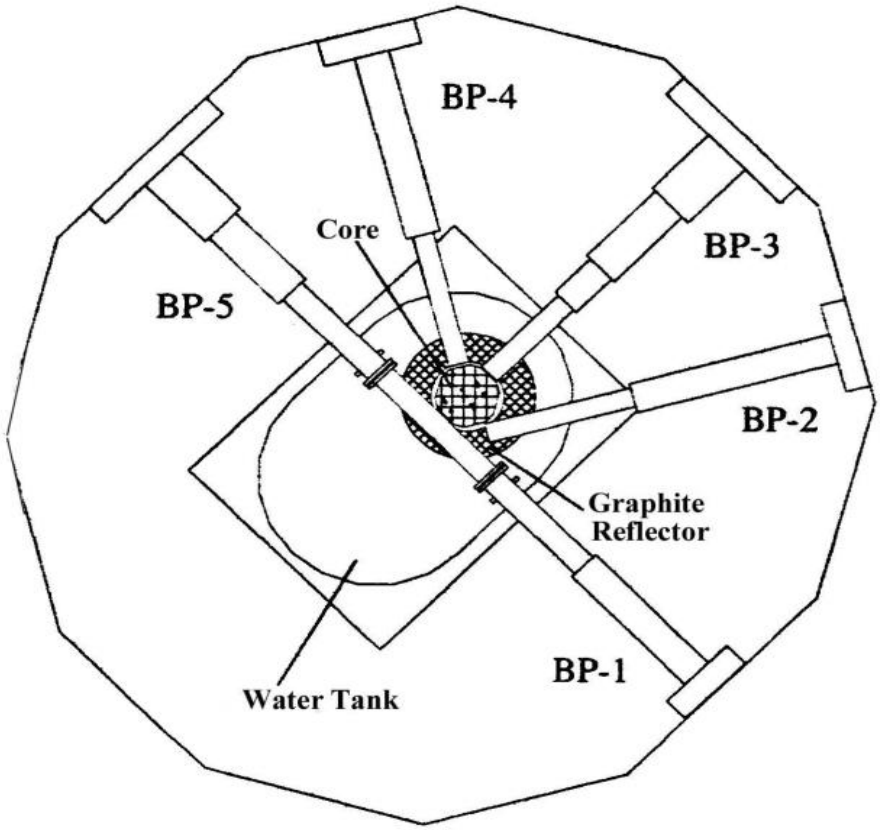

Figure 2. NETL Beam Port Configuration (Nuclear Engineering Teaching Laboratory, 2012)

3.3 Gas Activation

Prior to the decision of where this system should be located, activation calculations were performed to determine the quantities of ^{127}Xe and ^{37}Ar that could be produced within the reactor at various points. These activities all followed the same basis of assuming 100-hour continuous irradiations. A few things to keep in mind is that the University of Texas TRIGA reactor normally operates between the hours of 8am and 4pm on a normal 40-hour work week schedule, not including weekends, so a continuous irradiation does not portray a normal facility work week but merely serves to stand as a qualitative benchmark. Another

point of consideration for this benchmark would be that as the irradiation ran past 1 week the reactor would have created so many poisons that the overall power of the reactor would drop considerably even with all control rods withdrawn thus effecting the overall activity of the final product.

3.3.1 In-Core Irradiation

Pressure is one method to increase the overall activity produced within an irradiation due to a concentration of gas in a smaller volume. When considering in-core irradiations an assumption had to be made regarding the pressure to have corresponding volumes with the beam port irradiations. The following calculations were performed for pressures up to 200 psi. However, with the safety limits set by the reactor oversite committee (ROC) it is highly likely that the experimental pressure would in fact be limited to 20 psi for a canister within the core, or 80 psi if the vessel were to lay within the central thimble.

Using MCNP, the neutron energy flux profiles were created and tallied in 64 groups with the same energy bin software structure seen in CINDER-90 cross-sections. Flux weighted neutron radiative capture cross-sections were calculated to be 2.26 barns for ^{36}Ar and 2.73 barns for ^{126}Xe. These cross-sections were derived form a collapsed group approximation and are assumed to be valid for the total fluxes present within the core (E.A., personal communication, November 15, 2017).

Another key point of consideration is the neutron spatial distribution as a function of core height. This distribution takes a skewed cosine shape over the fuel region meaning that since the core fuel is 15 inches long there will not be homogeneity amongst the activation within the various in-core facilities (Figure 3).

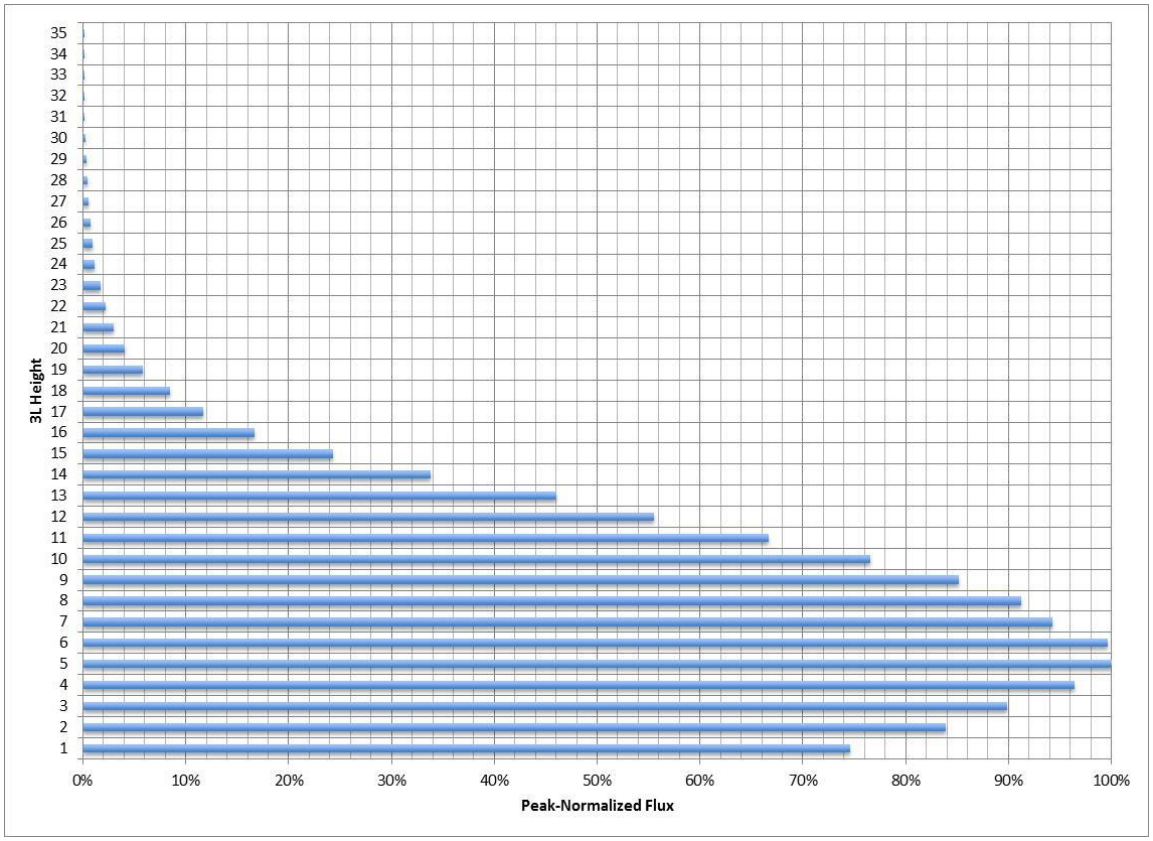

Figure 3. Neutron Flux profile of 3-Element Irradiator (Biegalski, 2016)

Taking these issues into consideration, a graph was constructed to show the activities that would be produced in the 3-element, 7-element, and central thimble facilities for both ^{37}Ar and ^{127}Xe, respectively.

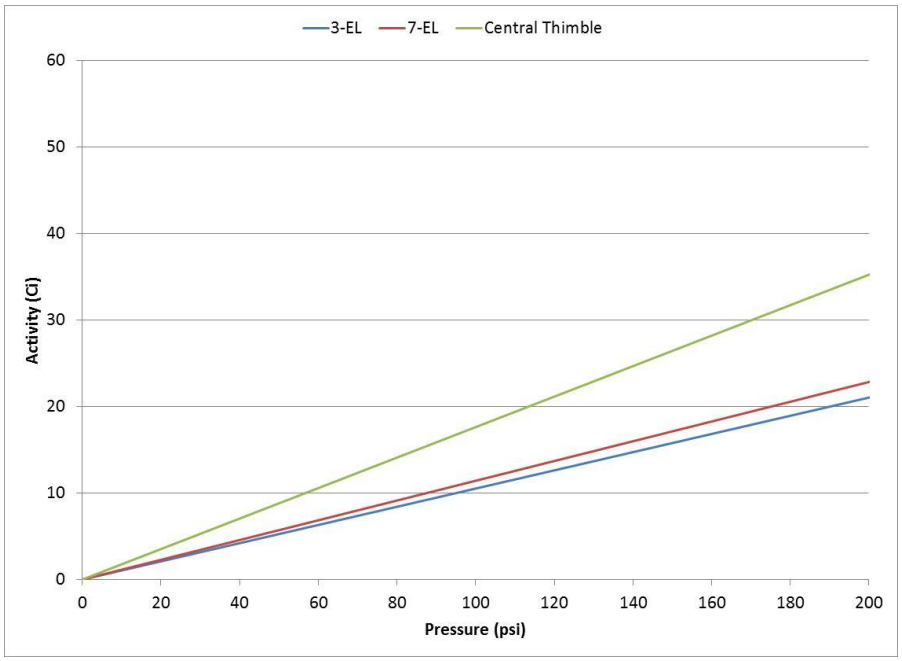

Figure 4. Activities of ^{37}Ar Produced in Various In-Core Facilities calculated with SCALE (Biegalski, 2016)

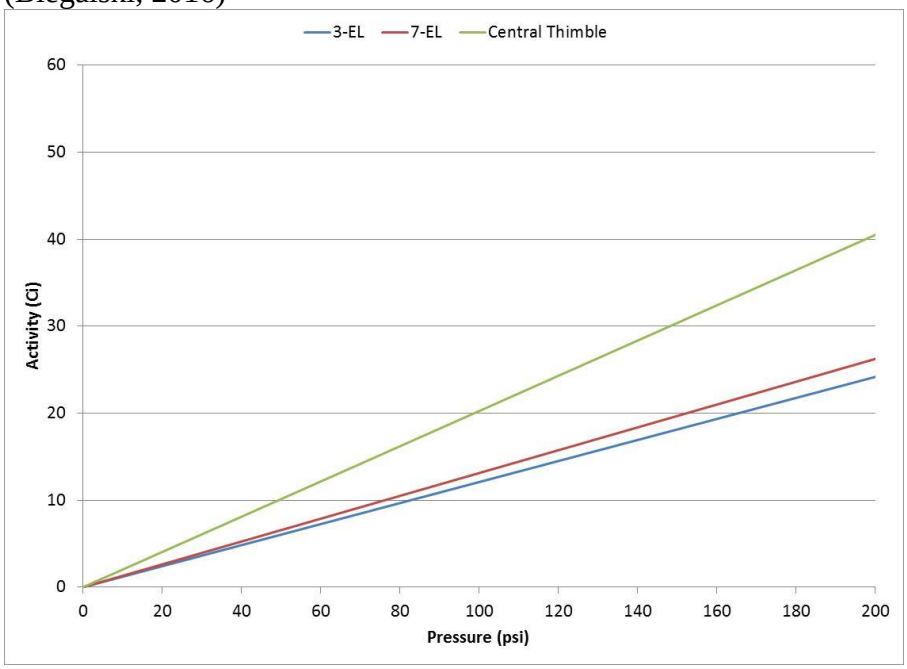

Figure 5. Activities of ^{127}Xe Produced in Various In-Core Facilities calculated with SCALE (Biegalski, 2016)

Parsing this data, it is clear that the Central Thimble has the highest possible activation given a 100-hour irradiation at 950 kW and 200 psi. This is primarily due to the fact that the neutron flux is the highest here than anywhere else in the reactor structure, despite its volume being the smallest.

3.3.2 Beam Port Irradiations

While the in-core facilities have the drawback of not being able to be operated at high pressures, they still have considerably higher flux than their counter part in the beam port facilities. However, the beam port facilities include much larger spaces for irradiation canisters that allow for both flexibility for the design as well as material makeup of the vessel. Given this flexibility, the feasibility of irradiating liquid Ar and Xe were explored for beam port irradiations (Biegalski 2016). Being able to liquify these gases would greatly increase efficiency by multiplying the density to facilitate higher activation upon irradiation.

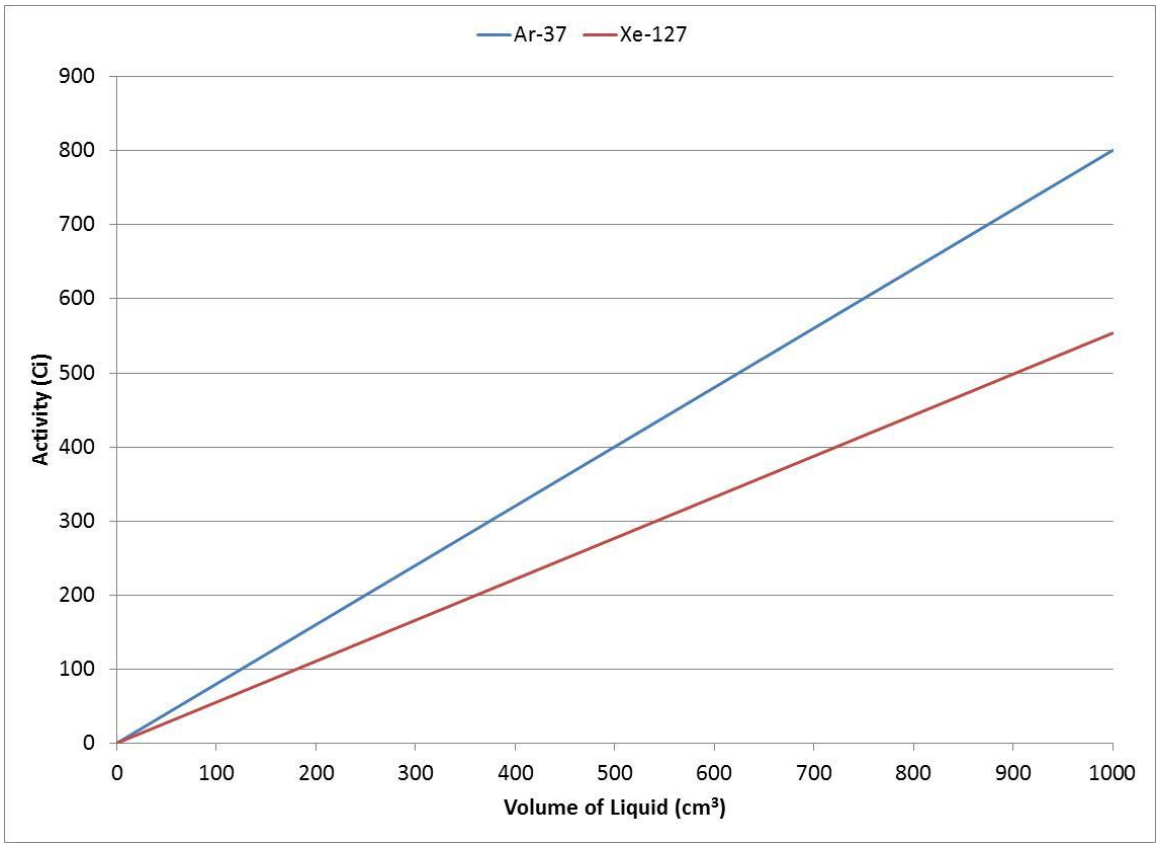

Figure 6. Activity of ^{37}Ar and ^{127}Xe produced in Beam Port 1 theorized cryogenic facility with solid ^{36}Ar and ^{126}Xe targets as calculated using SCALE (Biegalski, 2016)

These activation calculations were performed for both solid ^{36}Ar and ^{126}Xe within the near-core region of BP1 that sits adjacent to a graphite block. The total neutron flux used in these calculations was 7.0 x 10^{12} n cm^{-2} s^{-1}, and the model was still set for 100-hour continuous irradiation time. As a point of reference, BP3's cryogenic facility has a volume of 80 cm^3, which may work as a feasible volume, however this calculation was performed to 1000 cm^3 which could in fact go even higher for a given geometry and improved cryogenic ability of a system.

3.4 Safety Considerations

Given the nature of this experiment of sample activation and especially for one of this magnitude, several safety precautions exist such as dose to experimenters, public, and reactor structure integrity. Typical safety analysis for irradiations of novel gases assume instantaneous release of gas to the reactor bay area. Air concentrations within the bay must remain below 250 DAC (Derived Air Concentration) as set forth by the NRC:

> *"The concentration of a given radionuclide in air which, if breathed by the reference man for a working year of 2,000 hours (about 2 and a half months) under conditions of light work (with an inhalation rate of 1.2 cubic meters of air per hour), results in an intake of one annual limit on intake (ALI). Established DAC values are given in Table 1, Column 3, of Appendix B to Title 10, Part 20, of the Code of Federal Regulations (10 CFR Part 20), "Standards for Protection Against Radiation."*

Based on this information a release of 250 DAC would result in maxing out a radiation workers' annual limit on intake (ALI) in the reactor bay in an 8-hour day. Table 2 shows the limits and requirements that would have to be implemented to address radiation worker exposure concerns.

Table 2. DAC Limits and Maximum Production Values for ^{37}Ar and ^{127}Xe

Isotope	**DAC (µCi/ml)**	**Maximum Production for 250 DAC in Reactor Bay (Ci)**
^{37}Ar	1.0	1.03×10^{6}
^{127}Xe	1×10^{-5}	10.3

For in-core irradiations there will be additional safety concerns pertaining to the pressure of the irradiation vessel. The primary concern is given a rupture scenario that could induce reactor core damage. Because of this concern any pressure associated with a designed

vessel to be inserted into the core has to be limited between 20 – 80 psi, and future modeling and testing would need to be done to prove it met those safety set points.

Similar to the in-core facilities, the proposed cryogenic facility would also come with pressure concerns if the liquids/solid samples were allowed to flash back to a gas in a loss of coolant scenario. This situation must be proven to show that the structural integrity of the vessel would not impact the integrity of the reactor structure.

In conclusion, given the increase in sample density and activation rates a cryogenic facility would result in the most significant benefit to the activation levels and efficiency of the experiment. The increased densities would greatly outweigh the effect of a lower neutron flux present in BP1. However, with this being the ideal experimental scenario, significant effort would be required in the design, modeling and construction to build the cryogenic irradiation system within the safety requirements.

Chapter 4: Design Methodology

Careful design methodology is essential in creating a flexible system that meets the requirements and constraints of a given project. A multi-faceted project can create its own roadblocks when varying design parameters clash and are not thought out beforehand. This often leads to huge delays and backtracking to account for those errors before moving forward. To meet the needs of this project efficiently, the design was undertaken in three ways: design of the Cryo-System within specific facility parameters, efficient gas transfer mechanisms, and computational analysis for visualization and safety specifications.

4.1 Cryo-System

The design of the cryo-system is the central focus of this project and therefore, had to be taken on before any of the other facets of the project were developed to avoid conflict. This included looking at previous designs for alternative applications and morphing them into plans that would fit the needs of this new facility. Once the facility was designated to be placed in BP1, the requirements and constraints could start to take shape.

4.1.1 Requirements and Constraints

The way gas irradiations have previously been done was by filling a canister with the target gas at approximately atmospheric pressure and setting it within the reactor core at the highest possible power output for days to weeks. The geometry used previously held only about half of the target gas in the high-flux area of the reactor. From here the leap was made from simply using a gas to solidifying it by cooling it down to one point where it would receive homogenous activation and increase efficiency by 1000x due to the density

increase (Biegalski 2016). With this idea in mind we began design of the rest of the cryo-system.

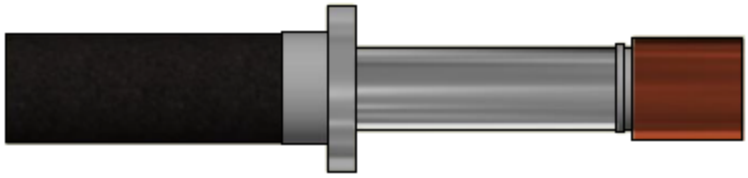

Figure 7: Original cold finger design (MCJ Cryomech, 2017)

Iterating upon this original design (Figure 7), the cold finger design began to morph into an irradiation canister, where a condensing body would mount to the copper cold head to focus the gas at the coldest point, and it would be surrounded in a vacuum jacket to help with thermal efficiencies in keeping the temperature low (Figure 8). Two different gas lines were attached to the condenser, one for gas transport, and the other for safety, as well as a vacuum line to maintain the correct pressure drop in the outer jacket. The irradiation canister was designed to sit inside the reactor structure just adjacent to the core where it would receive a high neutron flux. The canister was then attached to a 14’ flexible helium-transfer line that would feed back to the helium compressor sitting outside of the reactor core.

Figure 8: Updated cold finger design (Byrns, 2019)

Some other design features included small threaded holes on the outside face of the canister so that upon installation and removal, the experimenters could thread in a long pole for ease and safety in pulling the canister out of the beam port hole. A temperature sensor was also installed at the cold head-condenser interface where the experimenter will be able to monitor the temperature during the experiment to make sure the gases is staying in a solidified form, or to check for errors that would indicate possible failure.

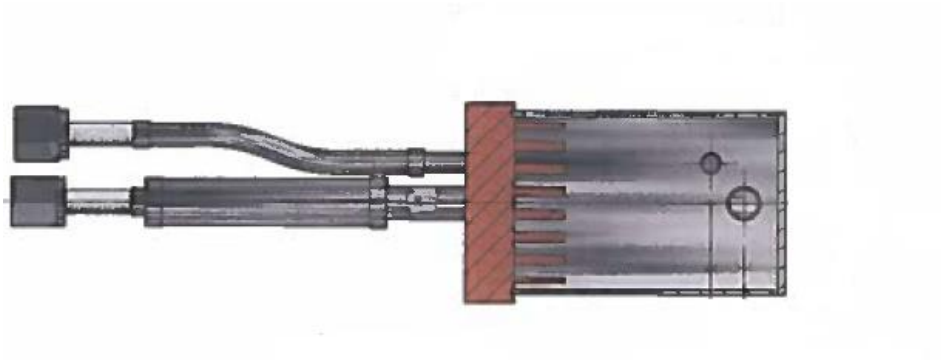

Figure 9: Cold finger fins (Byrns, 2019)

A major design change was to the inside of the condenser, on the copper face, where multiple horizontally oriented fins were added to significantly increase the surface area for gas to condense on. Another important design modification to note was the material selection process. With this canister sitting directly adjacent to the reactor core, materials other than the gas will activate and become radioactive. The material that would activate the most had to be evaluated to determine potential dose during removal and disposal. With the copper being the largest activation concern, other material selection for the canister and condensing vessel became less concerning. After extensive modeling (discussed in chapter 5) the canister passed safety approvals.

4.1.2 Heat Exchanger

Leading back from the irradiation canister, the flexible helium-transfer line runs back to the helium compressor unit that sits outside of the shielding so that it can be monitored during operations. A unique feature about this helium compressor is that to perform optimally it must operate with in very specific technical conditions, and a major facility change had to be made to create what became a chemically treated heat exchanger.

First, the water must remain within a specific pH and calcium carbonate level. This means that the water used must either be softened to get within the $CaCO_3$ specifications or there is access to de-ionized water in which the $CaCO_3$ spec is met, but the pH might be too high.

Parameter	Value	
Cooling Water	See Figure 5-1	
Maximum Inlet Pressure	110 PSIG	7.6 bar
Alkalinity	5.8 < pH < 8.0	5.8 < pH < 8.0
Calcium Carbonate	Concentration < 80 PPM	Concentration < 80 PPM

Table 3. Alkalinity and $CaCO_3$ Specifications (*Cryogenic Refrigerator Instillation and Operation Manual)*

Second, the flow rate and temperature must remain within a band as depicted in Figure 10, so a few parameters must be considered such as: heat induced into the water from the compressor unit and the pump, the heat removal rate of the heat exchanger given the temperature of the chilled water and these then have to balance out within the given specifications for successful operation.

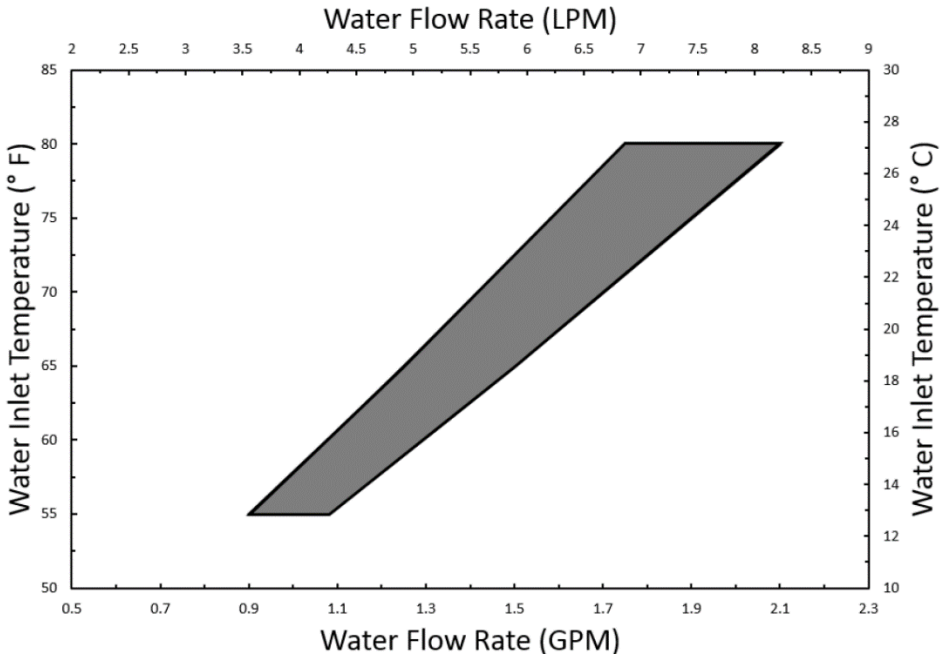

Figure 10. Temperature and Flow Rate Relationship Diagram (*Cryogenic Refrigerator Instillation and Operation Manual)*

The next phase of this project included constructing a system that would allow for water to transfer from the NETL's chilled water source across the reactor bay area and down to the compressor unit. This included over 80 feet of copper piping and over 20 feet of PVC in the lower connections between the water tank and the compressor itself. This project was split into two sections so that the chilled water would remain untouched by the treated water from the tank. The PVC section was also given multiple stages in the event the chilled water from the station prove to be too cold, the heat exchanger could be isolated from the rest of the loop and added back in when needed, or to pre-chill the water before the start of an experiment the compressor could also be isolated.

Figure 11. Heat exchanger as installed.

4.1.3 Safety Concerns

During the design process, safety precautions had to be built into the system for it to operate within the technical specifications of UT's reactor. Major safety concerns originated with the central focus of condensing gas into a small condenser, where in certain instances this gas has the potential to flash from solid to gaseous state, creating a large pressure wave that would threaten the integrity of the irradiation canister. Modeling was later done to prove that this could not occur under normal operating conditions, but prior to those

models, physical design changes were made to the irradiation canister and the gas manifold system.

NETL's reactor has a pressure limit on vessels within the reactor core that ultimately requires a valve release if 25 psi is ever reached within the vessel. This was originally the main reason for the experiment being moved from the 3-element facility to BP1. However, even with the move, the potential for a pressure vessel to be created meant that precautions had to be built in to help divert the flow of that pressure release in a safe manner.

4.2 Gas Manifold

During operation of the facility a transfer system must be in place to account for sending the gas into the condenser, removal, and any safety precautions along the route. To ensure these features were included a preliminary piping diagram was created as seen in Figure 12.

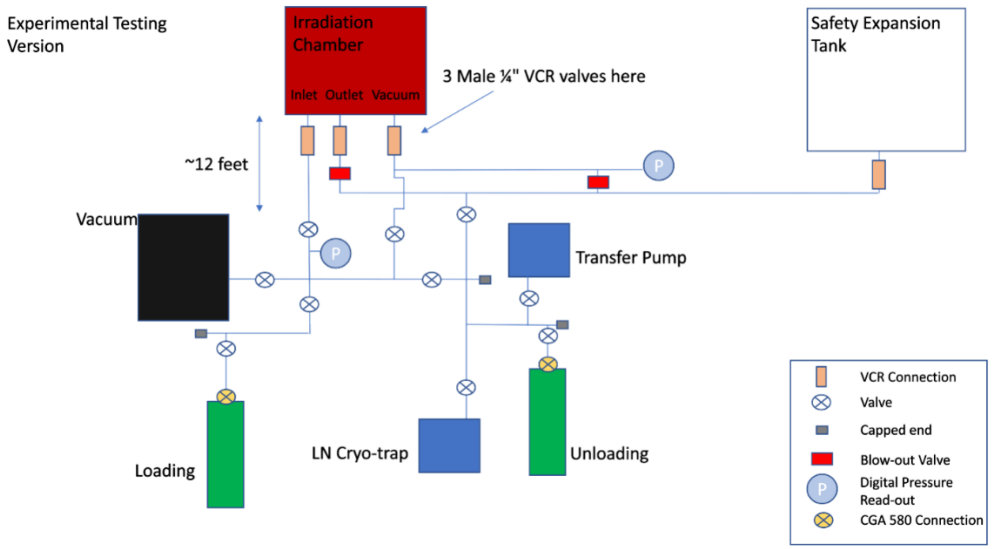

Figure 12. Gas manifold diagram

In this diagram it was important to include ways to isolate each of the individual routes to and from the condenser all the while considering how the gas could be saved in case of a leak or loss of coolant to the condensing vessel.

The first step is pumping and flushing the system with nitrogen to remove contaminants and create a pressure differential so that when the valves are opened the gas will move down the piping. Because of the isolation options the gas can be compartmentalized as it is fully removed from the loading tank and then sent to the condenser once the tank has been emptied. After the gas is trapped on the condenser the irradiation can commence.

After the irradiation is complete the gas will slowly be warmed up and then sent down the piping to the shipping tank. This step also has a few options within it in terms of how the gas will be unloaded. One option would be to simply warm up the gas and attempt to cryo-trap the gas back down on the piping, while the other would be a combination of using a transfer pump in conjunction with the cryo-trap to improve efficiency. These options will both be explored and detailed fully in the results chapter.

During this entire process, the ability to safely relieve pressure in the system as well as capture gases that may be highly activated was of utmost priority. This involved including several burst valves on the safety expansion pipe as well as the ability to isolate these pipes from each other to create an opportunity to repair the burst valves and return the gas to the condenser via cryo-trapping. While doing this the volumes of each individual line were calculated to account for enough gas flow rate given a failure scenario.

After incorporating design elements in the manifold for each of these steps, the pipe diagram was transferred from a 2D model into a 3D SOLIDWORKS model and a parts list was created (Figure 14).

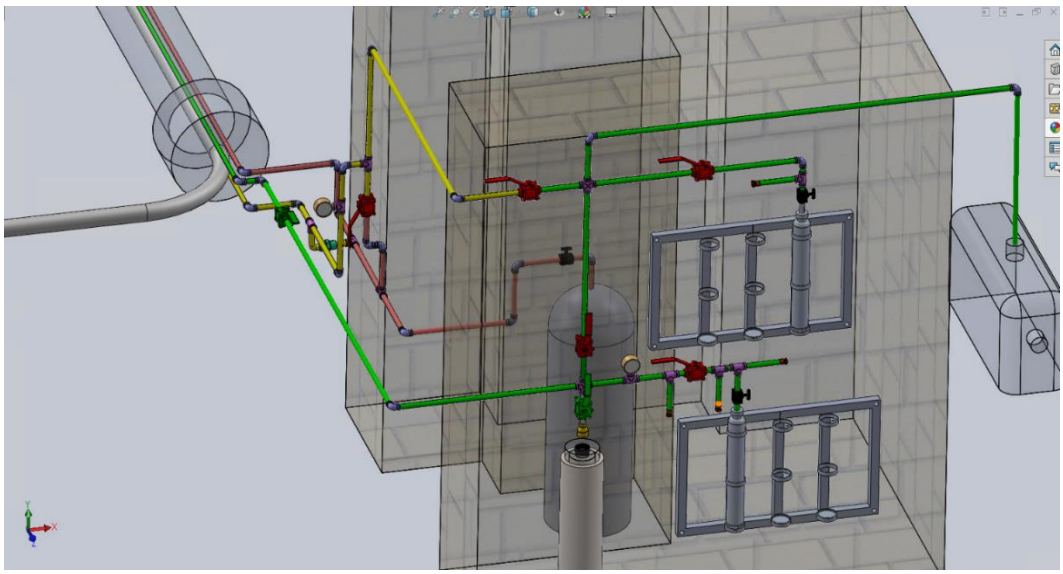

Figure 13. Gas Manifold SOLIDWORKS Model

The green line represents the loading/unloading transfer pipe, while the red is the safety expansion line and the yellow functions as a vacuum line. The biggest difference between the colors is that the yellow and red are both ¼" piping while the green was reduced to 1/8" to help improve gas transfer efficiency by reducing the amount of available dead volume.

The red and black valves pictured act as stand ins that account for various sized diaphragm and bellows valves. And there are multiple spots that are capped that create options for future additions to the system.

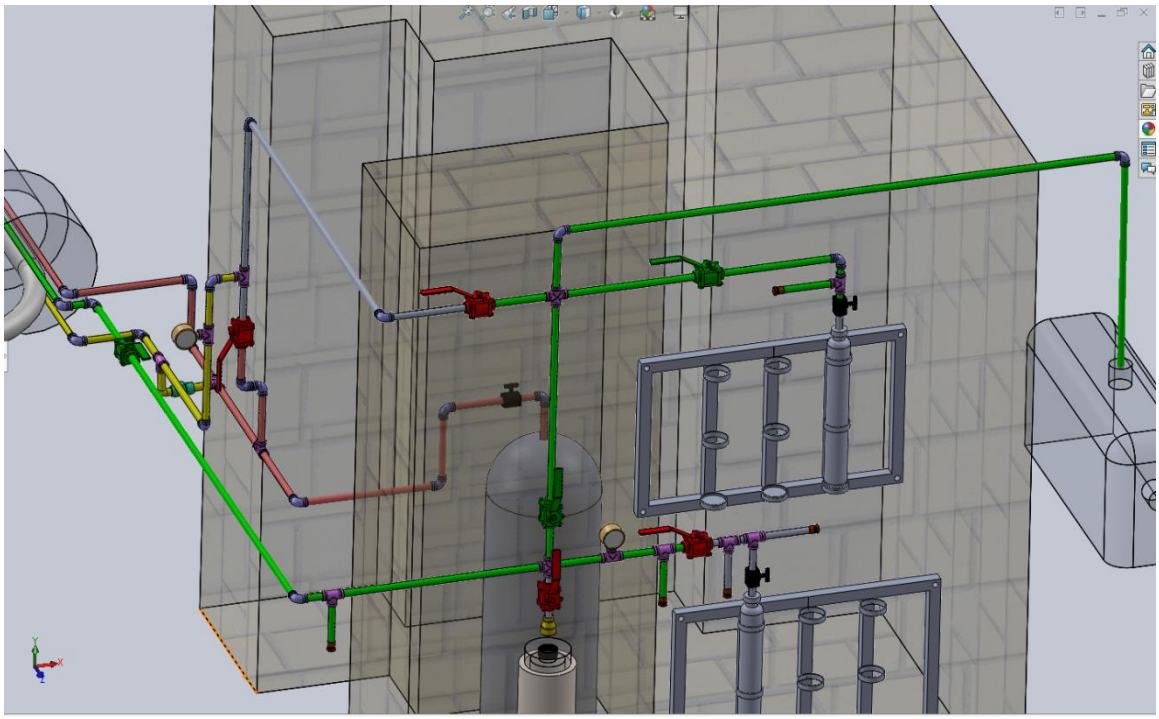

Figure 14: Manifold with valves in the “Loading” Configuration

4.2.1 Loading and Unloading Procedures

As seen in the figure above, this configuration of the piping, in which the green route signals the movement of the gas from the loading tank into the piping and then down into the cryo system via cryo-trap.

There have been multiple proposed ideas in which the gas shall be loaded into the piping before the cryo system is turned on, and due to the strengh of the cryo system it has been determined that the system will first under-go a “pump and flush” with nitrogen which entails loading the gas line to atmospheric pressure and then quickly pumping back down to a low vacuum pressure around 1 Torr. This will happen a few times to help cleanse the line of any unwanted gases or particles before loading in the target gas for irradiation. After

purging the line it will once again be pumped down to vaccum, have the valves to the vacuum pump closed and also open the valve to the target gas canister to charge the line to a pressure that corresonds with a volume for that specific irradiation. Once that pressure is met the valve on the canister will be closed, and preparations will begin to turn the system on. As the system begins to cool down the pressure drop should correspond with the freezing of the gas that resembles previously calcualted relationships during the experimental trial phase. When the system is then at a pressure and temperature that the experimenters set, and has stabilized, the reactor will then be turned on.

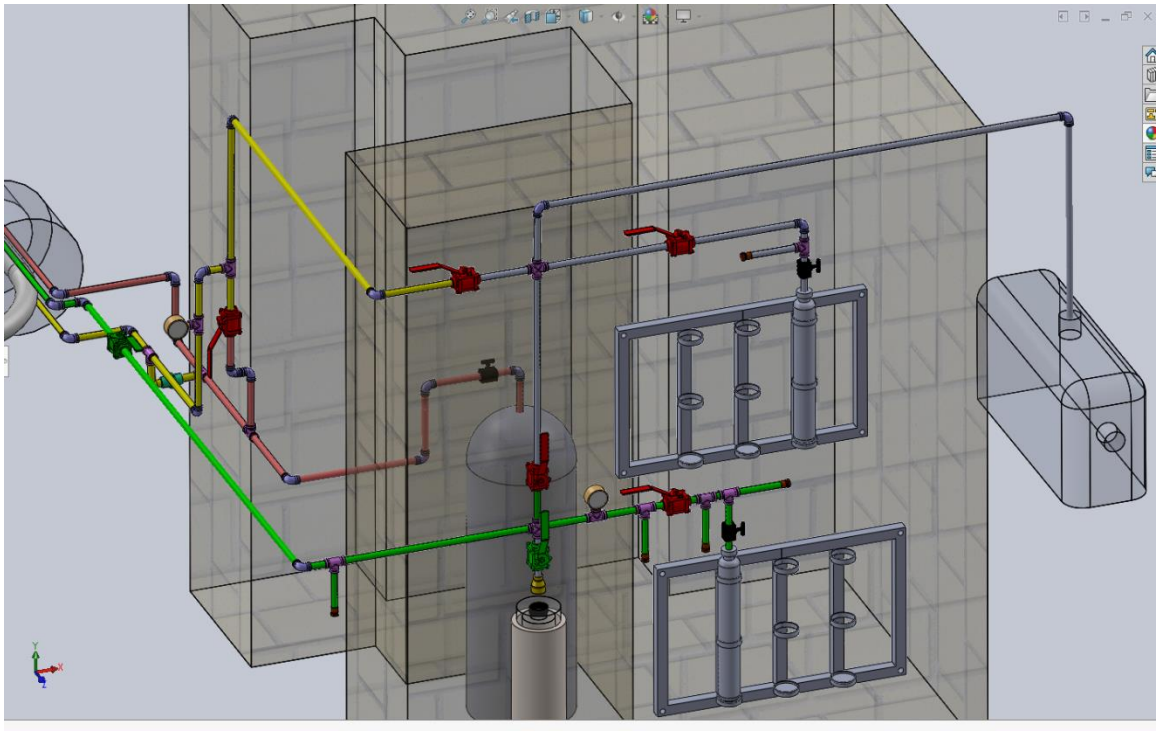

Figure 15: Manifold with valves in the “Unloading” Configuration

The figure above shows how the previously cryo-trapped gas will move out of the irradiation canister and back up the green loading/unloading pipe and back into the unloading tank.

During this phase of the experiment the gas will be radioactive and thus safety precautions were taken to limit dose to experimenters. The system will be allowed to warm up slowly and the gas will then begin to move down the gas tubes due to natural expansion. Once the system stabilizes one of two operations will occur: a transfer pump will be turned on to pull the gas from the tubes into a shipping canister, or a separate cryo-trap, utilizing a liquid nitrogen dewar, will be raised around a vial in which the gas will then be trapped again outside of the reactor beam port. These lines will all be shielded except for the valves so that they remain operable during this phase.

Chapter 5: Modeling

This chapter discusses the relationships and dependencies of the various modeling software utilized during this project. Each of these codes played a role in either design, safety, or a combination of both. Often one breakthrough in a given software would lead to multiple in another and vice versa.

5.1 MCNP

Monte Carlo n-Particle (MCNP) was used to model radiation dose and potential damage to the system and the surrounding area thus providing information to build safety precautions around. It was also used in developing the potential radiological dose releases given in the plume modeling from HOTSPOT and SCALE. ANSYS and SOLIDWORKS also worked hand in hand for developing the design and safety analysis of the system both inside and outside of the core. If a variable changed in terms of the gamma flux being higher or lower at the condenser location, the copper block would yield a different heating value and thus the potential for the flashing of gases may go up or down.

5.1.1 Theory

Monte Carlo n-Particle radiation-transport code (MCNP) is a general-purpose, continuous-energy, generalized-geometry and time-dependent analytical code designed to track many particle types over their respective broad energy ranges. This code was developed by Los Alamos National Laboratory (LANL).

MCNP 6.2 was utilized in providing all approximations of nuclear interactions within the materials of the proposed system, and the produced values from these interactions were

monitored by MCNP calculations following their energies. These reactions were marked by how a neutron or photon first reacted with a material, that material's ability to absorb or change that particle's direction, and then the resulting cascade of collisions that particle would undergo in its lifetime. Utilizing the F4, or FMESH tally, and an energy deposition, F6 or T-Mesh, a map of the resultant flux and deposited energies of the particles in the region of interest was created. To create a similar environment in which the system would be present, a geometrically accurate model of the TRIGA MARK-II reactor was used (Wilson 2017). The governing equation in MCNP:

$$l = \frac{-1}{\Sigma_t} \ln(\xi) \qquad [1]$$

where Σ_t is the macroscopic cross section of the material and ξ is a random number generated by MCNP. The equation represents the distance to the next collision a particle will have in the system. A particle is born with a specific speed, direction, and energy and then MCNP will calculate [1] for the particular material and then roll a random number. These values are then plugged back into the equation above to calculate the distance traveled by this particle. It will then calculate the type of collision it has and determine whether it will "survive" to have a new collision with a different material and thus the chain will continue. This will be repeated until the death of the particle by either a boundary cell condition, loss of energy, or capture.

This process will then be completed for a specific number of prescribed particles. These particle values can be gathered by inserting what is known as a tally at a specific location or surface and will have an associated relative error for the user to determine whether it is accurate enough to be acceptable.

For safety precautions such as shielding around the beam port and local dose levels when the system is removed the following equations below were utilized:

Absorbed dose

$$D = \frac{\Delta E_D}{\Delta m}\left[\frac{J}{kg}\right] \quad [2]$$

Absorbed Dose Rate

$$\dot{D} = \frac{\Delta D}{\Delta t}\left[\frac{J}{kg \cdot sec}\right] \quad [3]$$

Dose rate attenuated exponentially

$$\dot{D} = \frac{kSE\frac{\mu_t}{\rho}Be^{-u^D}}{4\pi r^2} \quad [4]$$

where B is buildup factor that is dependent on incident photon energy, the shielding material and its thickness, the source and shield geometry and the distance from the surface to the dose point.

5.1.2 Results

One of the largest potentials for danger in this experiment arises from the rate at which outside heating is applied to the condensed material. If this heating happens quickly, it could lead to gas flash boiling/subliming, and a subsequent pressure wave that could threaten the structural integrity of the condensing vessel. In this instance, the gamma-ray heating from the copper would prove to be the largest source of outside heating.

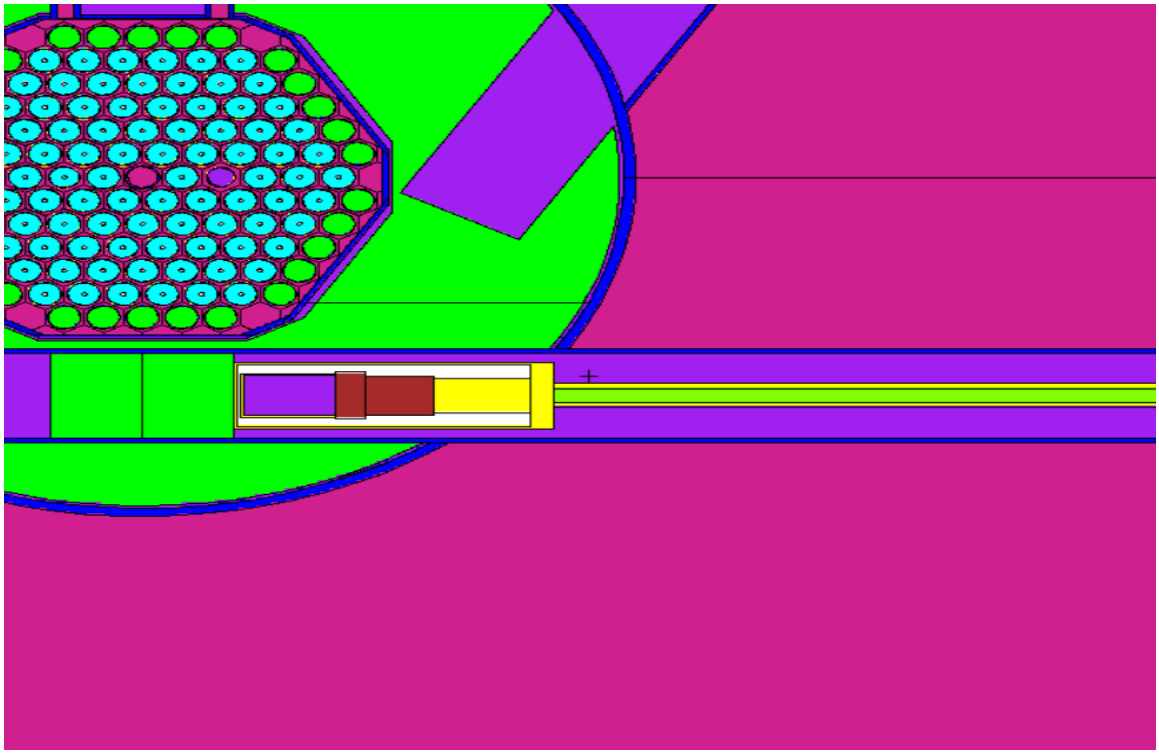

Figure 16. MCNP depiction of BP1 irradiation canister fully inserted into the beam port adjacent to the reactor core

To start to understand this value, an MCNP model of the reactor developed in prior work (Wilson 2017) was adapted depicting the location and geometry of the irradiation canister within BP1. An energy deposition T-Mesh was then taken of the beam port to look at neutron and photon energies deposited in the material after interaction. The resultant output file was then taken, and a conversion was applied to take the output unit of MeV/cm^3/Source particle, and convert into a rate of adiabatic temperature rise within the system, °C/minute, as shown in Table 4. From this calculation we can conclude that the outside heating induced from this particle deposition would not result in a gas flash scenario should loss of coolant occur.

Table 4: MCNP Energy Deposition Conversion

		Conversion			
Source Particles	8.02E+16	MeV	SourceParticle	Joules	= Joules
MeV to Joules conversion factor	1.60E-13	cm3 * Souceparticle	s	MeV	= s*cm^3
		J	s*cm^3	g	= s
		g*Celsius	J	cm^3	= Celsius
	In Condenser (SS 304 Stainless Stee	In Cold Head (101 OFE Copper	In Tubing (Aluminium)		
Max Energy Selected	3.54E-06	1.12E-05	1.01E-05	Mev/cm3/sourceparticle	
Heating power density	4.55E-02	1.44E-01	1.29E-01	Watts/cm^3	
Volume	6.93E+01	2.64E+02		cm^3	
Heating power	3.15	38.07	0.00	Watts	
Need specific heat of materials	0.502416	0.3852	0.9	J/g * celcius	
How to get Time rate of change of Temp:					
	11.04	2.67	6.96	seconds*cm^3/g * deg celcius	
Density	7.85	8.94	2.7	g/cm^3	
	0.011533807	0.041897815	0.05317772	deg C/s	
Temp change in materials	0.69	2.51	3.19	deg C/m	

5.2 ANSYS

5.2.1 Theory

ANSYS finite element analysis software is used to model structures, electronics, and machine components to be analyzed in regard to strength, elasticity, temperature distribution, fluid flow, and various other attributes. In the following section we will be exploring ANSYS and its many features that were utilized during this work. ANSYS Fluent was used in modeling multi-phase fluid flow and solidification, while ANSYS mechanical was utilized to develop models depicting the changes in pressure the system could potentially see during operation.

The Eulerian form of the conservation of mass equation is derived by applying the Reynolds Transport Theorem with f=1. This assumed value of "f" comes from integrating

the function "f" over the time-dependent region $\Omega(t)$ and taking the derivative with respect to time.

$$\frac{dM}{dt} = \frac{d}{dt}\iiint_{\Omega} \rho \, d\Omega = \iiint_{\Omega} \frac{\partial \rho}{\partial t} d\Omega + \oiint_{A} \rho \vec{\mathrm{V}} \cdot \hat{\mathrm{n}} \, \mathrm{dA} = 0 \qquad [5]$$

From here we apply the divergence theorem:

$$\iiint_{\Omega} (\frac{\partial \rho}{\partial t} + \nabla \cdot \rho \vec{\mathrm{V}}) \, d\Omega = 0 \qquad [6]$$

This integral is satisfied for an arbitrary volume taking the integrand to zero thus resulting in the differential equation form of the conservation of mass.

$$\frac{\partial \rho}{\partial t} + \nabla \cdot \left(\rho \vec{\mathrm{V}}\right) = 0 \qquad [7]$$

Where ρ is the fluid density, *t* represents is time, and $\nabla \cdot \left(\rho \vec{\mathrm{V}}\right)$ is the flow velocity vector field. From here it will be convenient to express the equation in common cartesian coordinate form by expanding the vector from the previous equation to include for x, y, and z dimensions.

For this situation we are dealing with a variety of compressible flows in which there exists a multitude of thermodynamic relationships that permit the conversion of energy into various forms. These include variables such as internal energy, specific heat ratio, enthalpy and of course the Ideal Gas Law relations. To solve this problem correctly the model will have to account for these physical laws and from there we will apply the Reynolds transport theorem to transform these laws to a Eulerian framework. This is done by setting up the energy equation in Lagrangian terms and inserting the heat transfer and work terms for pressure and viscosity. From there the pressure terms can be placed within the convection

term to introduce Fourier's law and greatly simplify the equation. After that we apply the Divergence Theorem to the surface integrals and since the control volume is arbitrary the sum of all the integrands must equal to zero to satisfy the equilibrium resulting in the following differential form of the conservation of energy equation:

$$\frac{\partial(\rho e_t)}{\partial t} + \nabla \cdot \left(\overrightarrow{\mathrm{V}}(\rho e_t + p\right) = \nabla \cdot \left(\mathrm{k}\nabla T + (\bar{\tau} \cdot \vec{\mathrm{V}}\right) + \dot{S}_g \qquad [8]$$

Where ρ is the fluid mass density and $\dot{S}_g$ is the generational source term that will include radiation heating and other physical effects present in the system. This will then be solved for by defining correct initial and boundary conditions.

5.2.2 Stress Equations

Often in pressure vessel cases failure mode and effects analysis (FMEA) is performed as a process for reviewing components and subsystems to identify possible failure modes in a system. For this case we are particularly interested in potential rupture of the condenser and consequential fracture of the irradiation canister while it is next to the reactor core resulting in a radiological release to the reactor bay. To understand whether a material has undergone failure in this situation the equivalent yield strength, or stress, was measured against the value of the material under pressure using the following equation:

$$\sigma_{eq} = \frac{1}{2}\sqrt{\left(\sigma_{xx} - \sigma_{yy}\right)^2 + (\sigma yy - \sigma_{zz})^2 + (\sigma zz - \sigma xx)^2 + 6\left[(\sigma zz)^2 + \left(\sigma_{yz}\right)^2 + (\sigma_{zx})^2\right]}$$

[9]

This equation represents a 3x3 stress tensor to view the equivalent stress as a scalar indicator to determine material failure. In this case, if the equivalent stress present on the material after being introduced to the pressure, is higher than the rated yield stress for the material the material would fracture.

5.2.3 Analysis

ANSYS was utilized for multiple simulation settings. These included the proof of concept that within this vessel, given operational conditions, that the subjected gas would begin solidification over time, and a pressure vessel analysis to simulate a worst-case scenario of a gas flash that could potentially lead to vessel rupture and leakage of highly activated gases.

5.2.4 Eulerian Modeling

The first of these simulations to be explored was the solidification scenario of these gases that would undergo, potentially, multiple phase changes before finding equilibrium. This took some time to understand how to best set up operating conditions in classical flow field theory to help with these various phase changes while being subjected to differing temperatures over time. But this simulation would be essential in setting up the future pressure vessel analysis for it would help in understanding the maximum volume of gas available to be present at one time within the condenser.

In ANSYS, we are presented with various system operating conditions to help govern the world in which this simulation is living. The first major decision was how to best describe this environment and how it was being observed which ultimately came down to a Eulerian or Lagrangian approach. In classical flow field theory, Lagrangian specification for a given flow field is a way of looking at the fluid motion where the observer tracks an individual particle as it moves through space and time, or its path line, however for this specific situation we couldn’t just look at one particle but had to observe all of them to understand how the average of the mass would behave. Hence, a Eulerian model was chosen as a way

of looking at the flow field that focuses on a specific location in the space though which the fluid flows as time passes, that location being the condensing body. In this method, conservation of mass, momentum, and turbulence transport all needed to be solved for, for all phases simultaneously.

5.2.5 Solidification

An important simulation for this work was explored in the form of a solidification/melting model that would be used to help describe the environment of the irradiation canister given the conditions of a copper face cooled by liquid helium, and incoming heating from gamma-rays produced from the de-excitation from the copper as well as the reactor core.

Instead of tracking the liquid-solid fraction explicitly, ANSYS Fluent uses an enthalpy-porosity formulation known as the “mushy-zone” which is treated as a porous zone with porosity equal to the liquid fraction in the volume. Appropriate momentum sink terms to account for the pressure drop and are also added to the turbulence equations to account for the reduced porosity in solid regions. Utilizing this feature a model was created to represent argon gas being present in the system and the system being turned on and cooled down, sucking the argon to the cold head via cryo-trap. The resultant figures depict solidification of argon occurring as the temperature approached 84 K which was viewed in a ratio of liquid to solid argon. The figure below is slightly mis-leading since it is unable to account for the 3 phases at once and thus we set the argon gas value to coincide with the liquid thus resulting in the entire condenser to be seen as a liquid, in red, versus the solid in blue. However due to the large fraction disparities, what we are actually viewing is the gas region, in red, and a small boundary layer between the blue and the red regions in which the liquid would reside.

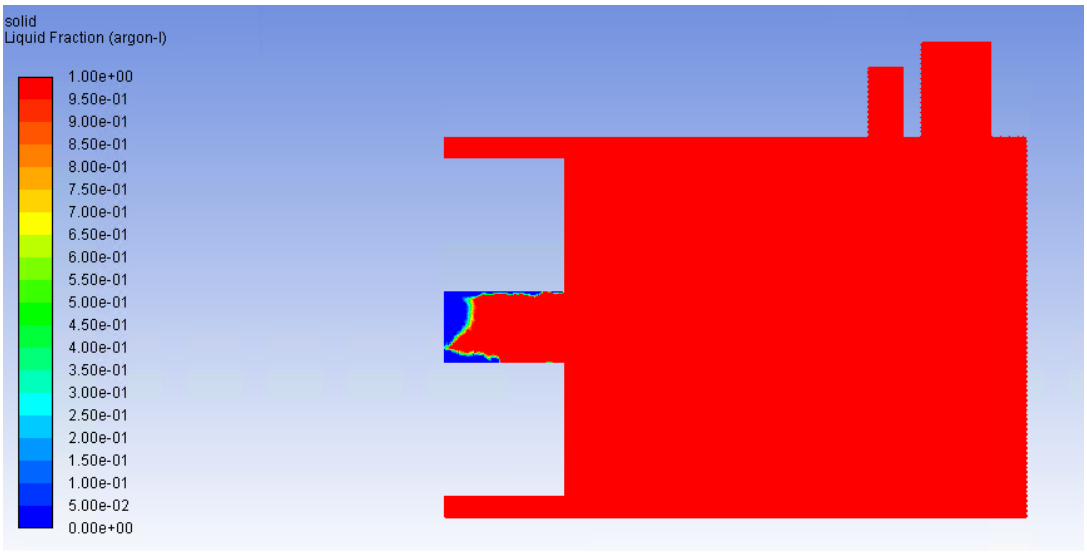

Figure 17. Liquid to Solid Fraction of Argon Present in Irradiation Condenser

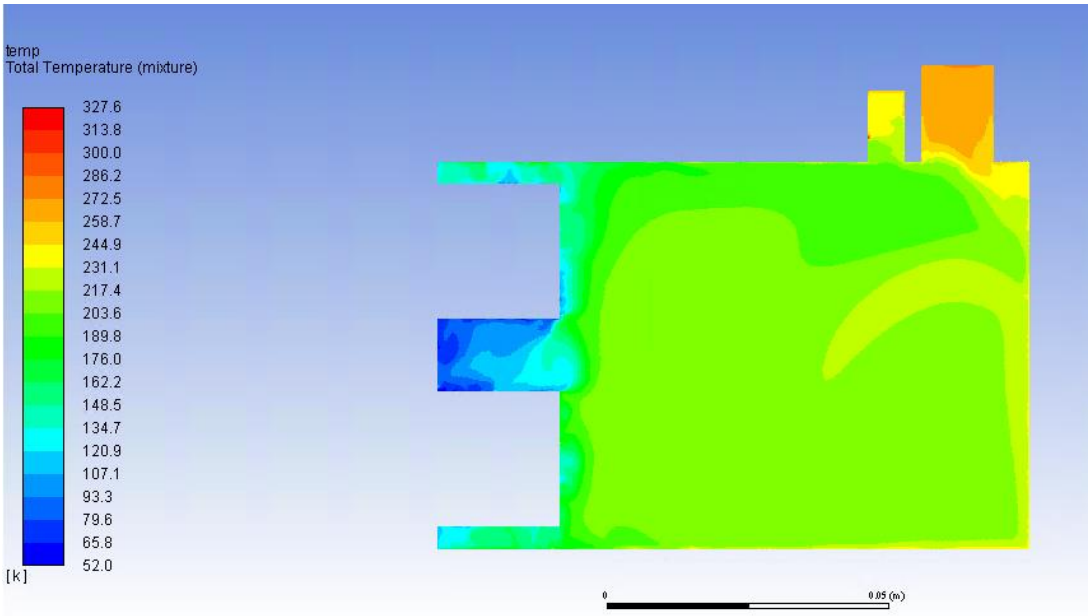

Figure 18. Total Temperature of Irradiation Condenser Solidification Model

These two models were built in 2D to save computational time and to allow for visualization of the solidification to occur. The difference between 2D and 3D modeling in this sense is that we do not have another directional component in which the gas particles could expand into thus limiting the interaction volume relative to the mass in a localized region, and therefore would cause phase change to happen more rapidly than it would in reality. However, we do see evidence that solidification of argon is occurring in the region closest to the copper face as evident in the liquid to mass fraction.

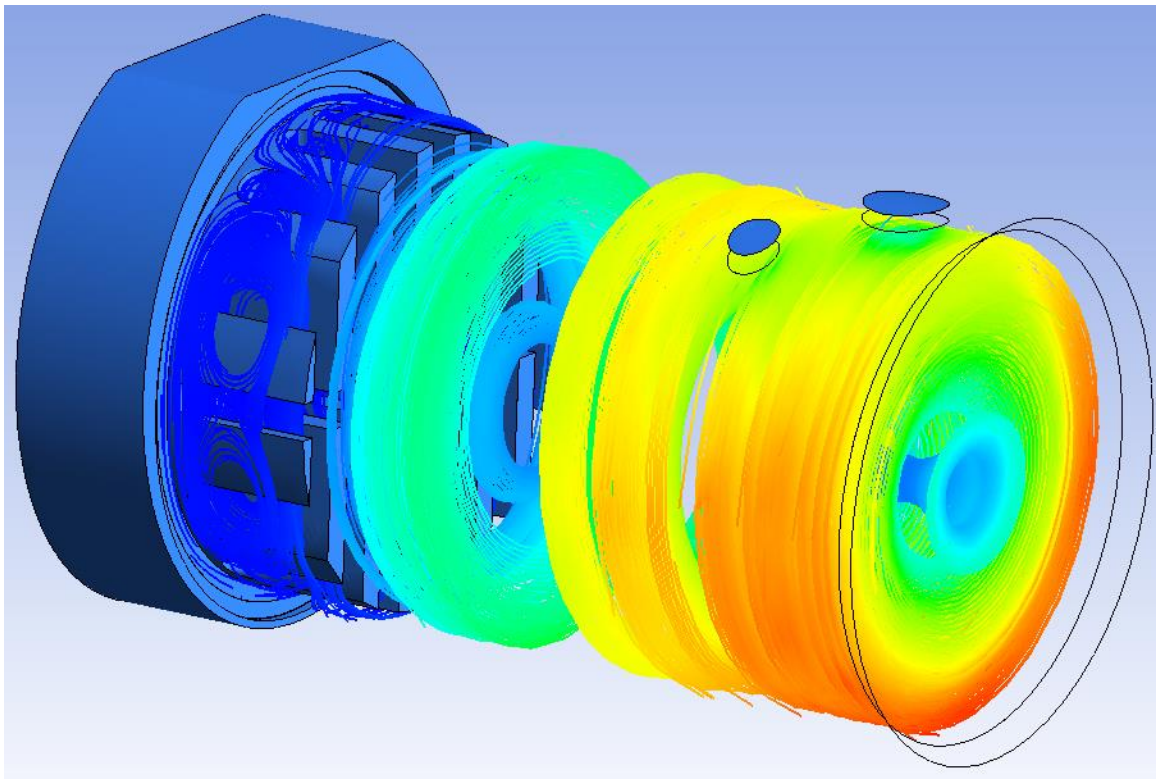

Figure 19. 3D Gas Velocity Profile Particle Tracking

Due to computational limits the solidification in 3D was too taxing to correctly track multi-phase flow while interfacing turbulence equations and porosity of the solid region so

instead we created a particle tracking model to show the velocity profile of 5000 individual gas particles and how they moved inside the condenser with no phase change. The resultant figure depicts velocities of 0 m/s in blue with steadily increasing speeds up to 0.05 m/s in red. This would indicate to me that the gas is not moving due to the temperature in that region, and if given the correct inputs would in fact change phase to a liquid or solid.

5.2.6 Pressure Vessel Analysis

When looking at the pressure vessel analysis we wanted to focus on two major stresses that would most likely be present in the operational environment the irradiation canister would be present in. These two stresses are the tensile stress, and the equivalent yield stress, both having to do with the resistance of an object to the force trying to tear it apart. The main difference between these two stresses is the that the equivalent yield strength relates to the minimum stress under which a material will deform permanently, whereas tensile strength describes the maximum stress that a material can handle before fracture, or breaking.

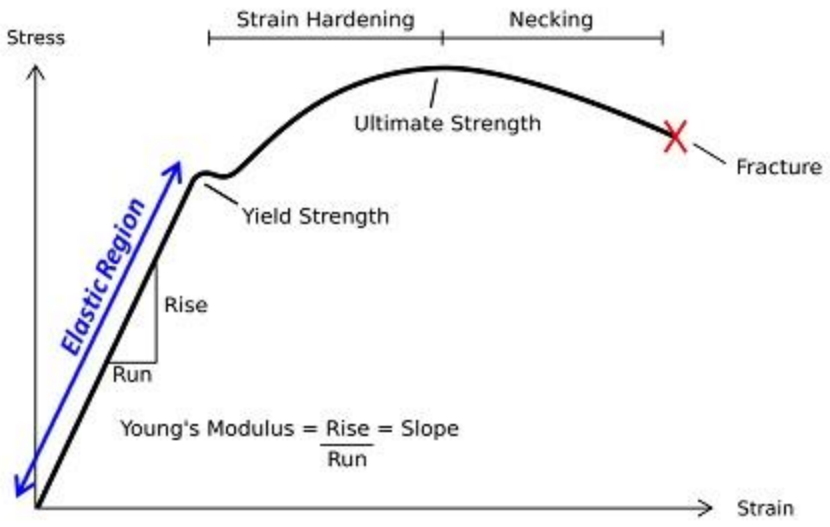

Figure 20. Stress-Strain Curve for a Ductile Material (Nuclear Power 2021)

The key thing to remember here is that the irradiation canister is not expected to undergo long periods of stress and rather only ever be subjected to one big pressure release, or flash, during a worst-case failure scenario. With a brittle material the graph would have initial higher slope that would then cut off at a fracture before ever stretching, thus there would be no elongation, or necking, period to the graph resulting in the graph shown in the figure below.

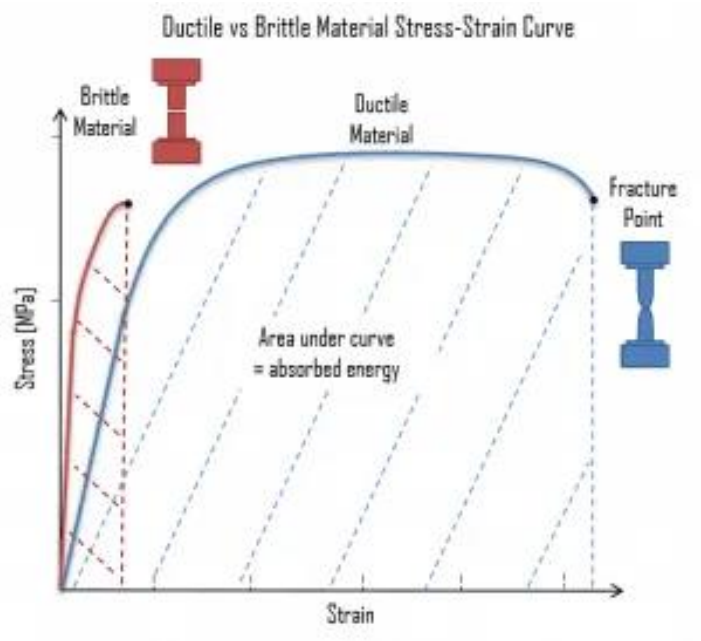

Figure 21. Stress-Strain Curve for a Brittle Material (Nipun, 2015)

To fully understand what kind of reaction our material will have we will need to plug in its exact specifications for these variables. Now the material that is in question is the condenser within the irradiation canister that is made up of 314 SS (UNS S31400) that is 0.125” thick on three sides but is mated with a copper face on one side through a brazing process.

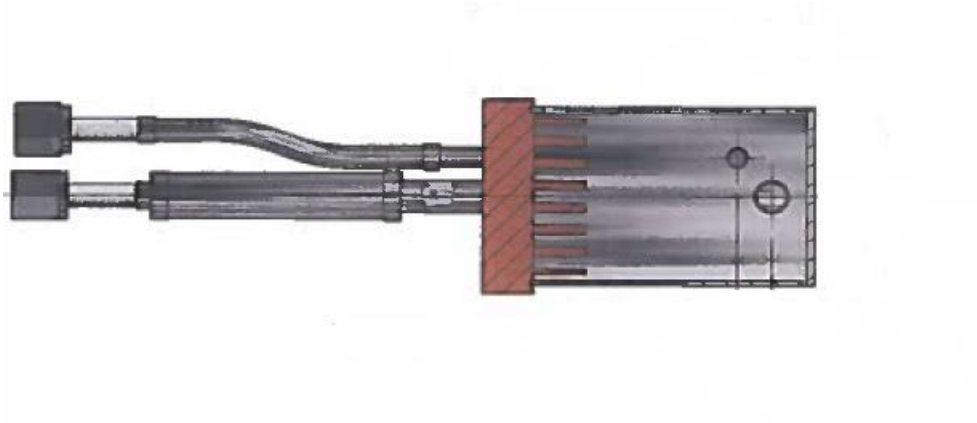

Figure 22. Condenser Top View (MCJ Cryomech, 2017)

At first, it was obvious that the side brazed to the copper was a point of concern in that it wasn't one material and a connection point, but upon further inspection it can be seen that the copper also surrounds the part of the condenser as the steel is actually seated inside of the copper thus providing it with extra wall thickness. That leaves the remaining three sides of the condenser in which to look at for failure points. Being that we are using SS 314, the pronounced yield plateau that is common in normal structural steels is nonexistent, so an equivalent yield stress is used in structural design (Rasmussen 2003).

5.2.7 Results

The Cryogenic Irradiation facility being installed into BP1 has the potential to produce mechanical stress due to pressure buildup inside of the condensing chamber. It has been shown through previously discussed results from the MCNP thermal energy deposition model that the frozen target gas will not undergo a pressure flash from solid to gaseous

phase simply due to gamma-ray heating in a “loss-of-coolant” event. However, for the purpose of this safety analysis report we will explore the three most likely scenarios regarding potential failure modes.

Within these failure modes we will look at the resulting equivalent yield stress that will give us a direct result on whether or not the system has fractured, and a safety factor to better understand how “in danger” the system is to failure. Equivalent yield stress is minimum point at which we will see permanent deformation to the system and the safety factor is calculated by the ratio of the strength of the material and the maximum stress in the part and is on a scale from 0 to 15 in this simulation. If the ratio drops below 1 we know there is failure somewhere in the condenser.

Scenario 1: Flash -- Max Volume of Ar (or Xe) in the vessel Flashes – 3.091 Liters at STP

This scenario represents the max volume of gas in the condenser with relation to the safety rating of 150 PSI. This volume was calculated using PV=nRT where pressure and volume are known, and we are solving for the number of moles present in the condenser.

This simulation resulted in the small temporary deformations of the condensing vessel shown in Figure 23 where the value of the tensile yield stress does not exceed the material limit; thus, no permanent deformation occurred. This is again verified in Figure 24 with the safety factor reporting a value of 4 in which a value less than 1 represents failure.

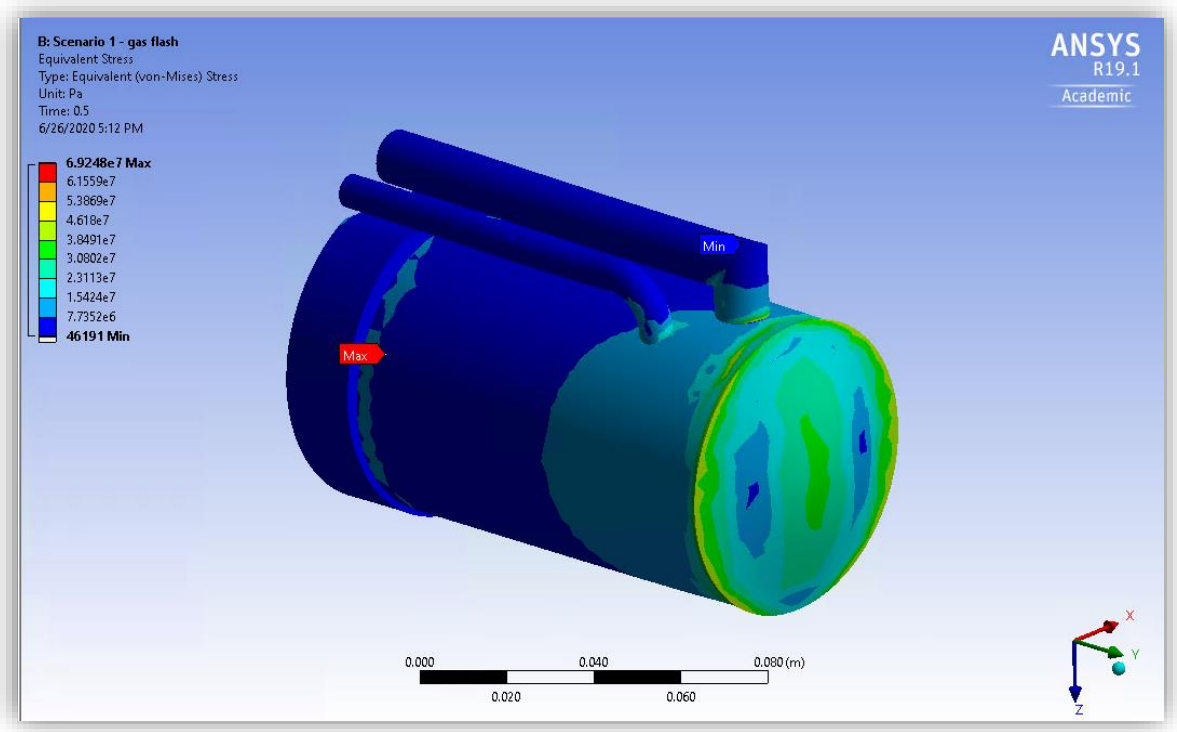

Figure 23. Equivalent Stress - Value 6.93 e7 Pa<2.15e8 Pa Tensile Yield Strength -- No Fracture

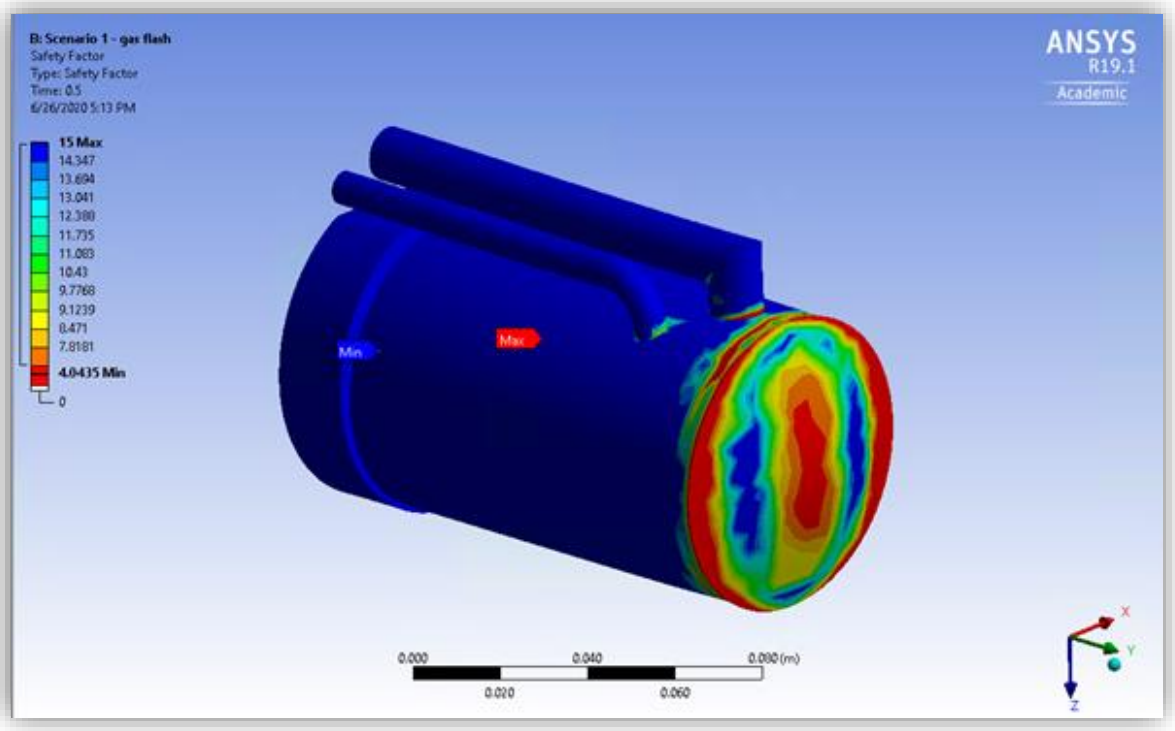

Figure 24. Safety Factor - Minimum value of 4.04 > 1 – No Failure of Condenser

Scenario 2: Gas Leak – Crack in gas line – 6 Liter (gas at STP) Flash

This scenario was based on the max volume of the actual condenser, and a rough estimate of the flow rate of the air into the condenser from a leak in the system. This model is the most variable dependent since the crack size and pressure differential at the time will considerably change the flow rate into the condenser. To calculate how much air would be present in the condenser, we calculated the total volume of air that would be needed to create the same pressure wave in the condenser as the Argon did at 3.091 Liters, and then back calculated, adding those volumes to arrive at the new pressure value. The idea behind this was that when we do the testing to see how the temp values change as gas is added to the system, we will be able to discern whether extra volume is present when this value

changes from the norm. Since we don't know that value, we erred on the safe side with a larger estimate of the volume of air being equal to the pressure safety factor of the condenser to create a worst-case scenario. Even with this new volume added, we still do not have a fracture failure within the condenser, just a larger temporary deformation.

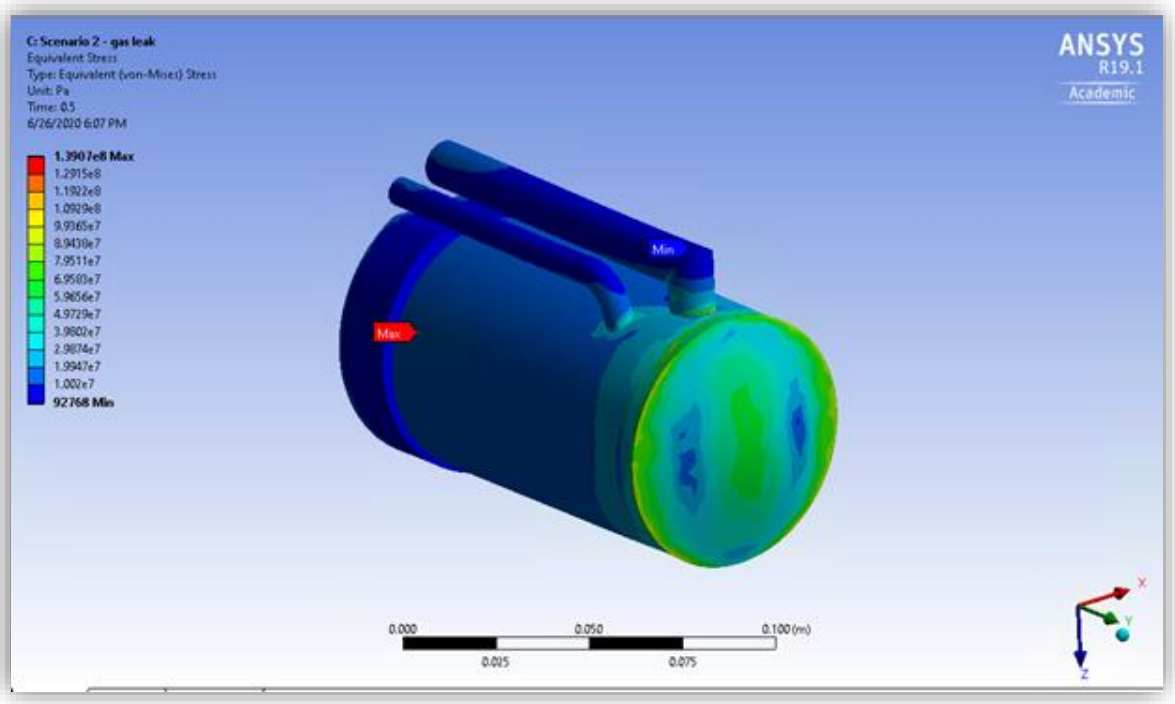

Figure 25. Equivalent Stress - Value of 1.39e8 Pa < 2.15e8 Pa Tensile Yield Strength -- No fracture.

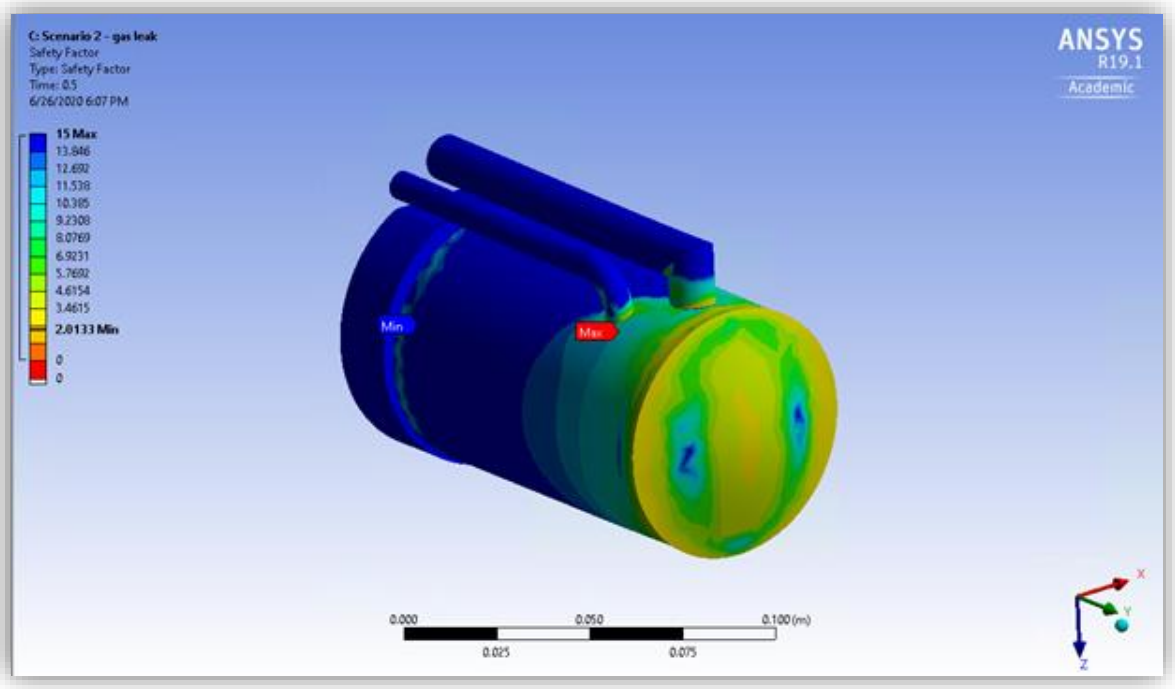

Figure 26. Safety Factor - Minimum value of 2.01 > 1 – No Failure of Condenser

<u>Scenario 3 - Failure Point – Find Volume that would induce fracture</u>

Since the previous two scenarios did not cause permanent deformation or fracture failure within the condensing vessel, we thought it was pertinent to this safety analysis report to include the volume and associated pressure value in which we do see these failures occur.

Permanent deformation and fracture failure occur at 4.64e6 Pa or an additional 7.6 liters, bringing the total volume to 13.7 liters of gas at STP

This would imply that an additional 10 liters of air (STP) were able to leak into the system undetected and the system underwent a loss of coolant fast enough to result in all 13.7 liters

of gas to sublime or evaporate, which would result in a small fracture at the end-cap of the condensing vessel.

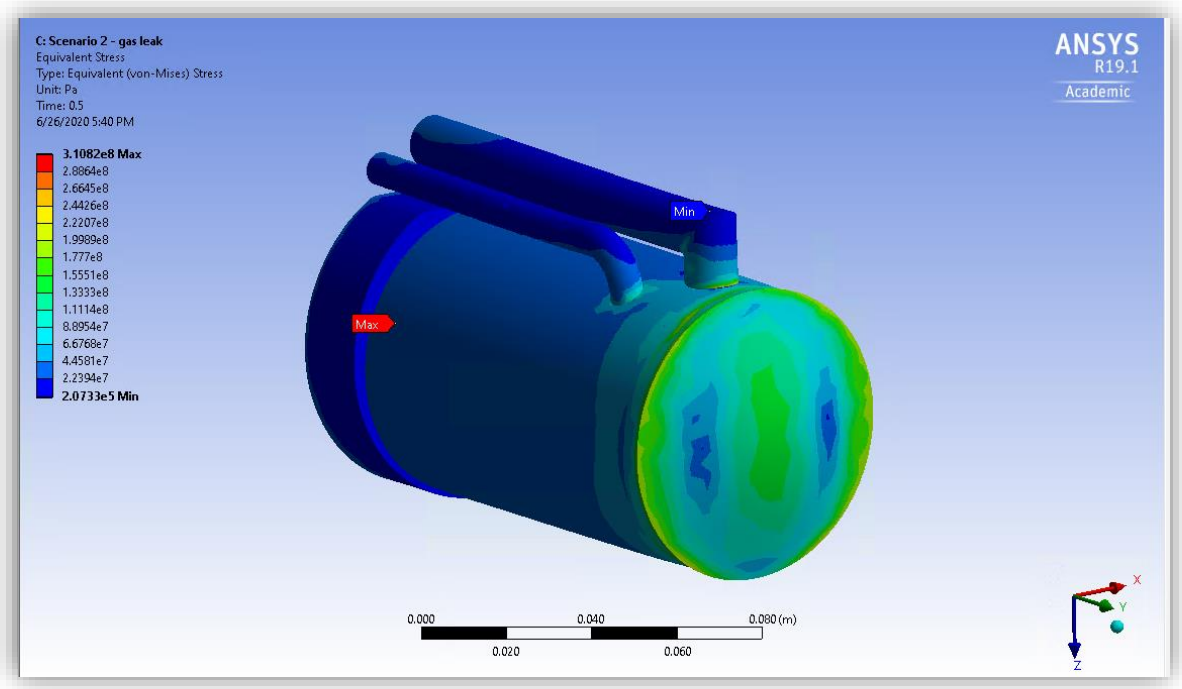

Figure 27. Equivalent Stress - Values over 2.15e8 are Fractures within SS304; the Larger Values (3e8) are within Copper Region

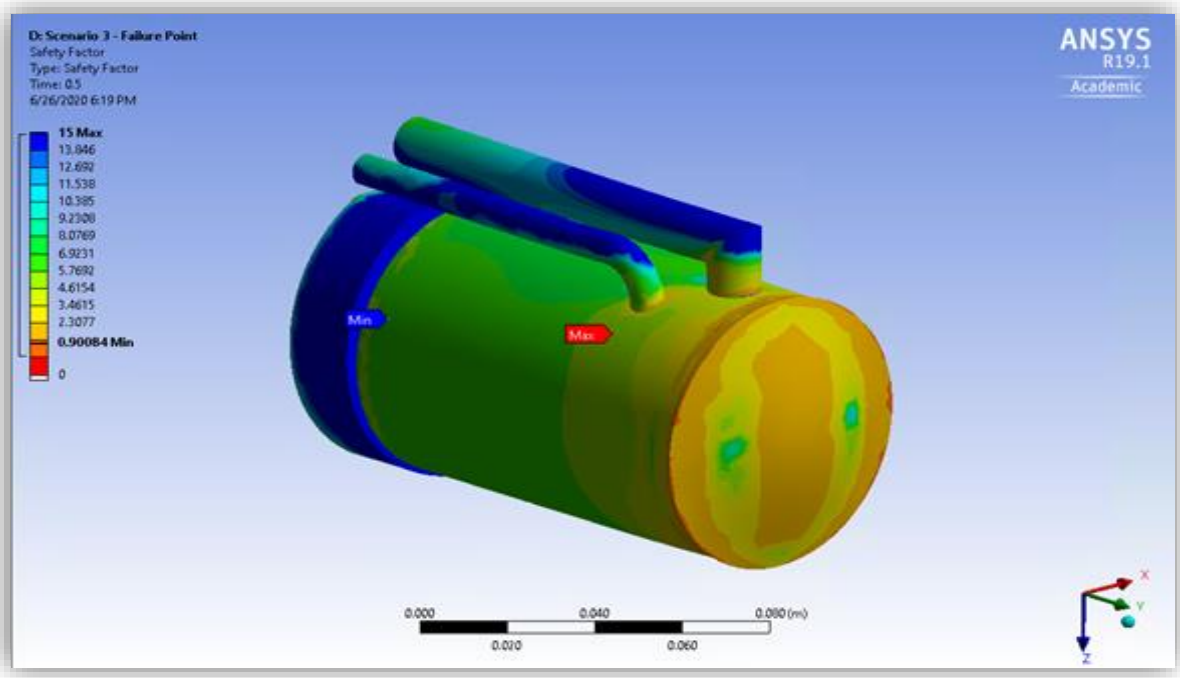

Figure 28. Safety Factor - Values Less than 1 Indicate Failure; Seen on End-Cap

In preparation of any safety failure resulting from a gas pressure burst, the irradiation canister will have two methods to fall back on. The first safeguard is the pressure release valves shown in Figure 28, previously denoted as the 5/16" Safety Tube, which would lead the gas down the line and into a larger safety expansion tank that is shielded outside of the reactor structure. Second, the canister has a naturally built in first line of defense—the vacuum which surrounds the canister that, in the event of a burst, will act as an immediate expansion tank for the gas.

One other matter that needs to be considered is the effluent concentrations at the closest receptor site to NETL. We assume that any release would be diluted into the 4,120 m^3 open

reactor bay volume. Additional dilution to the nearest receptor from NETL is on the order of 10^4 to 10^5 m^3 as calculated via CAP-88 which is nominally well within the DAC-to-effluent concentration ratio in 10 CFR 20 Appendix B. Nonetheless, maximum effluent concentrations should be evaluated for each operations request.

5.3 SCALE

For this portion of the modeling, SCALE 6.2 was implemented to solve for the activation and decay processes that would be happening during experimentation. Specifically, ORIGEN was used as a system for calculating the buildup, decay and processing of these radioactive materials. ORIGEN uses a matrix exponential method to solve a large system of first order differential equations with constant coefficients.

The goal of using this software was to understand what types of radioactive products would be created and how dangerous they could be. This would entail labeling radiation areas, release situations, and even activation of other materials based on the level of activity and the associated half-lives. The materials that were of highest concern were the large amount of copper present, as well as some smaller quantities of elements within the stainless steel such as manganese and chromium.

The following results are given for a 20-day cyclic irradiation in which the irradiation canister is subjected to 8-hour irradiations at 950 kW each day followed by a 16-hour decay period.

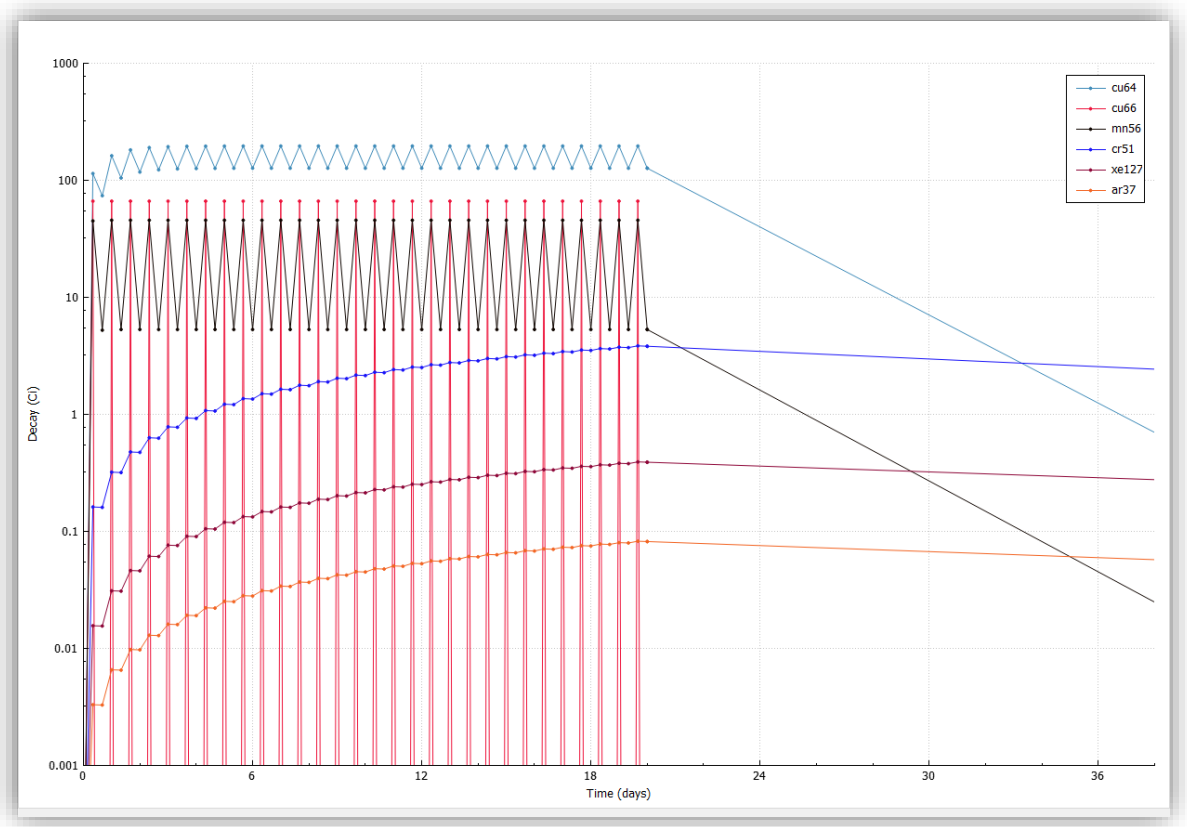

Figure 29: SCALE Irradiation Output – 20 Day cycle – 950 kW

Table 5 Activated Isotopes in Materials Used

	Days	cu64	cu66	mn56	cr51	ar37	xe127
Irradiation	20	126.80	3.80E-24	5.30	3.81	1.63	7.79
Activity (Ci)	40	2.24E-21	1.93E-29	2.25E-46	1.40	0.74	3.64

As can be seen from Table 5 above, the activity values for the structural materials are quite high but will slowly move to manageable levels after a few weeks of decay. The isotopes of greatest concern are Cu-64 and Mn-56, which have an activity level of 126.8 and 5.30 Ci, respectively, after the 20-day irradiation; just two weeks later, though, they are both less than 1 Ci. Given enough time to decay, the canister will be safe for removal without

concern for these isotopes being activated. The procedure for removal will include a review of the experiment to determine the activity level of these isotopes.

5.4 HOTSPOT

5.4.1 Theory

In the event of a radiological release from this experiment, a simulation, utilizing Hotspot software, was run to visualize the resultant dose and deposition contours for the local area surrounding NETL. These simulations were run for three different levels of activity based on realistic experiments that could result from use of the cryogenic irradiation facility.

Hotspot utilizes a variety of equations to govern how an isotope is released in various atmospheric dispersion models. Some of the main inputs are how an isotope is released, carried through the atmosphere, and later deposited; it will take into account environmental aspects such as wind speed and direction, as well as atmospheric stability factors. Prior to running a simulation, one must develop a series of inputs that best describe how an accident could occur and then how it would play out in a given environment.

5.4.2 Analysis

For an example scenario for a gas release in the reactor there would first need to be an isotope of interest and its assumed activity level. From this you would need to learn how

the facility deals with gas being released to the public and how its filtration system, or stack, is installed in the upper levels of the building. Taking that information, you can then tell the software from how high up the gas is released relative to the ground, its exit velocity, as well as the diameter of the stack. From there you input all the meteorological data as well as set multiple receptor locations to better track how the release affects the area at different intervals. Once those are all in place you can now begin to create various scenarios with these input parameters that alter the sample time, any sort of hold up in the atmosphere due to low wind speeds, and then create various levels of contours for dose and deposition to the surrounding area.

Given a previous understanding of how experiments of this nature had been run in the past it was easy to overlap those failure scenarios with this new system to create a series of potential cases that could result from a catastrophic failure from the cryogenic system. Given hotspots ability to create contoured plots that overlay google earth, it was only a matter of narrowing down a margin for maximum and minimum dose and deposition to the surrounding area. For this system we are going to be operating in various conditional settings from continuous runs, to time intervals over days and even weeks. So, taking that knowledge combined with previous calculations done in SCALE we were able to generate 3 failure scenarios to run in HOTSPOT.

5.4.3 Results

The following images were created after 3 scenarios.

Scenario 1

Scenario 1 represents a normal working volume at the end of an irradiation cycle producing 2 Ci.

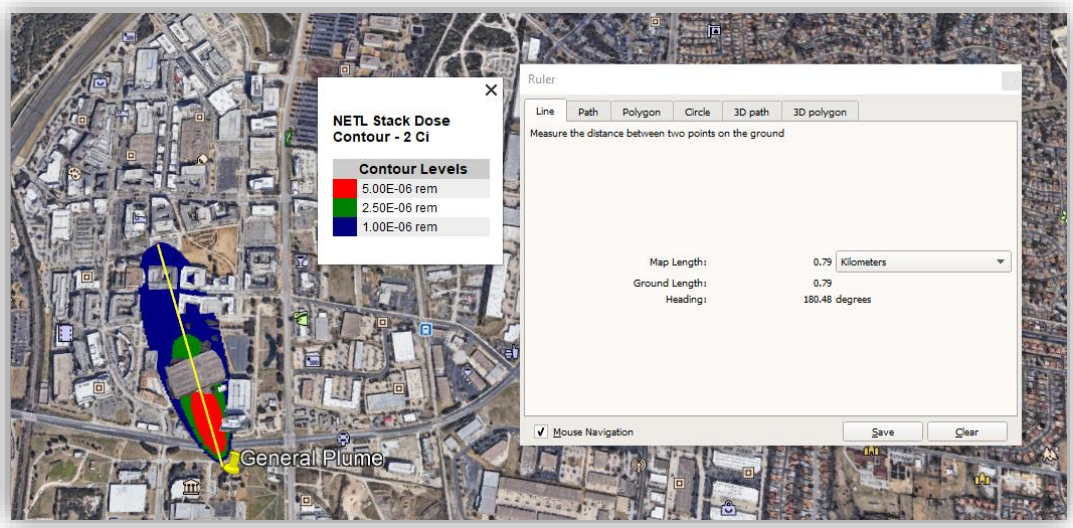

Figure 30. Scenario 1: 2 Ci – Dose Contour

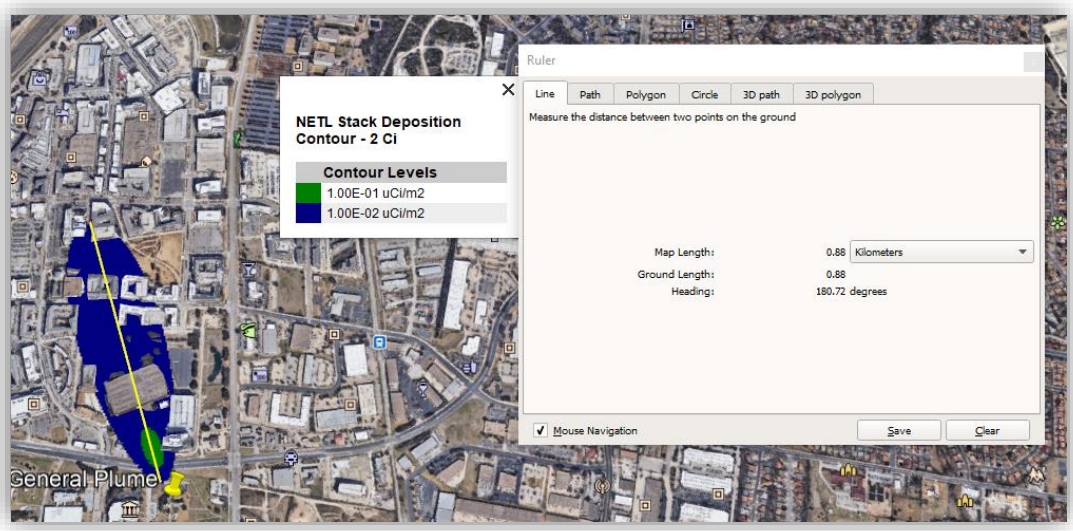

Figure 31. Scenario 1: 2 Ci – Deposition Contour

Scenario 2

Scenario 2 represents a 10 Ci activation cycle.

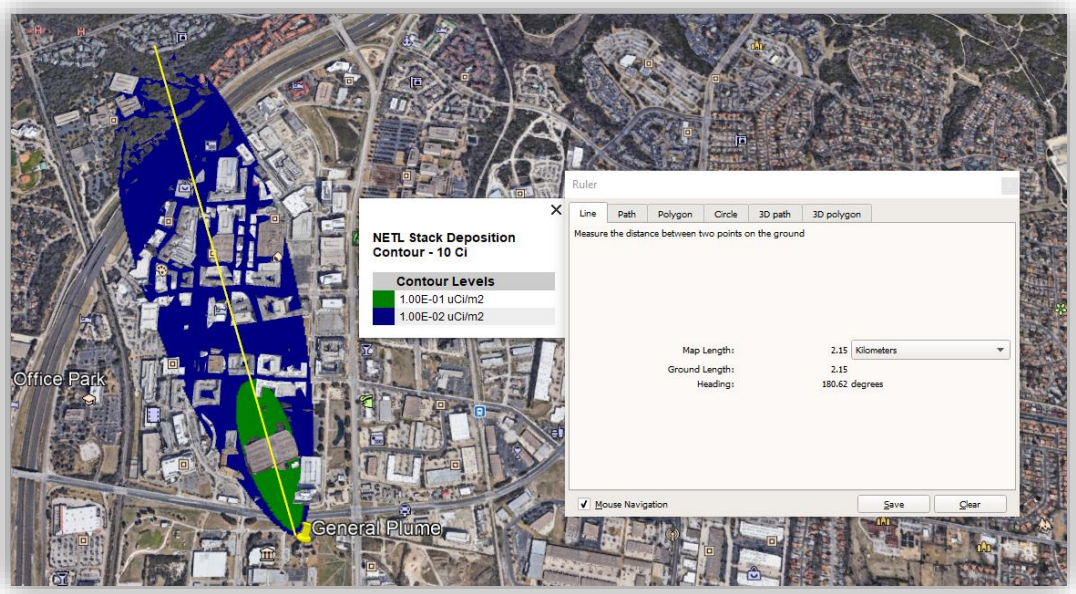

Figure 32. Scenario 2: 10 Ci – Dose Contour

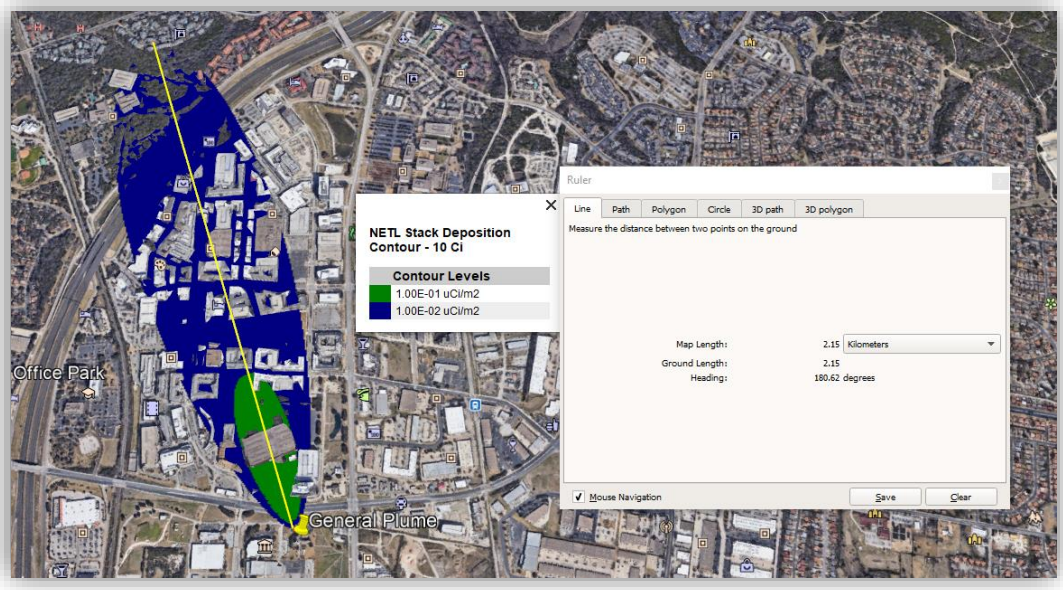

Figure 33. Scenario 2: 10 Ci – Deposition Contour

Scenario 3

Scenario 3 represents a 20 Ci production cycle with a worst-case scenario where the wind speed is low causing the cloud to hang longer in the air before dispersal, thus increasing dose to the local area.

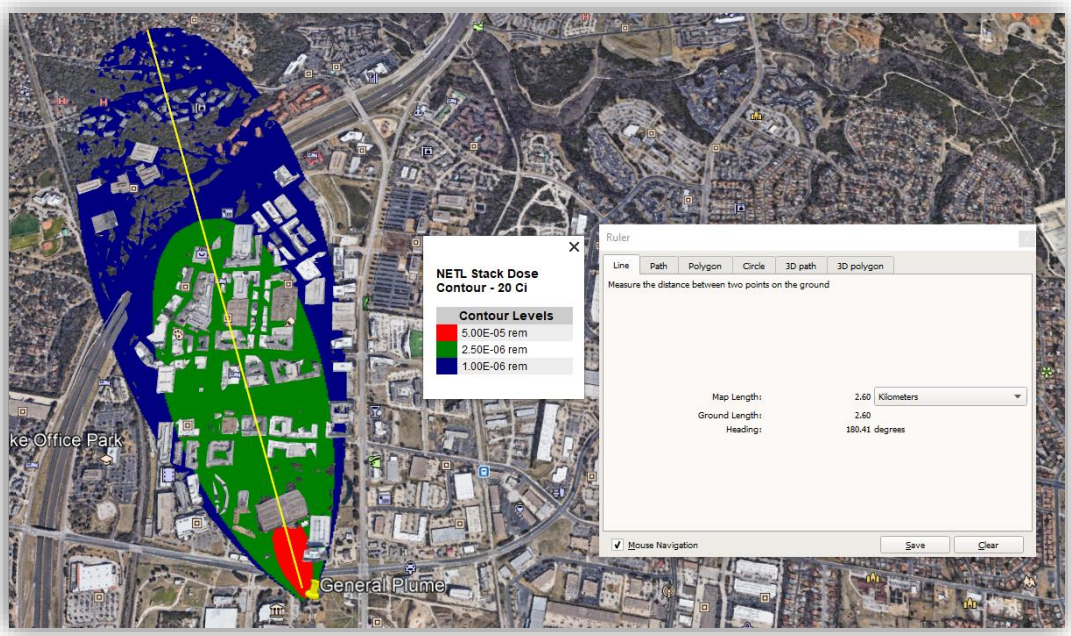

Figure 34. Scenario 3: 20 Ci – Dose Contour

Figure 35. Scenario 3: 20 Ci – Deposition Contour

In conclusion, under the assumption of a worst-case scenario in which all the gas during an experiment is put through the NETL Stack, the resultant dose and deposition of any of the prior gas release scenarios would not yield a dose to the public that would be large enough to surpass the minimum dose allowed to the public, which is 100 mrem per 10CRF20 regulations. The same goes for the resulting deposition contours plotted above.

5.5 SOLIDWORKS

5.5.1 Theory

SOLIDWORKS was used to create virtual 3D renderings of solid objects to aid in the design and construction of both the irradiation canister, gas manifold system, and reactor shielding during operations. Examples of these can be found in Figures 8 and 13 as well as the following depiction of the proposed shielding when the cryo system is fully installed into BP1.

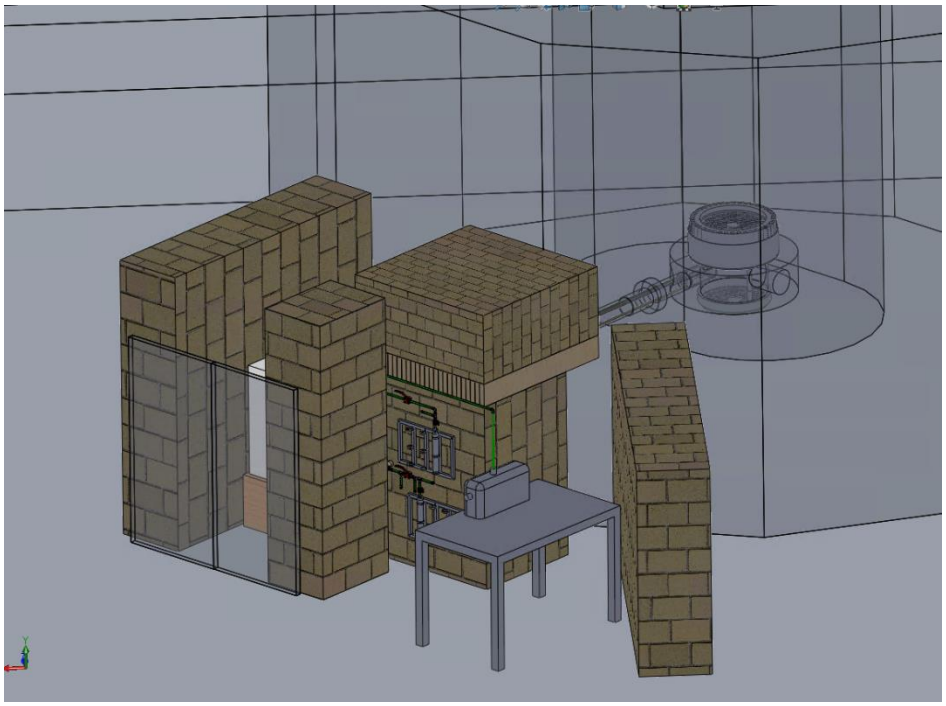

Figure 36. BP1 Reactor Shielding Isometric

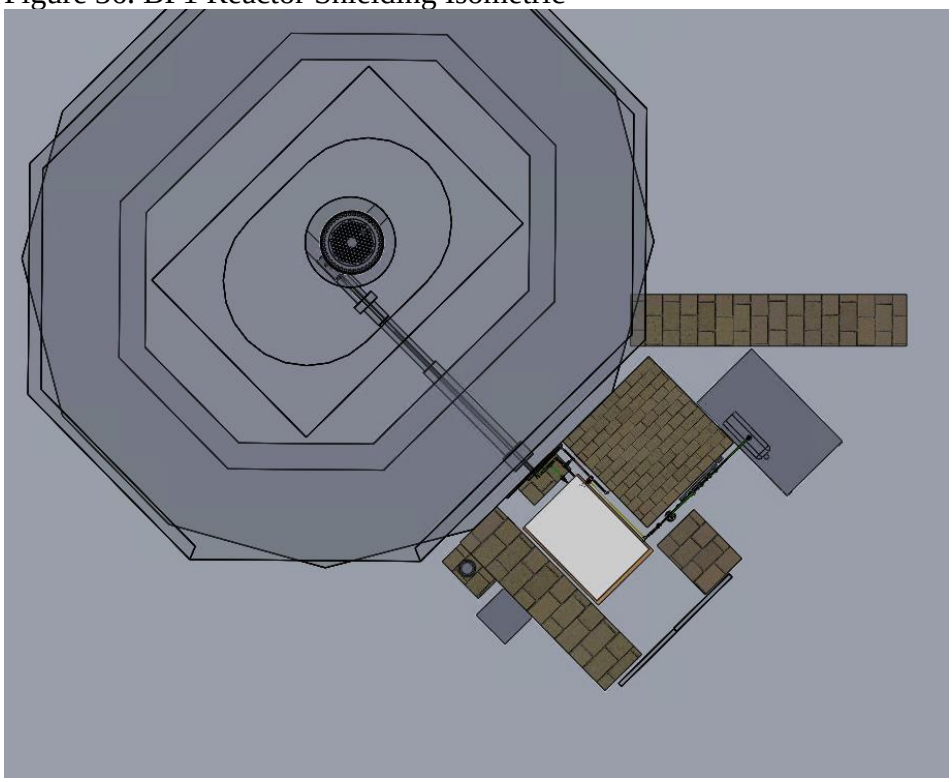

Figure 37. BP1 Reactor Shielding Top View

5.5.2 Analysis

After building a reactor containment structure, and reactor core scale model from the original engineering drawings we were able to come up with an accurate depiction of how the system would sit inside and out of the reactor. With this software we are able to then design safety measures, dimension piping, and present a to-scale model of how all of the components would fit together.

Chapter 6: Experimental Trials

Before any real testing begins in which a gas is loaded into the system in the reactor, there must be a set of preliminary results and understanding of how the system will behave so that it can be monitored for any unusual activity. These tests include cryo-head temperature stabilization and equilibrium, system power draw, and chilled water input equilibrium.

The most important goal of these tests is to create a reliable rate of change curve for how fast temperature can change with an empty canister as well as how much the temperature fluctuates at a given point. This will originally be measured by creating a minimum, maximum, and average temperature plot that will ultimately be filled in as more and more test are done at varying points. The goal will be to establish a frame of reference for when gas is loaded to see what the difference is between two things; the time it takes to achieve that temperature, and the stability at which the system can maintain at that given temperature. Once this is established a metric of "power draw" can be created to help in maintaining a safe work environment and monitor for leak deviations. One of the tools aiding in this goal is the CTC100 Temperature monitor that is equipped with a K-type thermocouple hooked up to the cryo cold-head that will provide a continuous reading of the temperature of the liquid helium as it is pumped to the cold-finger while the system is operational.

All while this is going on the helium compressor sits outside the reactor confinement structure and will have chilled water being circulated through it to aid in cooling the oil in the system necessary to pump liquid helium down to the irradiation canister. This water running through the helium compressor must remain within the given range shown in

Figure 10. With the system designed beforehand to account for heating form the oil inside as well as other outside factors, it will need to remain in this operational range for the duration of the experiment. That being said, it must also have a set of test points created for it to account for any deviation from the norm when undergoing the gas loading tests.

The start of these tests comprised of simply testing the system for pressurization and then how well it holds low vacuum. Once it was established that the lines to irradiation canister did not leak the testing could begin where the system was turned on and allowed to run for several hours while we collected various data points regarding the temperature and pressure of the system. During these tests vacuum was continuously pulled on the gas inlet line to simulate a “no-gas” situation. Because of the placement of the pressure gauge the cryo-system and the vacuum pump were allowed to work synonymously to simulate a perfect gas free environment while still reading the correct pressure output of the system.

Figure 38: Non-Gas Loading Experimental Set-Up

The value of these tests was two-fold, one being a monitoring of the system as it cooled down, and then another being how the system reacted to being heated up, which allowed for the gathering of significant factors that would later be implemented in the gas-loading trials. To successfully heat up the system and or control the temperature of the system it was found that it first needed to achieve its lowest temperature before any heating element was applied. This heating element came in the form of a singular 100-Watt resistive heater located on the back of the CTC 100 and that was connected to a thermocouple on the Cold-Head located outside of the reactor structure.

Figure 39: CTC 100 Temperature Controller

Figure 40: Cold-Head Helium Cooler

Once the system has arrived at its lowest temperature the heater can then be turned on and dialed to a “Set-Point” temperature that system will slowly react to. The heater is then controlled by three different algorithms known as the proportional, integral, and derivative feedback controllers that can be manually set to specific values to best fit the needs of the system. In this case, we wanted the temperature to slowly creep up to the set-point temperature with minimal oscillations and took this into account when configuring these algorithms. From here the system was allowed to heat up in a stepwise fashion to allow for a temperature to be reached, equilibrium to occur, and then a new set-point would be input to the controller.

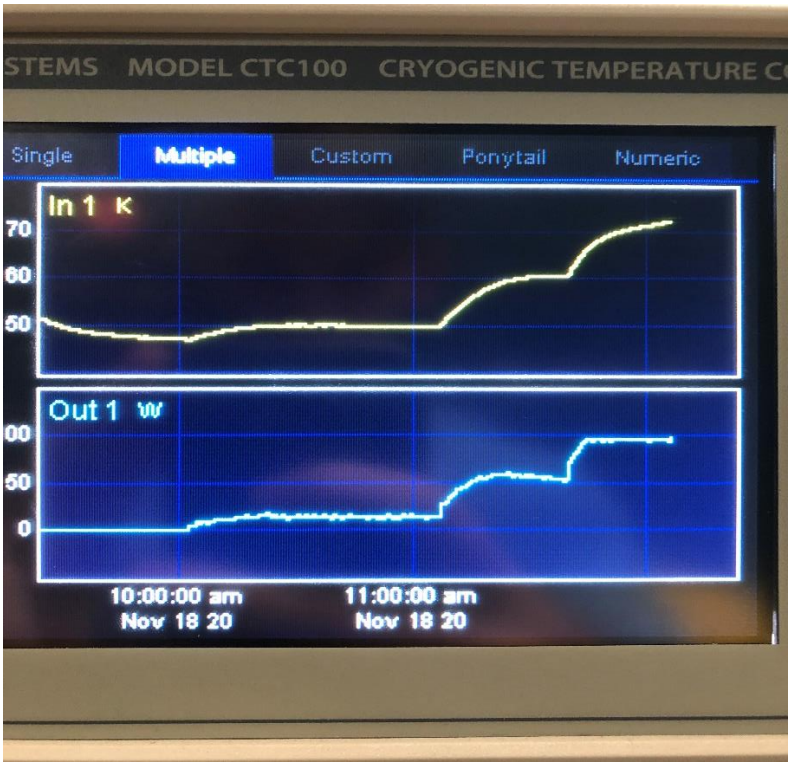

Figure 41: CTC Stepwise Heat Control

One of the most helpful things about this non-gas loading experiment is that we have the ability to run loss-of-coolant tests without fear of flashing gas in the system since there is no gas present during the run. From this test a regression line can be created to show how rapidly the system will heat up through various gas flash points that will indicate to us where potentially dangerous scenarios could occur and allow us to put in place the correct safety precautions to prevent those from happening.

With the Non-Gas-loading trials finished and the set points for these experiments created the experiment can proceed with the gas-loading trials. These trials will be comprised of both a nitrogen freeze test a well as, temperature set point and fluctuation monitoring.

The Gas-loading trials began by installing a 1/8” tube from the nitrogen cylinder directly into irradiation canister to simulate the length of line that would be installed into the reactor beam port of 133”. The 1/8” tubing was used here to limit the amount of volume in the gas line itself so that cryo-trapping the gas or pulling vacuum on the line would be more efficient. Once this was complete, we utilized the same pump and flush method until we were confident in the line being purged of any other significant quantity of gas. We then began loading nitrogen into the gas line and condenser to take the system up to atmospheric pressure, then the system would be turned on and temperature and pressure would start to drop. The vacuum chamber was open to the vacuum pump the entire time, but the rest of the gas lines were isolated so that only the helium compressor was working on the system. The goal of this experiment was to check the ability of the system to freeze off nitrogen at low pressures, an ancillary goal was to have the system cool down from a specific pressure and then heat back up to the same pressure to show that the system did not leak during the experiment.

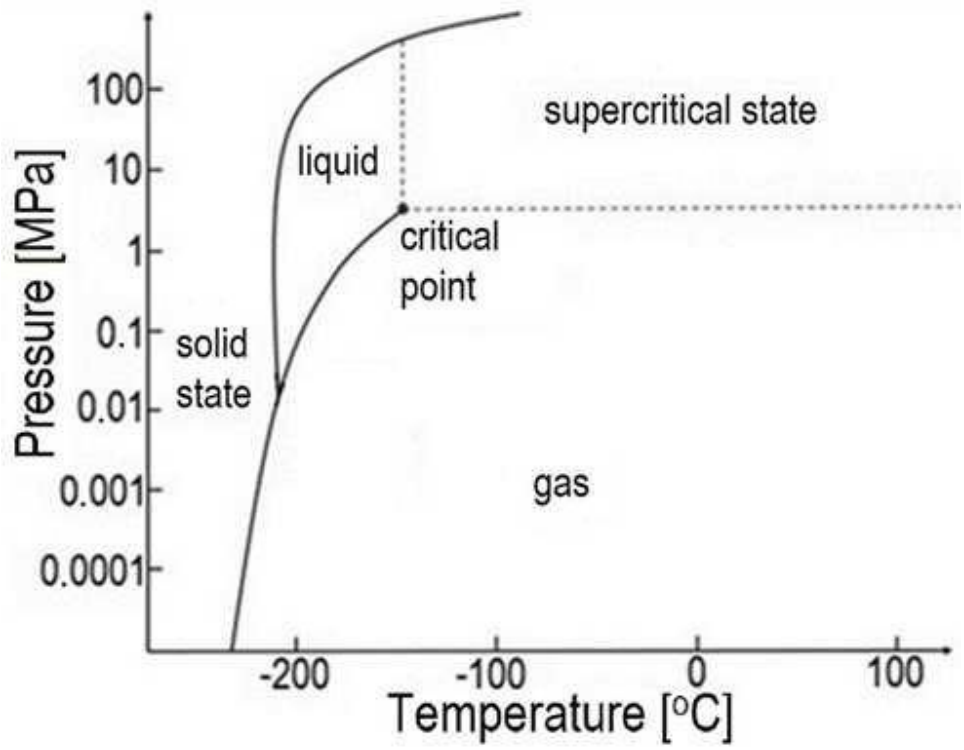

Figure 42: Nitrogen Phase Diagram (Frącz, 2017)

As the system cools down, we will be monitoring for any significant pressure drops that would indicate a freeze-off of the gas. The idea here is that if we do not have any freezing of the gas that we won't have to worry about creating ice balls from pin hole air leaks during a longer run. Another goal here is to establish the control of the system in terms of how rapid the frozen gas would return to a gaseous state during scenarios of controlled heating or straight loss of coolant to the system.

Chapter 7: Results

The goal for this system is to have the ability to load, freeze, controllably heat up, and unload pre-selected gases in a safe and time efficient manner. These tests included the pressurization, vacuum, and leak testing needed beforehand to verify there would be no issues with the experiments and to create a baseline of tests off of which future experimental results could be compared to track differences. Those objectives were tested in the following experiments.

7.1 Non-Gas Loading Results

This experiment was run first for safety reasons. Once the gas and vacuum lines had been tested and leak proofed, we wanted to start with the testing that would have the smallest safety risk involved. The main safety risk involved in cryo-system in general is having a leak in which outside air would be able to come in and freeze down inside the condenser at a rate almost undetectable either preventing the expensive target gases from being trapped in an area of highest flux, therefore decreasing activation levels, or in a worst case scenario, with enough air having frozen down, potentially flash back to gaseous form from a solid state that would induce a pressure wave large enough to fracture the canister.

With that in mind this experiment was run in a very procedurally oriented manner especially given this would only be the first time the system had ever been fully tested. This trial was run three different times each time slightly different from the previous based on new things learned. The following graphs depict the cooldown and heat up times, temperatures and pressures from Non-Gas Loading Test 1.

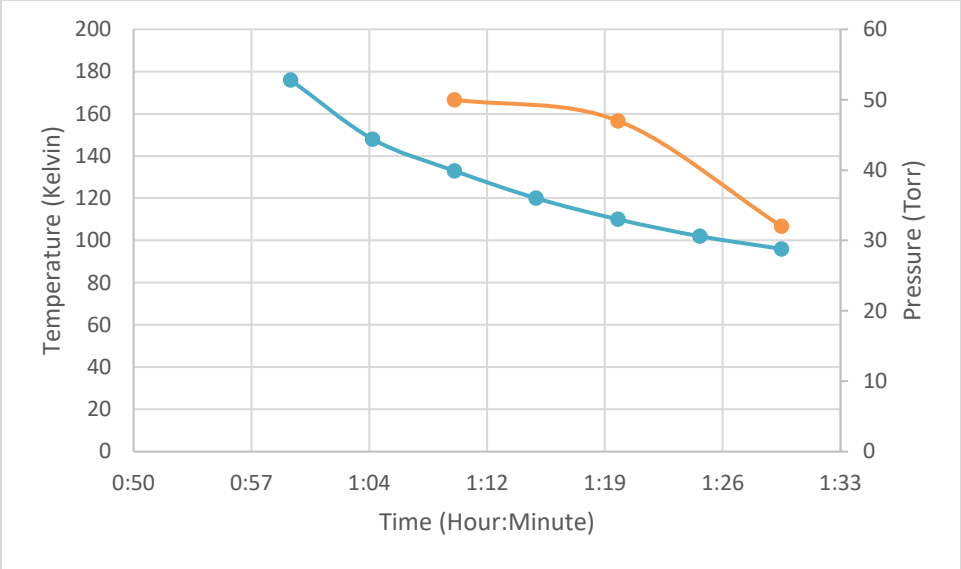

Figure 43. Test 1 Temperature vs Pressure

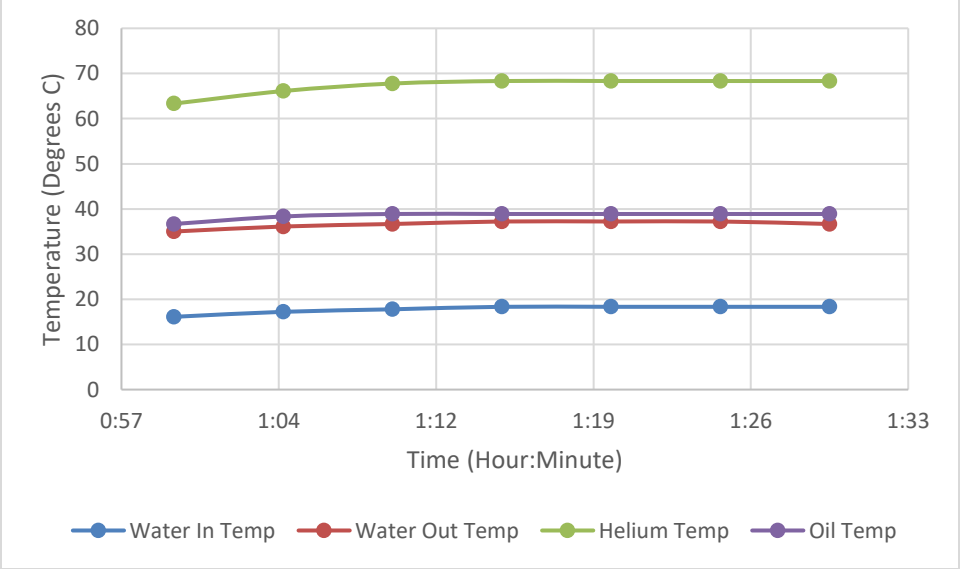

Figure 44. Test 1 Helium Compressor Temperature Statistics

During this experimental set up, we pumped vacuum on the gas line down to 50 Torr closed that valved and then opened the valve to the vacuum canister surrounding the condenser and had the vacuum pump the entire time. We were also attempting to watch and record

each section so there were less data points in this experiment that would be corrected for in future work. The system shows that it rapidly starts to drop temp and then after 120 K mark, we begin to see the pressure become affected as it also starts to drop as is expected. As this was happening, we were also monitoring the compressor values to verify that it was operating within its bounds in terms of flow rate and temperature of the chilled water, as well as the helium and oil temperatures. From this experiment we wanted to see these values remain steady and reach an equilibrium point which they seem to quickly approach from Figure 44 above.

From Test 1 we were able to learn that the heat exchanger and helium compressor operated together exactly as expected and so we turned our attention to the cold finger temperatures and pressures for Test 2. We additionally begin to track the pressure differential and current output of the helium compressor to look for changes in how hard the system is working to cool down. This could potentially help indicate if there is a leak in future experiments by showing the system working harder of if a loss of pressure occurs in one of the lines and the helium is not getting to the cold finger.

The results of Test 2 are listed in the following figures:

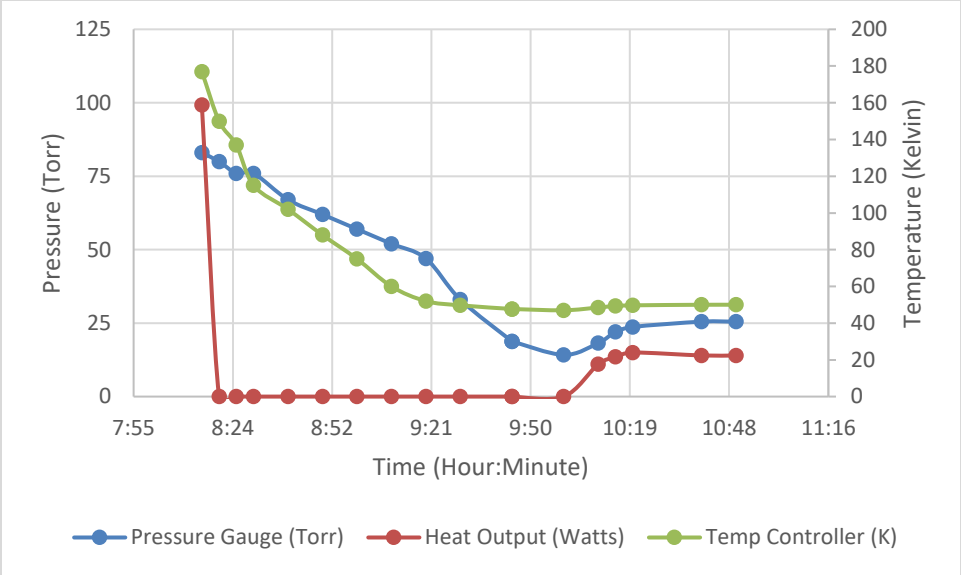

Figure 45. Test 2 Temperature, Pressure and Power Consumption

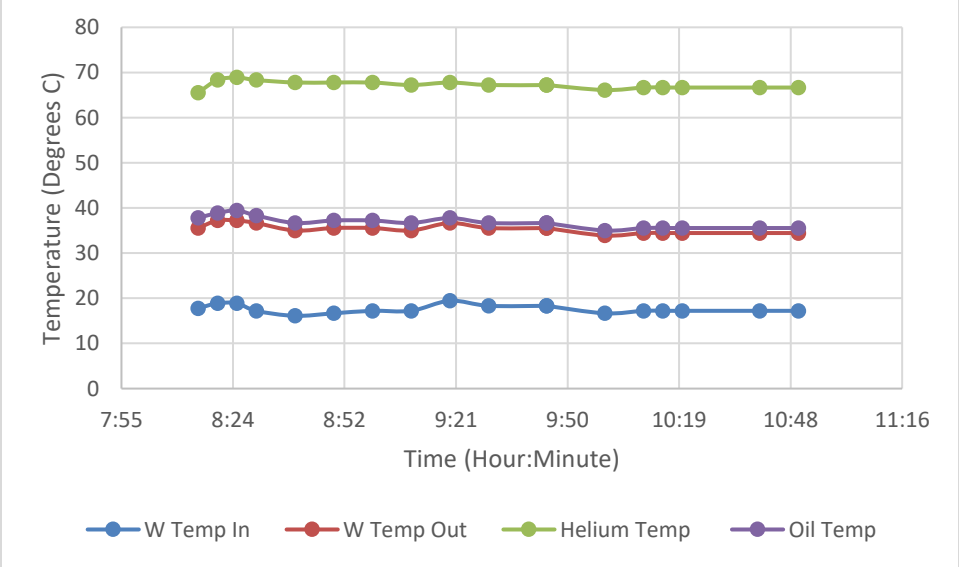

Figure 46. Test 2 Compressor Temperatures

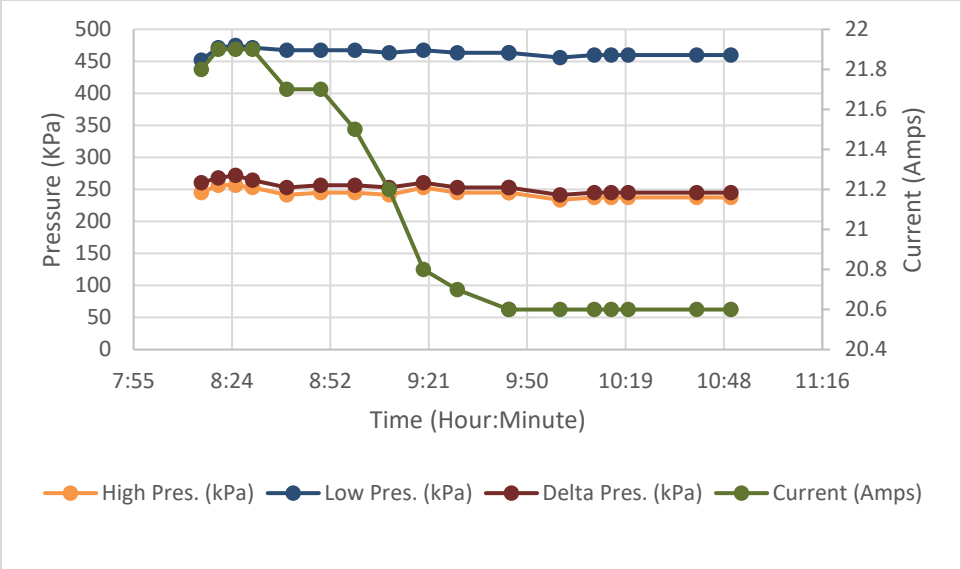

Figure 47. Test 2 Compressor Pressures

After all the things learned in Test 1, we wanted to begin Test 2 with testing out the CTC 100 temperature controller by setting the PID feedback controller to 250 K. However, it was quickly realized that this system was just too powerful to control at that temperature and after it blew by that mark, it was quickly turned off as can be seen at the 8:24 mark in Figure 45 when the temperature starts to decrease with a steeper slope due to the heater going from working at max capacity of 99 Watts to 0 watts. From that point on, Test 2 became a test of how low of a temperature the system can achieve and how does that reflect in the pressures of the gas line as well as the helium compressor temperature and pressure statistics.

From this test, we learned that the bottom out temperature for the system is around 47 K, and we also noted a trend for the pressure in the gas line that mirrors this drop as well as stabilizes when the system reaches its lowest temp, in this case, that pressure being 14 Torr.

From here the PID was turned back on and set to 50 K which was achieved 20 minutes after it was turned on and the system was then able to hold that temperature within a very low error.

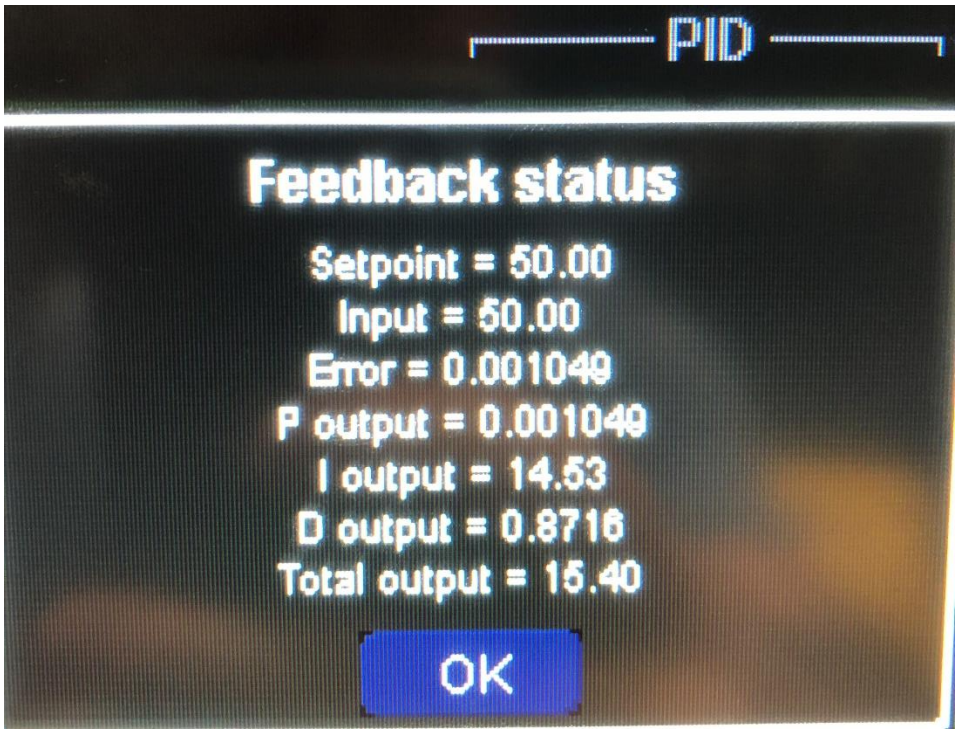

Figure 48. PID Feedback Controller Error at 50 K

Once this set point had stabilized, we then set the controller to 60 K, let that stabilize, and then move to 75 K to see if we could start to see any larger pressure changes.

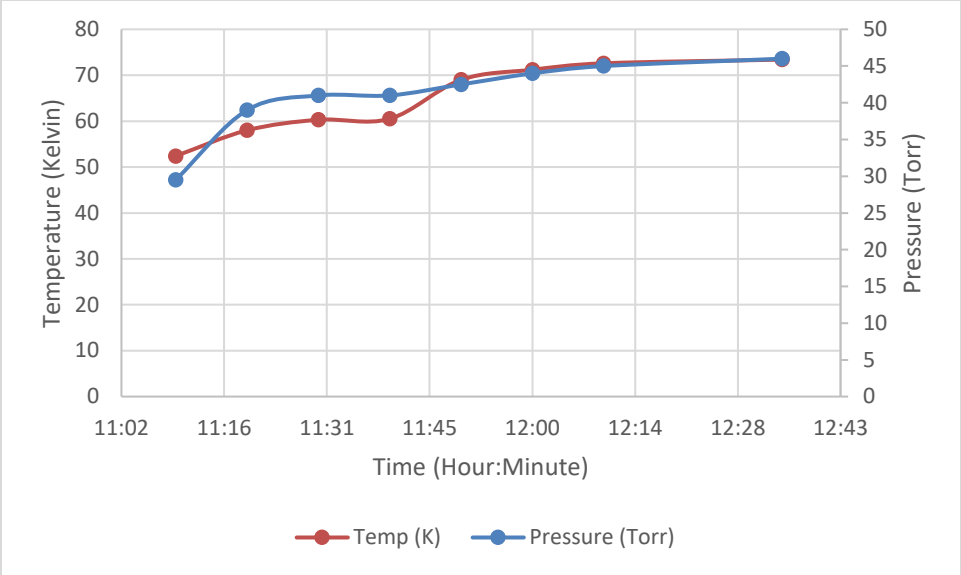

Figure 49. Test 2 Heat Up to Check for Large Pressure Changes

However, once the temperature reached around 73 K it became apparent that the heating element on the temperature controller system was maxed out therefore losing any further capacity to control the system past this point. It was also noted that no large pressure changes were occurring which would indicate that there had not been any significant air leak into the system and no flashing was occurring. After surmising this Test 2 to be a success, and there were not any air leaks into the system, we added one last phase to the test as seen below in Figure 50.

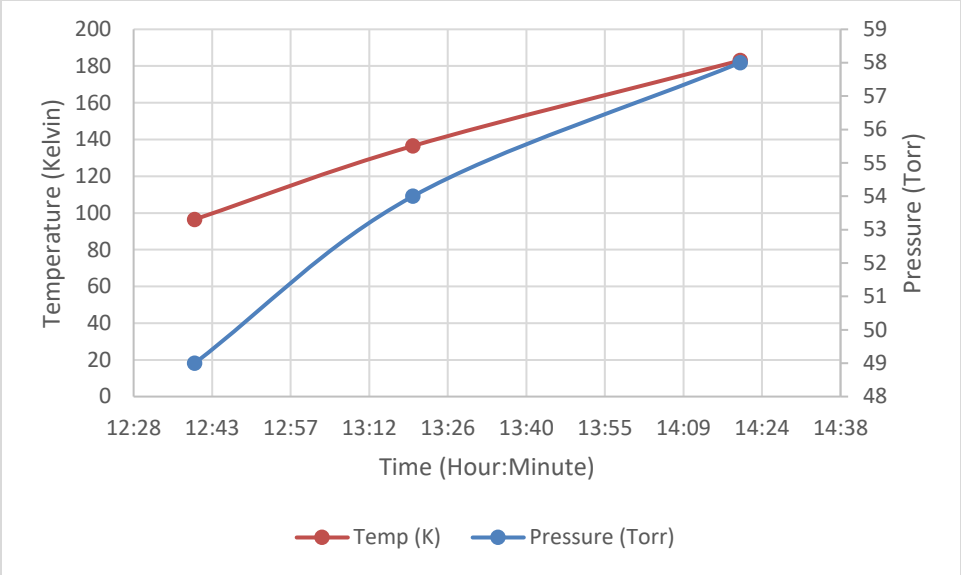

Figure 50. Test 2 Loss-of-Coolant

This was the last major question in the non-gas loading trials to answer, and since we were in a safe environment and it had been proven that there were no leaks, no gas flashes could occur. With this complete. we shut off the system and began to track the changes in temperature and pressure over the remaining time. It was found that the temperature, coming from a previously cryo-state environment and only being controllably warmed up to 74 K would only heat up at ~.45 K per minute given a complete loss of coolant from the helium compressor, and that the pressure as well dropped extremely slow. This was great news for the project, and it meant that in any failure scenario with equipment, with no heat input, we would never be in immediate danger of flashing the contents of the irradiation chamber. This situation will change when it is in the presence of the reactor due to the heat coming from nuclear interactions, but this was a great starting point that would allow me to do more loss of coolant testing with gas as long as the system was outside the reactor.

Of the many things learned in Test 2, it was also brought to our attention that there was no real idea of the range of control we had over the cold finger and thus it was decided that we needed to create a regression line from previously provided calibration data for the system so that we could track the actual temperature the cold finger was at while the temperature of the cold head was monitored simultaneously.

Table. 6 Temperature Correlation for Cold-head and Cold-finger (*Cryogenic Refrigerator Instillation and Operation Manual)*

Cold-Head Temp (K)	Cold-Finger Temp (K)	Input heat (Watts)
42.5	55.9	0
54.9	80	42.5

From this data set provided a regression line was created for each of these situations so that we could then predict the temperature change based off that relationship.

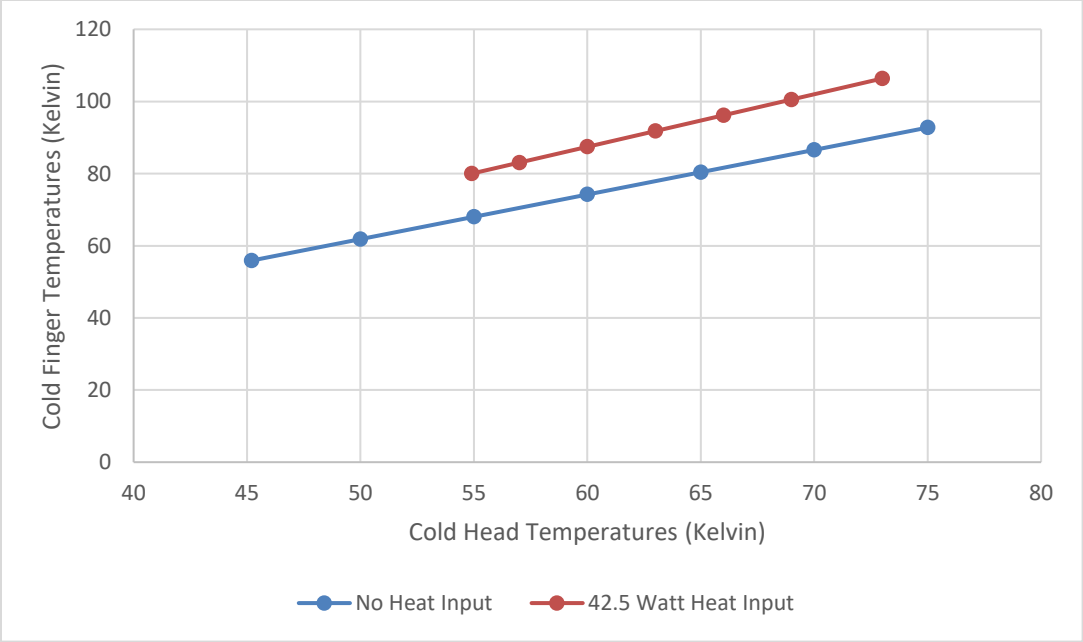

Figure 51. Temperature Regression Calculated from Cryomech Data

The data represented above in Table 6 come from 4 data points provided by Cryomech. Two of the data points being a temperature reading at the cold head and the cold finger without heat input, and the other two with a heat input of 42.5 watts, representing heat input from the reactor. Because of the small number of data points, we wanted to go ahead and re-create this test ourselves with and without gas to verify the data and check for any discrepancies. The results representing heat up of the cold-head with and without gas loaded into the canister are shown in Figures 52 and 53.

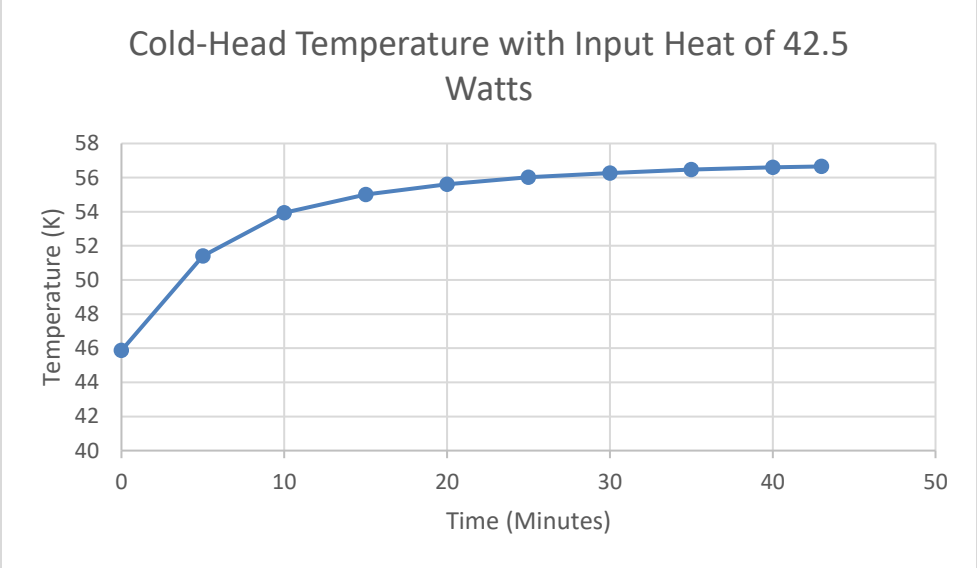

Figure 52. Cold-Head Temperature Response Test No Gas Loaded

From this test we can see the temperature level off at 56 K which is slightly above the temperature listed from the initial testing done by Cryomech. There is no real way to verify the temperature at the cold-finger follows the provided temperature correlation, but we can create testing environments to explore the differences between a gas-loaded and non-gas loaded system.

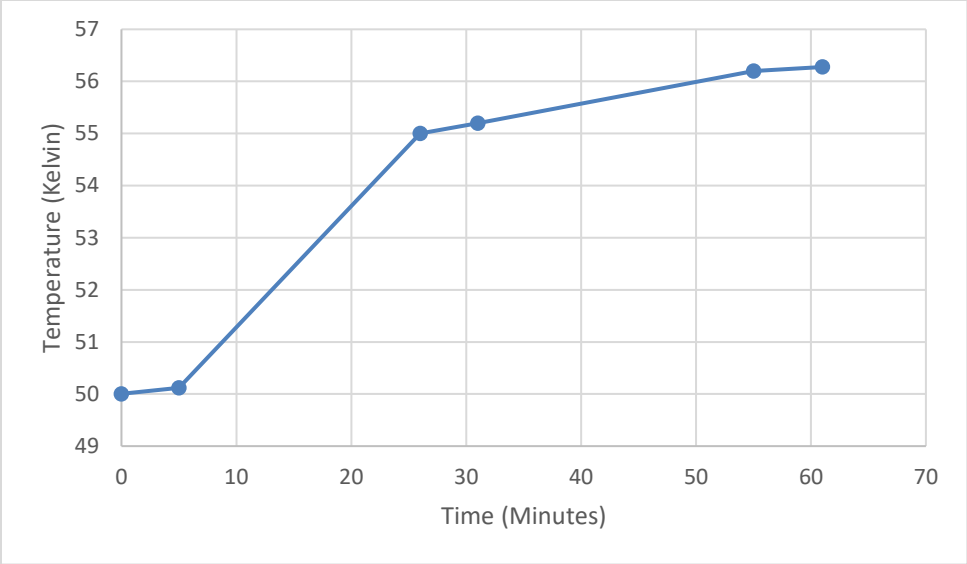

Figure 53. Cold-Head Temperature Response Test with Xenon

Figure 53 had Xenon loaded into the system and was heated at regular intervals of temperature correlating to 50 and 55 K and then the controller was set to equilibrate at 42.5 watts. From these two figures we can see that the system behaves very similar whether gas is present or not and arrives at similar temp of 56.2 K when introduced to 42.5 watts of input heat.

This result of both tests equilibrating at the same temperature was the goal of the test in that any discrepancy between the values with or without gas loaded into the system would have created another factor of how the temperature changes when heat is applied. Because we know they behave the same we are now only relying on the temperature testing done by Cryomech is correct.

With Test 2 being very successful and having verified the temperature correlations, a final test could be undertaken to gather a large amount of data points while operating the system from cool down through heat up. This will act as a standard for the future comparison with the Gas loading trials to see if there are different loads on the system in terms of time it takes to cool down as well as pressure differences.

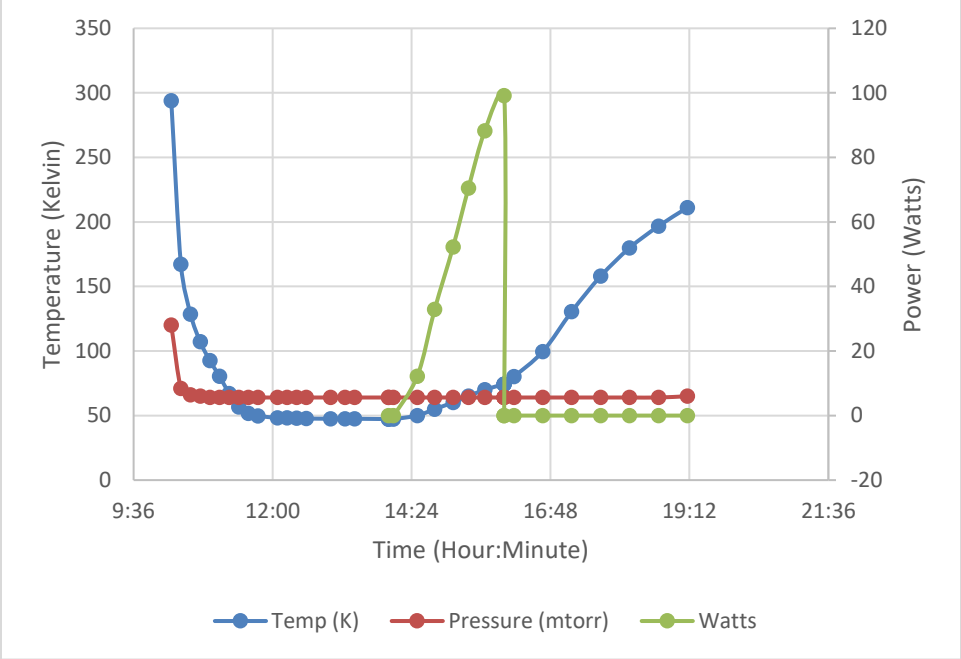

Figure 54. Test 3 Temperature, Pressure, and Power Draw

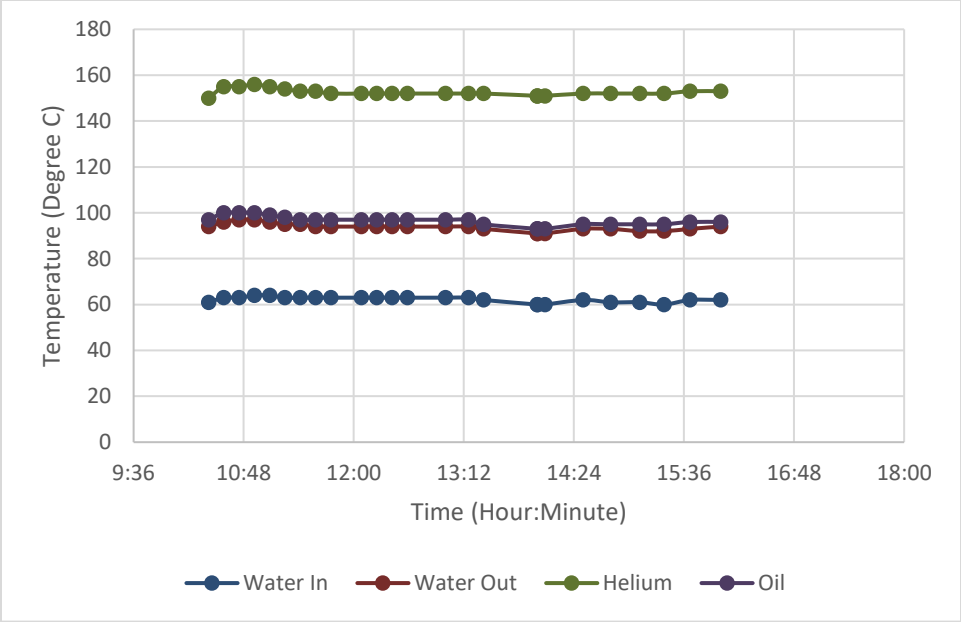

Figure 55. Test 3 Compressor Temperatures

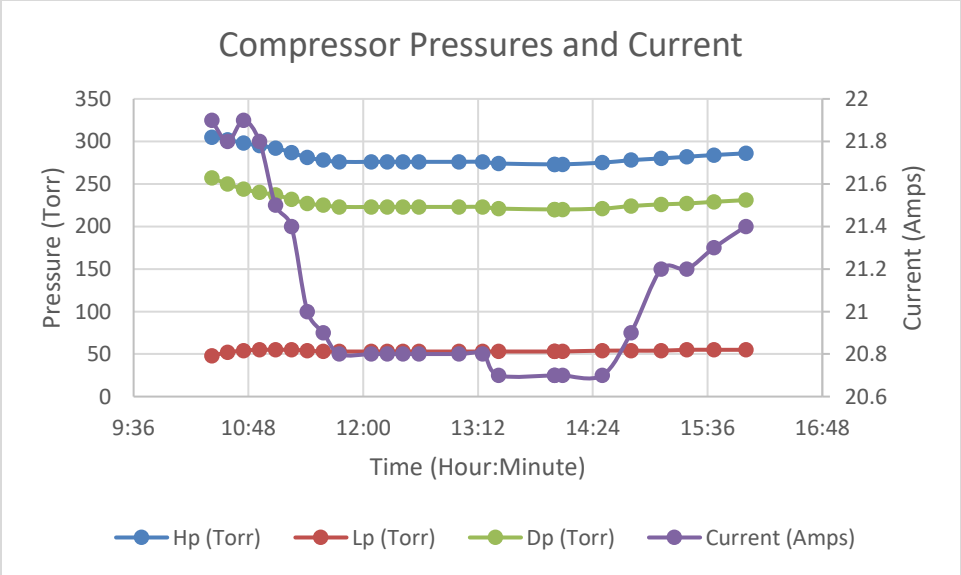

Figure 56. Test 3 Compressor Pressures and Current

For this last test we deemed it made the most sense to pull vacuum on the gas line and canister at the same time to simulate a "gas free environment" for the duration of the

experiment. This would ultimately bring us to the lowest temperature the system was able of achieving as well as continuously reassuring there was no gas leaking into the system. We would then be able to clearly track temperature over time as well as the pressures of the compressor and wattage input into the CTC 100. This test now provides us with a set of standards to compare to when we start the Gas loading experiments, this will allow for conclusions to be drawn based on changes in pressure, temperature, time to achieve temperature, and power draw.

7.2 Gas-Loading Results

The following results come from two Nitrogen Freeze test and one Xenon Freeze Test. During these experiments the ultimate goal was to, after pulling vacuum, load the condenser with the chosen gas to atmosphere pressure, cool the system down, slowly warm it up as down in the NGL testing, and then draw similarities and differences between the two. Goals that were made accomplished during these tests include check to see if the pressure of the loaded system returned to the same value after letting it heat up over the course of 12 hours, as well as check to see if freezing does occur for a specific gas at low pressures and to note the associated pressure drop.

During the first test we watched as the cold head temperature approached the 63 K mark that would signal, we were reaching the freezing point of nitrogen of 77 K at the cold finger. The following graphs show how the temperature is behaving almost identically to the NGL testing as if the system is strong enough it doesn't notice it is filled with gas, however as we approach the freezing temperature, we notice a significant pressure drop in a matter of 30 minutes as we drop from 420 Torr to 43 Torr signaling that we are in fact freezing off the nitrogen in the condenser.

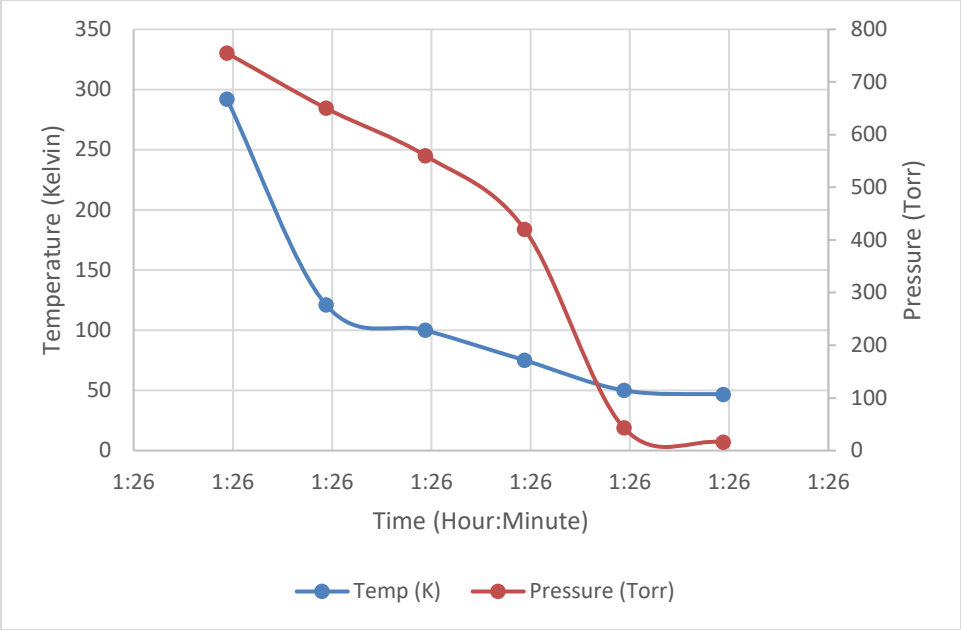

Figure 57. Nitrogen Freeze Test 1 Temperature and Pressure

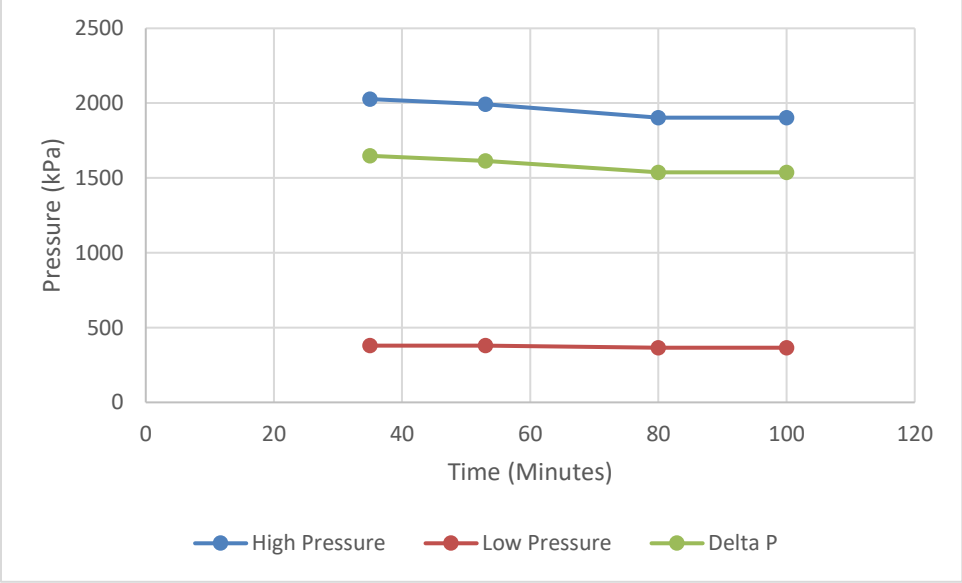

Figure 58. Nitrogen Freeze Test 1 Compressor Pressures

During this test, we also briefly noted the helium compressor's statistics to watch and see if the volume of gas would make a difference in how hard the system had to work to cool

that mass down. From the figure above it shows that is not the case as the numbers report identical to that of the NGL testing. After the system was allowed to reach its "bottom out" temperature of ~ 46 K we began to slowly heat it up with the resistive heater built into the CTC 100 and watched for any differences between the rates in the NGL testing phase.

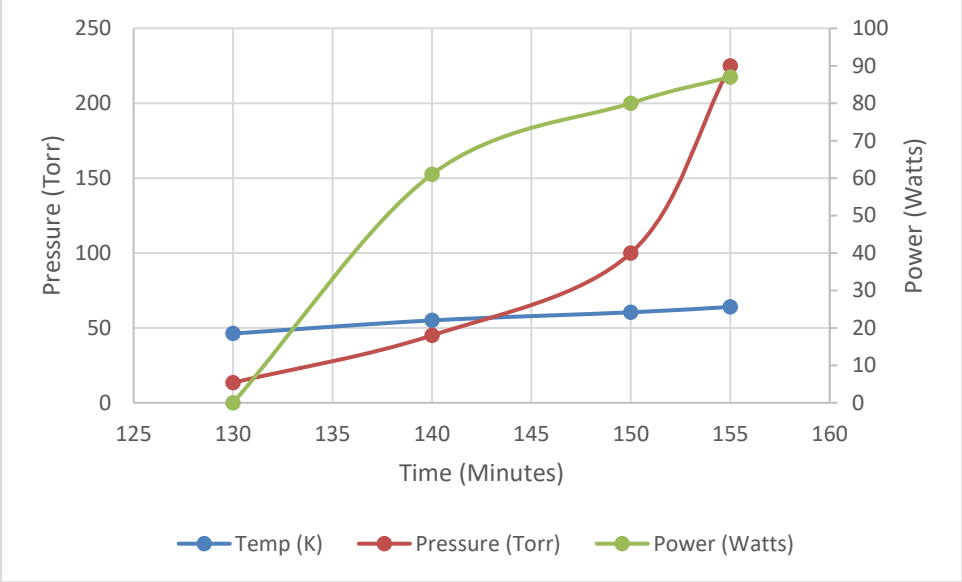

Figure 59. Nitrogen Freeze Test 1 Canister Heat-Up

After watching a pressure spike similar to the drop seen during the "cool-down" phase of the experiment we turned the system off and let it attempt to return to its original start points.

In the morning when returning to the lab, after letting the system heat up naturally, the temperature controller and pressure gauge read out 293k and 755 Torr exactly the same values as the start of the test indicating there were no leaks in the system and concluding in a successful test.

Nitrogen Freeze Test 2 has the same effect that the NGL test 2 had in that it improved on all of the Test 1 data taking and focused in on areas where potential discrepancies could form such as the pressure drops and heat up phases of the experiment. More time and data points were taken for these metrics as shown in the following graphs.

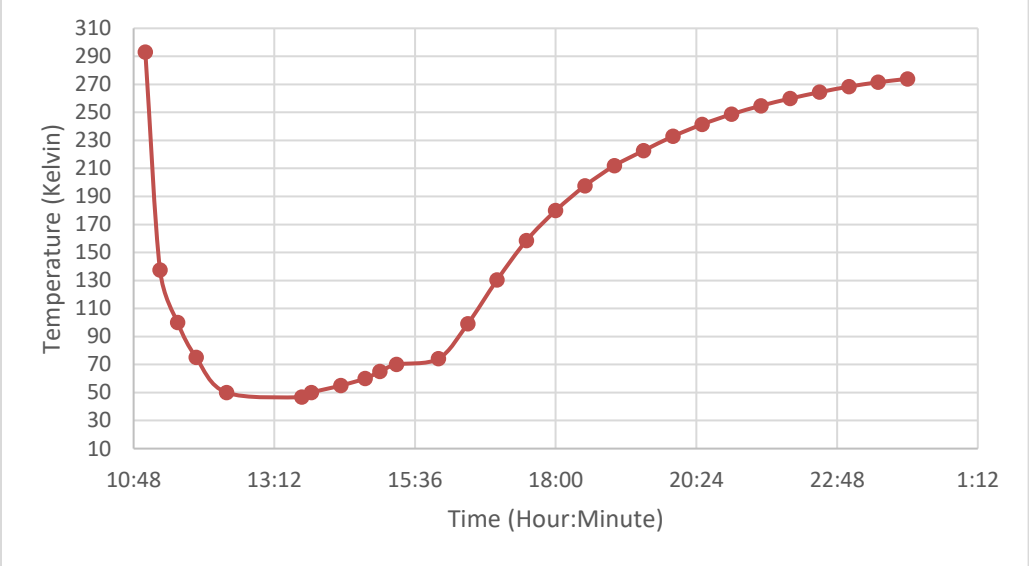

Figure 60. Nitrogen Freeze Test 2 Temperature

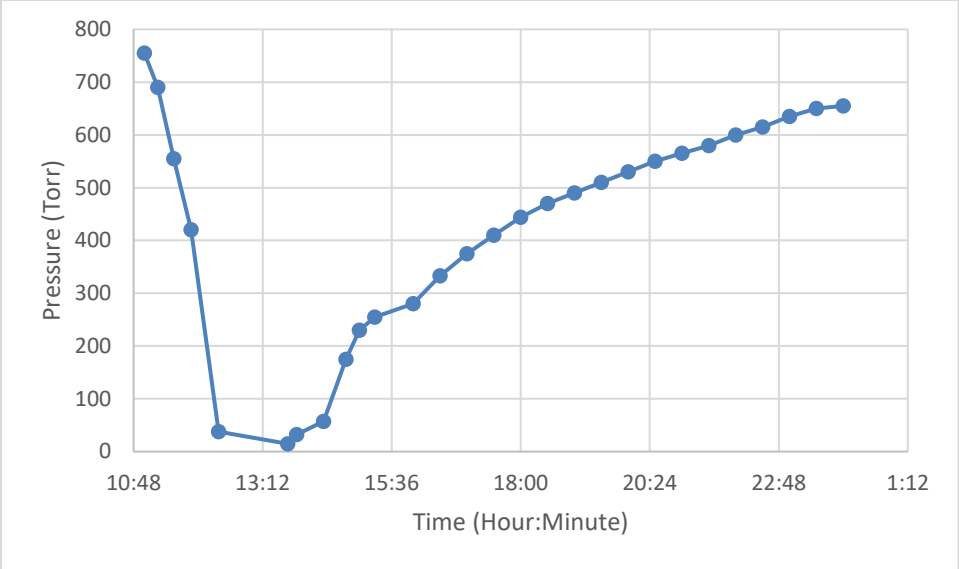

Figure 61. Nitrogen Freeze Test 2 Gas Line Pressure

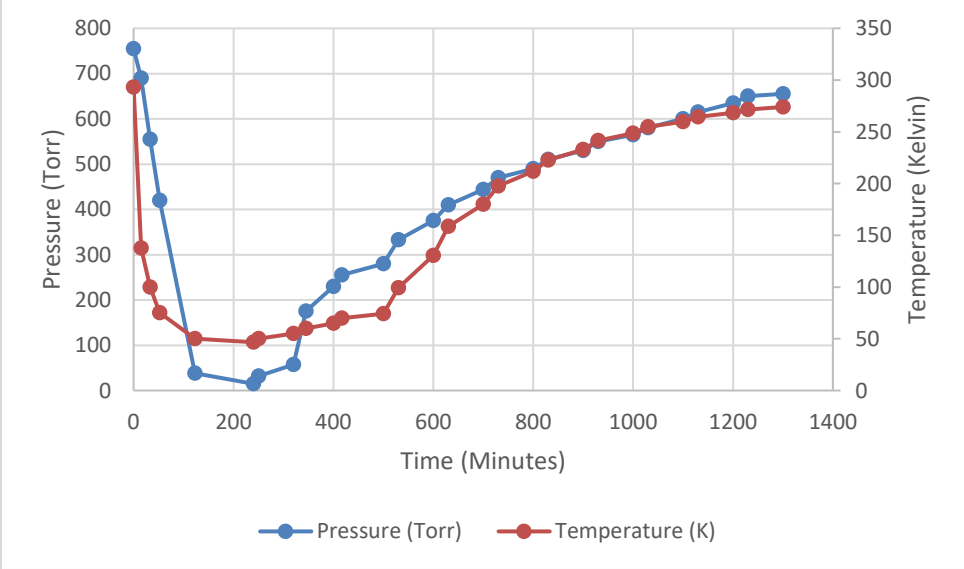

Figure 62. Nitrogen Freeze Test 2 Pressure vs Temperature

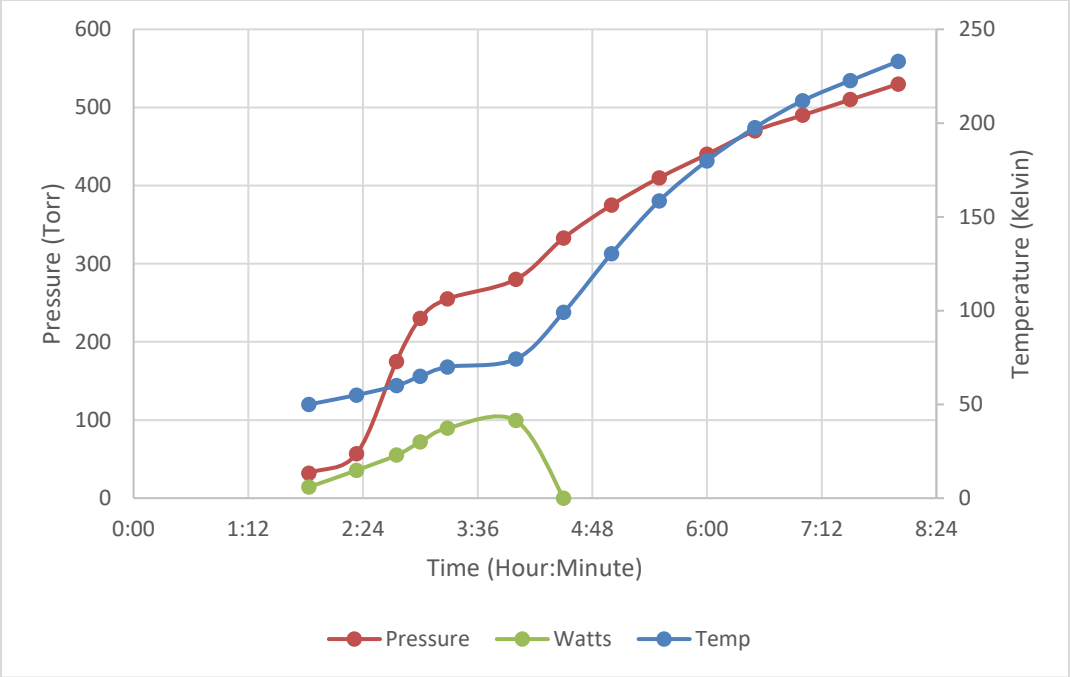

Figure 63. Nitrogen Freeze Test 2 Canister Heat Up

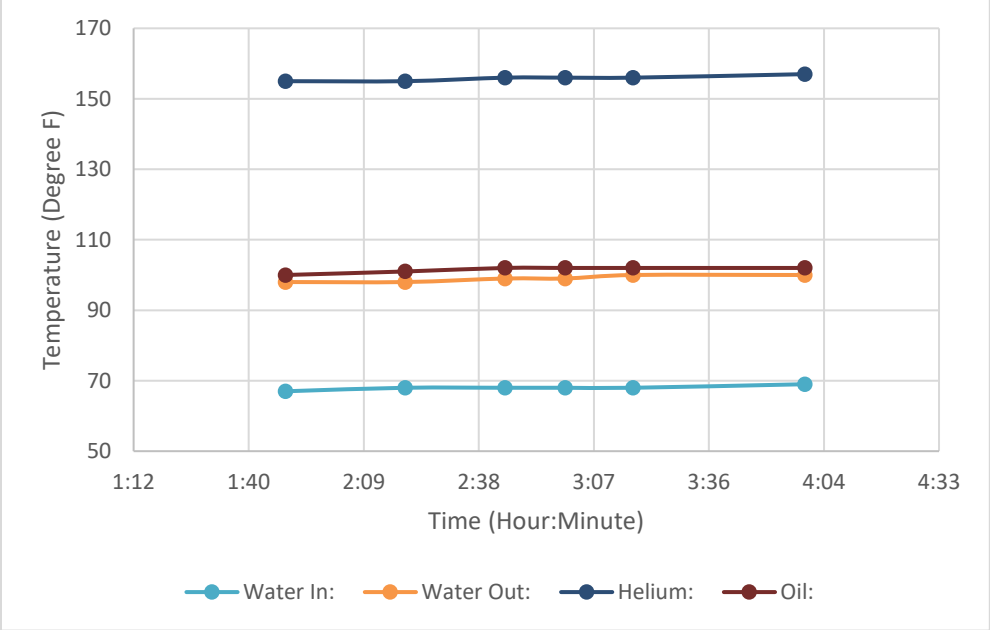

Figure 64. Nitrogen Freeze Test 2 Compressor Temperatures System Heat-Up

During this test it was noted that the chilled water being received by NETL was running 10°F above normal indicating that potentially one of the chilled water plants was shut down due to it being the day before a holiday. This had a non-insignificant effect on the experiment due to the chilled water loop running the helium compressor was directly affected causing temperatures to run ~4 °F higher and not allowing the system to reach its normal "bottom out temperature" of ~46 K as well as the pressure being ~ 1 Torr higher. It was because of this anomaly that the compressor's temperature statistics started to be monitored in the heat up phase of the experiment. As the temperature, pressure, and wattage were monitored it became evident that with a gas loaded system time to heat up the system would take a much longer time, which makes sense due to the added mass in the condenser.

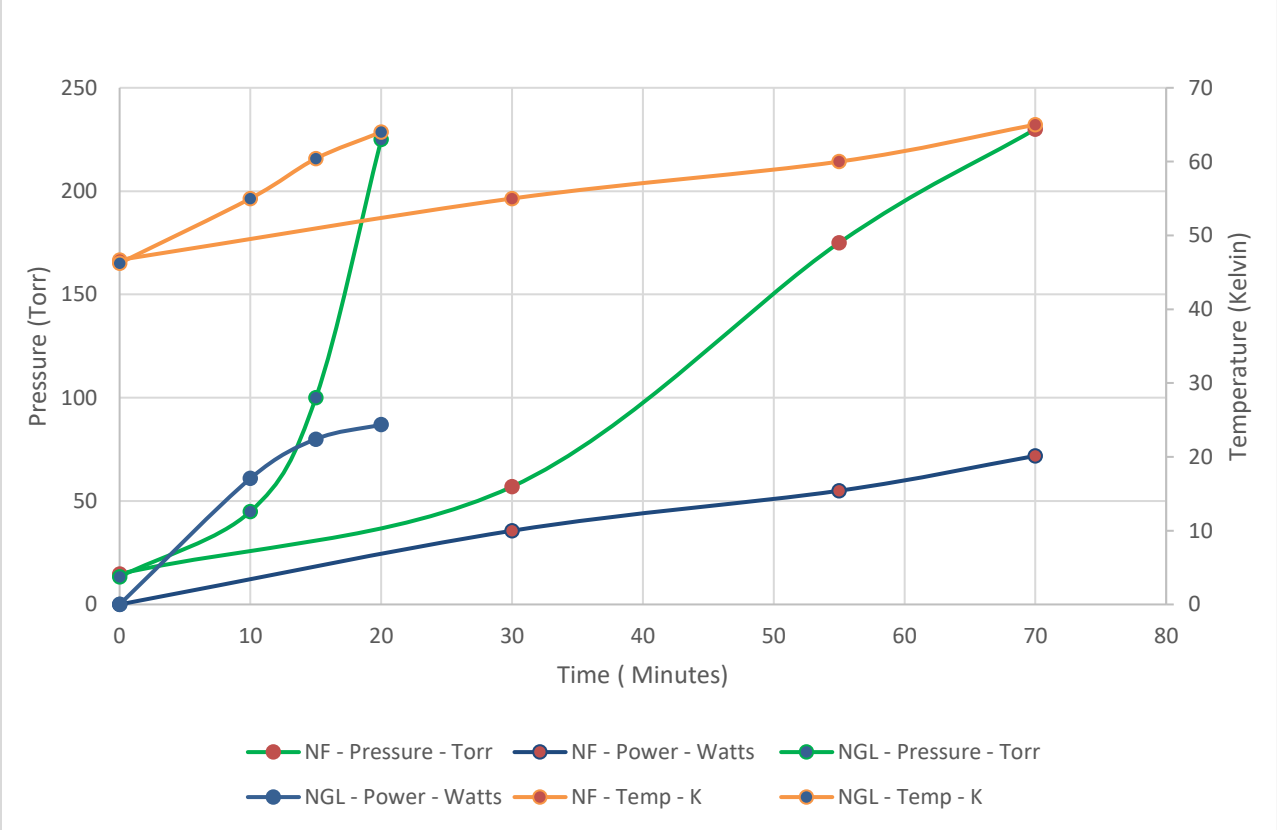

Figure 65. Non-Gas-Loading Test vs Nitrogen Freeze Test Heat-Up

With this test complete it is time for the final test of inserting Xenon into the system to watch is behavior as we start the cryo system.

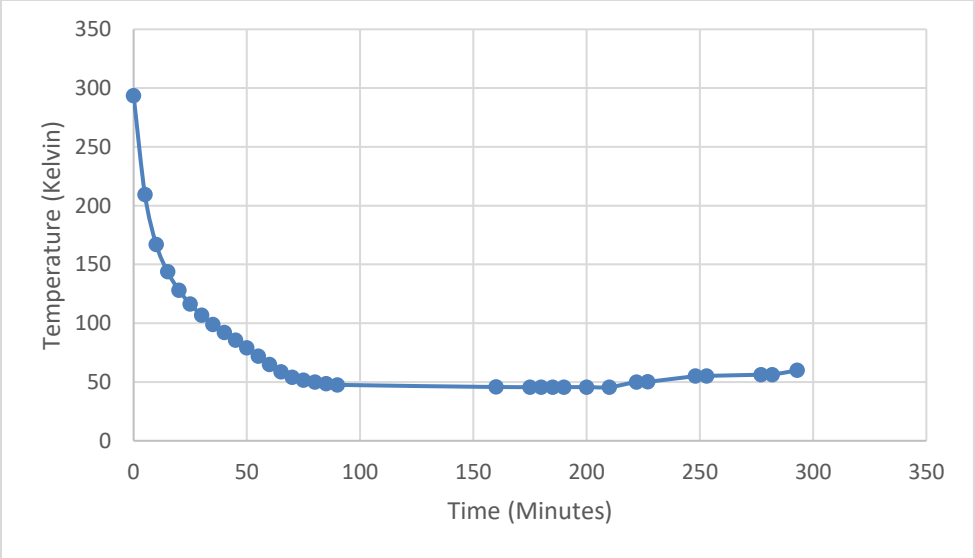

Figure 66. Test 3 Xenon Loading Temperature

Due to the type of pressure gauge used in this experiment the pressure read out was only valuable for very low-end ranges of 1-5 Torr. This is because the pressure gauge used works on thermal conductivity and was only calibrated for a variety of gases, none of which were xenon. The closest to Xenon in thermal conductivity that it was calibrated for was Krypton and due to that relationship between the two we could extrapolate to verify that we would still be able to see a pressure drop during the xenon freezing, despite the system being at low pressures.

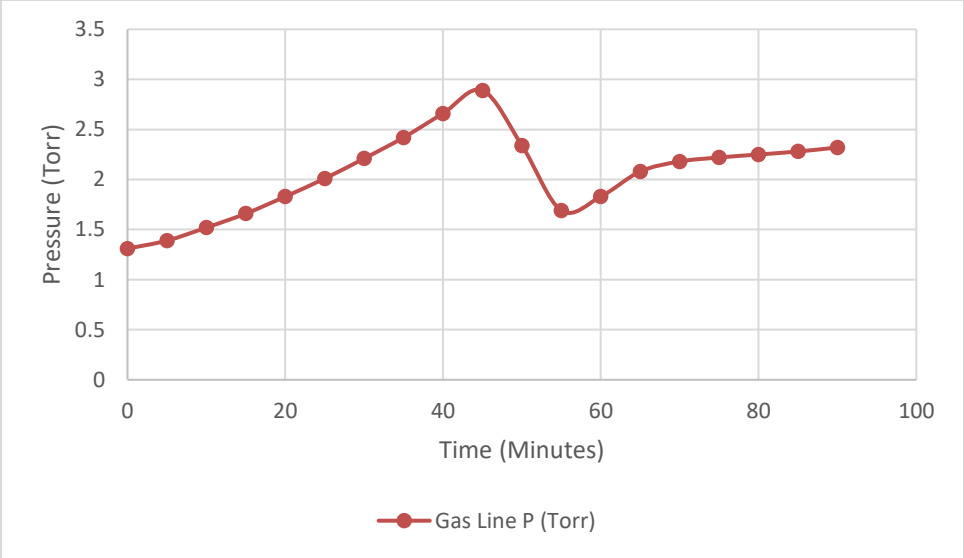

Figure 67. Test 3 Xenon Loading Gas Line Pressure

As seen in the figure above, in correlation with a temperature value of 85.7 K, there is a distinct pressure drop in the system. If our regression is correct, this should correlate with 105 K with no heat input, however we also must remember we are also at ~ 2 Torr which changes the phase diagram of Xenon and puts the freezing point right in the 100 – 105 K range as shown in the figure below.

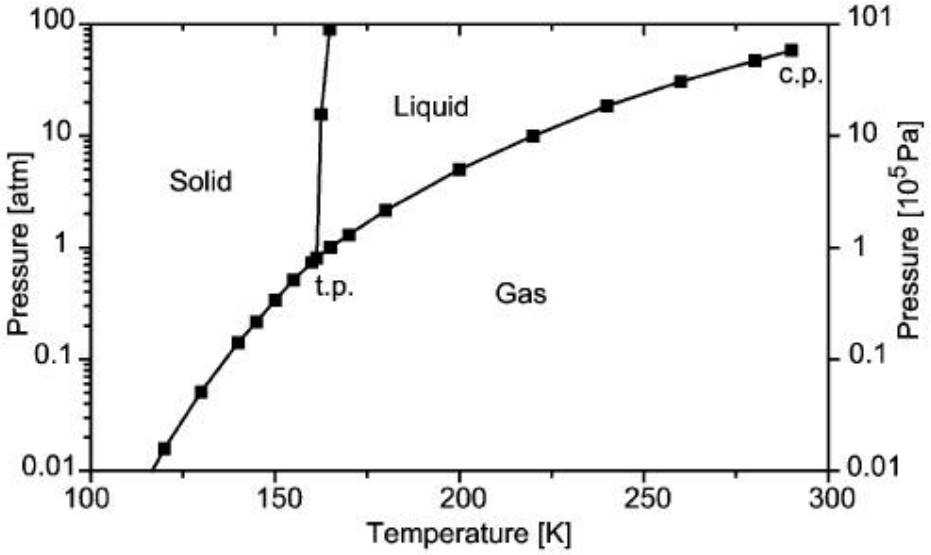

Figure 68. Xenon Phase Diagram (Borgosano, 2012)

However, it is also evident that there is a leak of air into the system estimated at a rate of 0.001 Torr/second which would be equivalent to .005 liters/hour of air. This was noted and the test was closely monitored for any other signs that the compressor was working harder to condense the air and xenon. The test continued without any other issues.

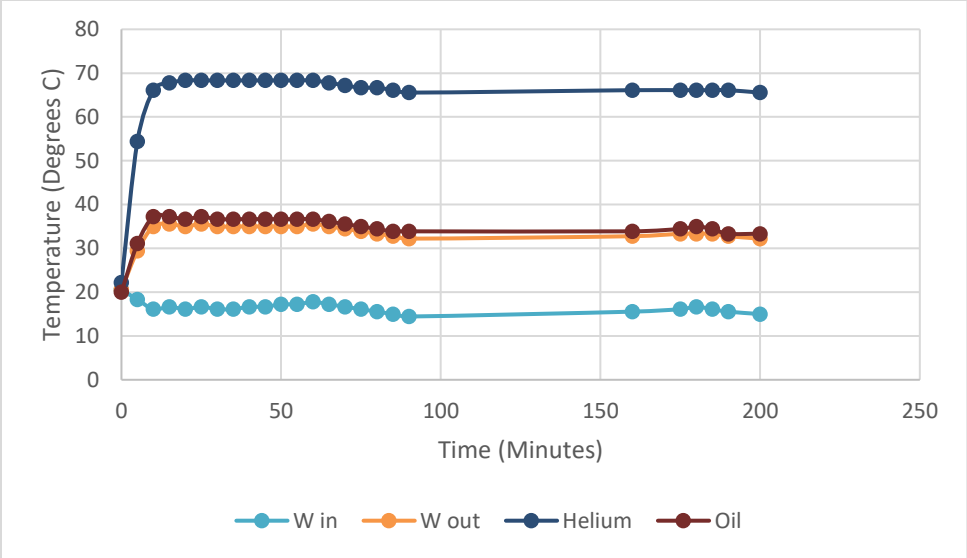

Figure 69. Test 3 Xenon Loading Compressor Temperatures

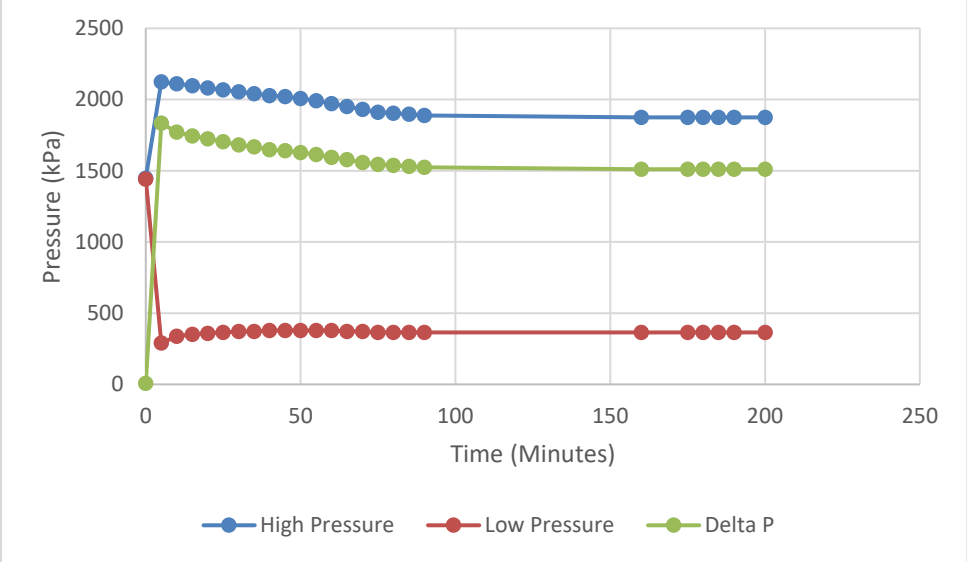

Figure 70. Test 3 Xenon Loading Compressor Pressures

From the figures above we saw no real difference in pressures or temperatures during this test as they approached equilibrium, equilibrated, and maintained both constant pressures and temperatures throughout the remainder of the experiment.

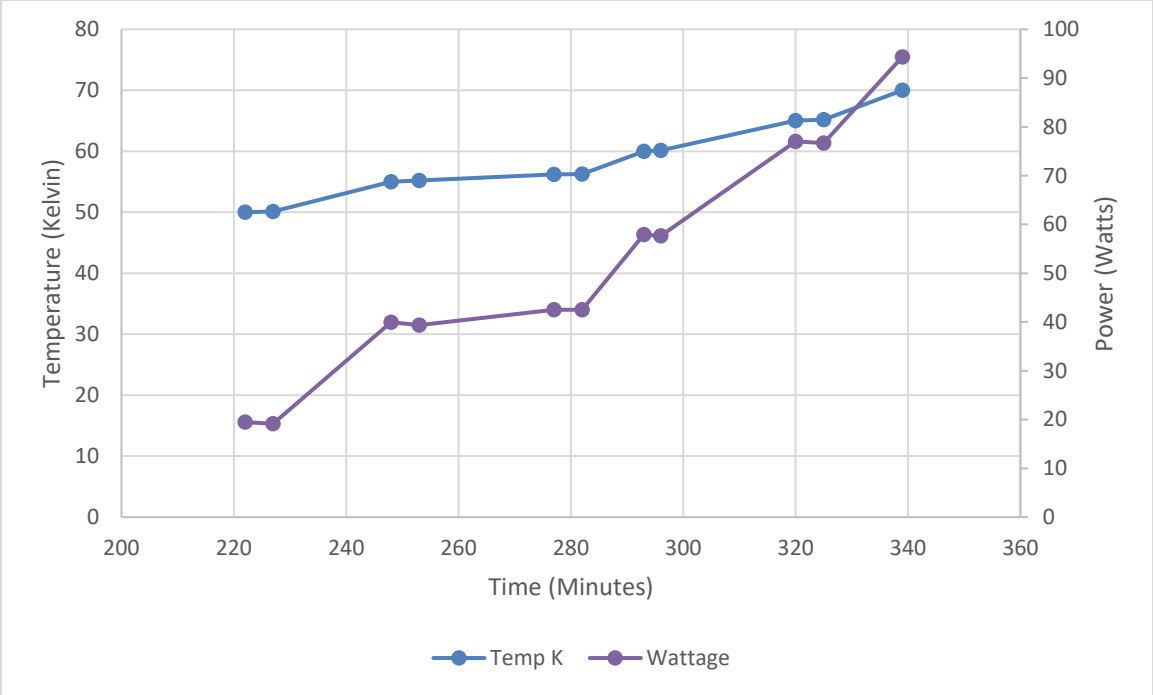

Figure 71. Test 3 Xenon Loading Heater Power vs Temperature

This figure was created to demonstrate the relationship between the heat input and the temperature. From this we can see how, through the use of the PID controller, the CTC 100 is able to approach a temperature, slightly pass it and then adjust the wattage to account for the error and then equilibrate over time. A more finely tuned PID could potentially take this to an exact temperature through the first iteration, however this would take exponentially longer. For the sake of time the PID setting were left as previously set and the system was only allowed to equilibrate for 5 minutes once the desired temperature had been reached.

Chapter 8: Conclusions and Future Work

With the system successfully tested and temporarily set up for both gas loading and unloading we conclude with the system performing satisfactorily with the ability to freeze down to 46 K on the cold head, 55 K on the cold finger, and warm up incrementally from that point with control well past 100 K. This will allow for the freezing of the target Xenon and Argon gases as well as safety measures to prevent other gases from returning to the gaseous phase from liquid or solid state too rapidly. With these steps proven the project can now progress into future phases including testing the trapping efficiency of the cold finger, max and min gas volumes that can be frozen at one time, and the ability to mix gases into one run.

The first and foremost next step to undertake is to create a way to measure the trapping efficiency of the system. By that, there needs to exist a measurement system in place to look at volume of gas before and after the system operates, this can be done in a rudimentary fashion by simply looking at pressures, but to get a full picture of how the gas is settling inside of the irradiation condenser the system must be installed into the reactor, loaded with gas, and then have that gas run at a specific power level and counted for its activation. After this step is done, we can form a base line on activity, and from here we can then increase the volume incrementally to understand how effectively the gas is being targeted in the condenser. From simple calculations we can create a prediction curve for how much the activity should increase based on the increase in the number of atoms of the supposed gas and from there derive an efficiency of the cryo-trap.

Within this step comes the task of installation into the reactor which in itself is a time-consuming task that will take planning in terms of how to load the system, procedures for what steps are taken first, and then tests for how effective the radiation shielding is around the facility. From the current simulations the dose to the surrounding area will be negligible, but the need for a real-world experiment is pertinent to demonstrate the streaming that will occur from the long tubes next to the reactor core.

Once the system is installed into the core and these experiments begin, another test that will work hand in hand with the efficiency calculation will be the minimum and maximum values of gas that we can load into the system and have a significant read out from activation after a run. From this we should be able to find a minimum amount of gas necessary to achieve a specific activity and then the real prize will be finding the point at which we saturate the system and see a plateau in activity despite increases in volumes. This will be extremely important for future orders or experiments that will be run on this facility so that the experimenters will be able to know their operational bounds.

After these initial tests are completed any other experiment whether it be loading multiple gases or cooling and heating in various cycles will be valuable in that they will be a “first of a kind” for this type of system and thus will provide new information available in the ability to produce tracer gases.

REFERENCES

1. Carrigan, C.R., Sun, Y. Detection of Noble Gas Radionuclides from an Underground Nuclear Explosion During a CTBT On-Site Inspection. *Pure Appl. Geophys.* **171,** 717–734 (2014). https://doi.org/10.1007/s00024-012-0563-8
2. Aalseth, Craig E., Day, Anthony R., Haas, Derek A., Hoppe, Eric W., Hyronimus, Brian J., Keillor, Martin E., Mace, Emily K., Orrell, John L., Seifert, Allen, and Woods, Vincent T. *Measurement of 37Ar to support technology for On-site Inspection under the Comprehensive Nuclear-Test-Ban Treaty*. United States: N. p., 2011. Web. doi:10.1016/j.nima.2010.09.135.
3. Burnett, J.L., Davies, A.V. On-site inspection for the radionuclide observables of an underground nuclear explosion. *J Radioanal Nucl Chem* **303,** 2073–2079 (2015). https://doi.org/10.1007/s10967-014-3739-0
4. Sun, Y., Carrigan, C.R. Modeling Noble Gas Transport and Detection for The Comprehensive Nuclear-Test-Ban Treaty. *Pure Appl. Geophys.* **171,** 735–750 (2014). https://doi.org/10.1007/s00024-012-0514-4
5. Carrigan, Charles R., Sun, Yunwei, Hunter, Steven L., Ruddle, David G., Wagoner, Jeffrey L., Myers, Katherine B. L., Emer, Dudley F., Drellack, Sigmund L., and Chipman, Veraun D. *Delayed signatures of underground nuclear explosions*. United States: N. p., 2016. Web. doi:10.1038/srep23032.
6. Jordan, Amy B., Stauffer, Philip H., Knight, Earl E., Rougier, Esteban, and Anderson, Dale N. *Radionuclide gas transport through nuclear explosion-generated fracture networks*. United States: N. p., 2015. Web.

doi:10.1038/srep18383.The Non-Proliferation Experiment and Gas Sampling as an On-Site Inspection Activity (Carrigan 1994)

7. "Bateman Equations - Radioactive Decay." *Nuclear Power*, www.nuclear-power.net/nuclear-power/reactor-physics/atomic-nuclear-physics/radioactive-decay/radioactive-equilibrium/bateman-equations/.
8. Jerzy Cetnar, General solution of Bateman equations for nuclear transmutations. Annals of Nuclear Energy 33 (2006). January 2006.
9. *Cryogenic Refrigerator Installation and Operation Manual*. Cryomech. 2020. Cryomech | The Original Innovators
10. Kayleigh Byrns. (2019, May 13). Custom Condensing Chamber. (12-30671-11).
11. Kayleigh Byrns. (2019, May 13). CHCS180Y02 Outline Drawing. (12-30671-11).
12. MCJ Cryomech. (2017 August 10). CHCS110 Final Assembly. (106-[CCHCS110]-2.
13. Frącz, Wiesław & Janowski, Grzegorz & Ryzinska, Grazyna. (2017). Selected aspects of manufacturing and strength evaluation of porous composites based on numerical simulations. Scientific Letters of University of Rzeszow Technology - Mechanics. 31-43. 10.7862/rm.2017.03.
14. Borgosano, Francesco. (2012). Studies of the influence of thermodynamical parameters on the production rate of hyperpolarised 129Xe and the degree of hyperpolarisation.
15. MCNP® USER'S MANUAL Code Version 6.2 Los Alamos National Laboratory report

16. LA-UR-17-29981.
17. MCNP® Version 6.2 Release Notes Los Alamos National Laboratory report
18. LA-UR-18-20808.
19. Biegalski, S.R., Tipping, T.N. & Klingberg, F.J. Preparation of radioxenon and radioargon mixed sources for IFE14. J Radioanal Nucl Chem 307, 1837–1840 (2016). https://doi.org/10.1007/s10967-015-4398-5
20. "PART 20—STANDARDS FOR PROTECTION AGAINST RADIATION." Www.nrc.gov, 1 Dec. 2015, www.nrc.gov/reading-rm/doc-collections/cfr/part020/full-text.html.
21. Wilson, William Hamill. "Advancements in Radionuclide Monitoring Technologies Used to Detect Indications of Nuclear Explosions." The University of Texas at Austin, 2017.
22. Nipun, Nipun. "Difference Between Stress and Strain." *Pediaa.Com*, 2 Oct. 2015, pediaa.com/difference-between-stress-and-strain/.
23. "Ductility - What Is Ductile Material." *Nuclear Power*, 2021, www.nuclear-power.net/nuclear-engineering/materials-science/material-properties/ductility/.

Appendix A – MCNP Code

```
***** UT-TRIGA - Core Model 01/26/00 ***** Case:
c
c Updated by Ryan Lester for Cryogenic Irradiation Facility Installment in BP1
c Last Updated 6-2020
c
c
c    Geometry version 3.30
c    Coordinate origin on core axis at core midplane
c    Experiment tubes, empty beam ports, empty RSR
c    TRIGA33d as reference calculation w/rod position TR7; w/det.
c
c    67890123456789012345678901234567890123456789012345678901234567890123456789012345
c    ****0*********0*********0*********0*********0*********0*********0*****
c    Problem geometry cells.
c    ****0*********0*********0*********0*********0*********0*********0*****
c    0         -100  -110  +120                $Problem region
c              +150  +155                     $Hex core region
c    ****0*********0*********0*********0*********0*********0*********0*****
c    Cells   0 - 199 Basic TRIGA reactor core components
c    ****0*********0*********0*********0*********0*********0*********0*****
c    Reactor core configuration
c    Cells 0 - 9 core grid, plates and holes
  0  1  -1.0   -202  +206                    $Core region
```

```
          -231  +232  -233  +234  -235  +236
          -241  +242  -243  +244  -245  +246
      FILL=1                          $+150  +155
 1  2  -2.7   -206  +207                  $Lower grid plate
          -211  +212  -213  +214  -215  +216
          -221  +222  -223  +224  -225  +226
      FILL=3                          $+150  +155
 2  2  -2.7   -203  -201  +202              $Upper grid plate
      FILL=5                          $+150  +155
c    ****0*********0*********0*********0*********0*********0*****
c    Define configuration U = 1 to 5
 3  1  -1.0   -101  +102  -103              $Core lattice
          +104  -105  +106       U=1  LAT=2
      FILL=-7:7 -7:7 0:0
    1 1 1 1 1 1 1 1 1 1 1 1 1 1 1                  $D17 E23
    1 1 1 1 1 1 1   1  06  06  06  06  06   1   1      $E22
    1 1 1 1 1 1  06   8   8   8   8   8   8  06   1
    1 1 1 1 1  06   8   8   8  08  08   8   8  06   1  $E7  E6
    1 1 1 1  06   8   8   8 9(7) 08   8   8   8  06   1  $D5
    1 1 1  06   8   8   8   8   8   8   8   8   8  06   1
    1 1  06   8   8   8   8  08  08   8   8   8   8  06   1
    1   1   8   8   8 9(7) 08  10  08 7(7)  8   8   8   1   1
     1  06   8   8   8   8  08  08   8   8   8   8  06   1 1
      1  06   8   8   8   8   8   8  08  08   8  06   1 1 1
       1  06   8   8   8 9(7)  8   8  08   8  06   1 1 1 1
```

```
          1  06   8   8   8   8   8   8   8 06   1 1 1 1 1
           1  06   8   8   8   8   8   8 06   1 1 1 1 1 1
            1   1  06  06  06  06  06   1   1 1 1 1 1 1 1
                       1 1 1 1 1 1 1 1 1 1 1 1 1 1 1
c
c    ****0*********0*********0*********0*********0*********0*********0*****
  4  1  -1.0   -205                U=2
  5  2  -2.7    #4                 U=2
c    ****0*********0*********0*********0*********0*********0*********0*****
  6  2  -2.7   -101  +102  -103              $Cell lattice
             +104  -105  +106       U=3  LAT=2
        FILL=-7:7 -7:7 0:0
     3 3 3 3 3 3 3 3 3 3 3 3 3 3 3
     3 3 3 3 3 3 3   3  02  02  02  02  02   3   3
     3 3 3 3 3 3 3  02   2   2   2   2   2   2  02   3
     3 3 3 3 3 3  02   2   2   2   2   2   2   2  02   3
     3 3 3 3 3  02   2   2   2 9(7)  2   2   2   2  02   3
     3 3 3 3  02   2   2   2   2   2   2   2   2   2  02   3
     3 3 3  02   2   2   2   2   2   2   2   2   2   2  02   3
     3 3  02   2   2   2   2   2   2   2   2   2   2   2  02   3
     3   3   2   2   2 9(7)  2  10   2 7(7)  2   2   2   3   3
      3  02   2   2   2   2   2   2   2   2   2   2   2  02   3 3
       3  02   2   2   2   2   2   2   2   2   2   2  02   3 3 3
        3  02   2   2   2 9(7)  2   2   2   2  02   3 3 3 3
         3  02   2   2   2   2   2   2   2  02   3 3 3 3 3
          3  02   2   2   2   2   2   2  02   3 3 3 3 3 3
```

```
              3   3  02  02  02  02  02   3   3 3 3 3 3 3 3
                        3 3 3 3 3 3 3 3 3 3 3 3 3 3 3
c
c    ****0*********0*********0*********0*********0*********0*********0*****
  7  1  -1.0   -200                 U=4
  8  2  -2.7    #7                  U=4
c    ****0*********0*********0*********0*********0*********0*********0*****
  9  2  -2.7   -101  +102  -103               $Cell lattice
           +104  -105  +106       U=5  LAT=2
       FILL=-7:7 -7:7 0:0
     5 5 5 5 5 5 5 5 5 5 5 5 5 5 5
     5 5 5 5 5 5 5  5  04  04  04  04  04   5   5
     5 5 5 5 5 5  04   4   4   4   4   4   4  04   5
     5 5 5 5 5  04   4   4   4   4   4   4   4  04   5
     5 5 5 5  04   4   4   4 9(7)  4   4   4   4  04   5
     5 5 5  04   4   4   4   4   4   4   4   4   4  04   5
     5 5  04   4   4   4   4   4   4   4   4   4   4  04   5
     5   5   4   4   4 9(7)  4  10   4 7(7)  4   4   4   5   5
      5  04   4   4   4   4   4   4   4   4   4   4  04   5 5
       5  04   4   4   4   4   4   4   4   4   4  04   5 5 5
         5  04   4   4   4 9(7)  4   4   4   4  04   5 5 5 5
           5  04   4   4   4   4   4   4   4  04   5 5 5 5 5
             5  04   4   4   4   4   4   4  04   5 5 5 5 5 5
               5   5  04  04  04  04  04   5   5 5 5 5 5 5 5
                        5 5 5 5 5 5 5 5 5 5 5 5 5 5 5
```

```
c
c    ****0*********0*********0*********0*********0*********0*****
c
c    Reactor core structure
c    Cells 10 - 29 reflector inner core shroud
10  2  -2.7   -300  +302  -303  +202          $Alignment ring
11  2  -2.7   -300  -202  +352                $Alignment ring
           (+231: -232: +241: -242:
            +233: -234: +243: -244:
            +235: -236: +245: -246)
12  2  -2.7   +305  -306  +307                $Shroud loading
           (-311  +312  -321  +322
            -313  +314  -323  +324
            -315  +316  -325  +326)
13  2  -2.7   -301  -352  +304                $Alignment ring
           (+331: -332: +341: -342:
            +333: -334: +343: -344:
            +335: -336: +345: -346)
14  2  -2.7   +231  -331  -233  +236          $Reflector plate
            -352  +306
15  2  -2.7   -232  +332  +234  -235          $Reflector plate
            -352  +306
16  2  -2.7   +241  -341  -343  -345          $Reflector, bp3
            -352  +306  +363
17  2  -2.7   -242  +342  +344  +346          $Reflector plate
```

```
          -352  +306
18  2  -2.7   +233  -333  -331  -343          $Reflector plate
          -352  +306
19  2  -2.7   -234  +334  +332  +344          $Reflector plate
          -352  +306
20  2  -2.7   +235  -335  +332  -345          $Reflector plate
          -352  +306
21  2  -2.7   -236  +336  -331  +346          $Reflector plate
          -352  +306
22  2  -2.7   +243  -343  -241  -233          $Reflector plate
          -352  +306
23  2  -2.7   -244  +344  +242  +234          $Reflector plate
          -352  +306
24  2  -2.7   +245  -345  -241  -235          $Reflector plate
          -352  +306
25  2  -2.7   -246  +346  +242  +236          $Reflector plate
          -352  +306
26  2  -2.7   +241  -363  +364  -360          $Reflector BP3
27  2  -2.7   -361  +362 -100          $Reflector BP1&5
c    ****0*********0*********0*********0*********0*********0*********0*****
c    Cells 30 - 39 reflector outer shroud structure
30  2  -2.7   -355  +361                  $Reflector cyclin
          -350  +351  -352  +353
31  2  -2.7   +355  +363                  $Reflector cyclin
          -350  +351  -352  +353
```

```
32  2  -2.7   -370  +371  -372  +373          $Cylinder, top
33  2  -2.7   -374  -375  +376               $Cylinder, bot
           (+331: -332: +341: -342:
            +333: -334: +343: -344:
            +335: -336: +345: -346)
34  2  -2.7   -370  +374  -375  +377          $Reflector edge rang
35  2  -2.7   -352  -371  +380  +381          $Reflector rsr unit
36  2  -2.7   -380  +300  +381  -382          $Reflector rsr unit
37  2  -2.7   -352  +301  -300  +381          $Reflector rsr unit
38  1  -1.0   +370  -351  -377  +120          $Edge ring error
c    ****0*********0*********0*********0*********0*********0*****
c    Cells 40 - 49 reflector graphite moderator
40  4  -2.25    -400  +401  -402  +403         $Reflector graphite
41  4  -2.25    -400  -403  +375  -404  +361
            (+411: -412: +421: -422:
             +413: -414: +423: -424:
             +415: -416: +425: -426)
           #(-361  +405)                 $Graphite, bp1&5
42  4  -2.25   (-400  -403  +375  +404  +363
            (+411: -412: +421: -422:
             +413: -414: +423: -424:
             +415: -416: +425: -426))
           #(-406 +408) #(-407 +409)        $Graphite, bp3
43  8 -1.15e-3 (+371 -351 -373 +403)     #40
                                    $graphite void
```

```
                                    $ <fix this ?>
44  8 -1.15e-3 (-351  -403  +375  -404  +361
             (+331: -332: +341: -342:
              +333: -334: +343: -344:
              +335: -336: +345: -346)) #41    $graphite void
45  8 -1.15e-3 (-351  -403  +375  +404  +363
             (+331: -332: +341: -342:
              +333: -334: +343: -344:
              +335: -336: +345: -346)) #42    $graphite void
46  8 -1.15e-3  -304  +403  -301
             (+331: -332: +341: -342:
              +333: -334: +343: -344:
              +335: -336: +345: -346)        $graphite void
47  8 -1.15e-3  +301  -371  +403  -381         $graphite void
c    ****0*********0*********0*********0*********0*********0*****
c    Cells 50 - 59 pool coolant water
c    exterior core water, above and below grid plates
50  1  -1.0   -203  +201  -110               $Upper gridplate
51  1  -1.0   +203  -302  +202  -110          $Upper gridplate
52  1  -1.0   +302  -300  +303  -110          $Upper gridplate
53  1  -1.0   -305  -306  +307               $Lower gridplate
54  1  -1.0   -307  +120                    $Lower gridplate
           (-311  +312  -321  +322
            -313  +314  -323  +324
            -315  +316  -325  +326)
```

```
55  1  -1.0   -207  +306                $Lower gridplate
          (-231  +232  -241  +242
           -233  +234  -243  +244
           -235  +236  -245  +246)
56  1  -1.0   -206  +207                $Lower gridplate
          (+211: -212: +221: -222:
           +213: -214: +223: -224:
           +215: -216: +225: -226)
          (-231  +232  -241  +242
           -233  +234  -243  +244
           -235  +236  -245  +246)
57  1  -1.0   -351  +371  +372  -110          $Upper reflector
58  1  -1.0   -374  -376  +120              $Lower reflector
          (+311: -312: +321: -322:
           +313: -314: +323: -324:
           +315: -316: +325: -326)
59  1  -1.0   +306  -376                $Lower reflector
          (+331: -332: +341: -342:
           +333: -334: +343: -344:
           +335: -336: +345: -346)
          (-311  +312  -321  +322
           -313  +314  -323  +324
           -315  +316  -325  +326)
c    ****0*********0*********0*********0*********0*********0*********0*****
c    Cells 60 - 69 pool coolant water
```

```
c    exterior core water, around reactor core assembly
c 02  8 -1.15e-3    (-406 +408)
c    *TRCL (+35.255  -06.222  -6.985  30 120  90   60  30  90) $BP2
c 04  8 -1.15e-3    (-407 +409)
c    *TRCL (-22.871  +13.216  -6.985  60  30  90  150  60  90) $BP4
950  8 -1.15e-3 -150 +160 -165
     *TRCL (-60.00    00.00   00.00   00  90  90   90  00  90) $NP
951  8 -1.15e-3 -150 +160 -165
     *TRCL ( 57.96   -15.53   00.00   00  90  90   90  00  90) $NPP
952  8 -1.15e-3 -150 +160 -165
     *TRCL ( 42.43    42.43   00.00   00  90  90   90  00  90) $FC
60  1  -1.0   +350  -355  +361
           (-100  -110  +120) #950 #951       $Beam ports 1&5
61  1  -1.0   +350  +355  +363
           (-100  -110  +120) #950 #952
          #(-406 +408) #(-407 +409)          $Beam ports 2&4
62  1  -1.0   -363  +364  +360  -100          $reflector BP3
63  1  -1.0   -350  +351  +352  -110          $reflector cylinder
64  1  -1.0   -350  +351  -353  +120          $reflector cylinder
65  1  -1.0   -370  +374  -377  +120          $reflector edge ring
66  1  -1.0   +300  -371  +303  -110          $RSR removal
67  2  -2.7   +370  -351  -375  +377          $edge ring error
68  2  -2.7   -351  +370  -372  +373          $edge ring error
c    ****0*********0*********0*********0*********0*********0*********0*****
c    Cells 70 - 79  beam port structure
```

```
c    bp 2 & 4 structure
71  2  -2.7    (-406  +430)
                 +350  +355  -100          $Reflector BP2
72  2  -2.7    (-407  +440)
                 +350  +355  -100          $Reflector BP4
c    beam port 3 structure
73  2  -2.7     +461  -462  -464             $Reflector BP3
74  2  -2.7     -463  +464  +461  -100        $Reflector BP3
75  1  -1.0     +241  -364  -461             $Reflector BP3
76  1  -1.0     +463  -364  +461  -100        $Reflector BP3
c    beam port 1, 3, 5 cavity
77  4 -2.25 +450  -362  -451 +800          VOL =    $Reflector BP1 graphite
78  8 -1.15e-3  +462  -464  -453             $Reflector BP3
79  4 -2.25  -450  -362  +455                $Reflector BP5 graphite
c    ********** Cells 80 - 89 beam port cavity
c    ********** beam port 1 **********
 81  8  -1.15e-3  +451  -362  -100 +800  +815 +816            VOL=1   $air around canister
800  3  -7.8      -800 +801 +802 +803 +804 +805 +806 +807
              +813 +814 +816                              $outer canister
807  0            -807 +801 +802 +803 +804 +805 +806 +813 +814          $outer canister
vacuum
801  3  -7.8      -801 +802 +803 +806 +808 +813         VOL=88.483987   $condenser
808  8  -1.15e-3  -808 +806 +813                  VOL=303.16135   $condenser air
804  9  -8.96     -804 +802 +803                  VOL=115.83358   $copper fins
814  9  -8.96     -814 +802 +803                  VOL=265.45196   $copper-helium interface
```

```
805  3  -7.8      -805 +803 +806 +813 +816                    $last steel
802  3  -7.8      -802 +811                                   $1/2inchpipe
811  12 -1.5e-3   -811                                       $1/2inchpipeAr
813  3  -7.8      -813 +802 +812 +811                         $1/2inchpipeconnection
812  12 -1.5e-3   -812 +811 +802                              $1/2inchpipedconnectionaAr
803  3  -7.8      -803 +810                                   $5/16inchpipe
810  12 -1.5e-3   -810                                       $5/16inchpipeAr
806  3  -7.8      -806 +803 +809 +810                         $5/16connection
809  12 -1.5e-3   -809 +803 +810                              $5/16connectionAr
815  3  -7.8      -815 +816                                VOL=1   $outer-helium transfer line steel
816  14 -1.15e-3  -816                                       $inner-helium transfer line
c **************************beam ports 2,3,4,5 ******************
82  8 -1.15e-3 (-430  +408) +350  -100  VOL=1   $Reflector BP2
83  8 -1.15e-3  +453  -464  -100       VOL=1   $Reflector BP3
84  8 -1.15e-3 (-440  +409) +350  -100  VOL=1   $Reflector BP4
85  8 -1.15e-3  -455  -362  -100       VOL=1   $Reflector BP5
c    Cells 90 - 94  rsr unit
c     rotary specimen rack
90  8 -1.15e-3  +300  -303  +352  -371         $RSR unit
91  8 -1.15e-3  +300  +304  -352  -380         $RSR unit
92  8 -1.15e-3  +300  -304  -380  +382         $RSR unit
c    ****0*********0*********0*********0*********0*********0*****
c    Cells 100 - 199 Fill universe for reactor core grid
c                 Basic core components U = 6 to 9
c    ****0*********0*********0*********0*********0*********0*****
```

```
c    Cells 100 - 109 graphite reflector elements
100  1 -1.0     #101  #102  #103
             #104  #105  #106        U=6      $element clad
101  2 -2.7     -623  -609             U=6      $lower fitting
102  2 -2.7     -605  -620  +621        U=6      $end closure
103  4 -2.25    -605  -621  +622        U=6      $graphite
104  2 -2.7     -605  -622  +623        U=6      $end closure
105  2 -2.7     +620  -608             U=6      $upper fitting
106  2 -2.7     +605  -607  -620  +623  U=6      $element clad
c    Cells 110 - 119 reactor pulse control
c      transient control rod
110  1 -1.0   #(-502  -511  +516)      U=7      $element clad
111  2 -2.7     -500  -510  +511        U=7      $end plug
112  2 -2.7     -500  -511  +512        U=7      $spacer plug
113  6 -2.52    -500  -512  +513        U=7      $absorber
114  2 -2.7     -500  -513  +514        U=7      $spacer plug
115  8 -1.15e-3 -500  -514  +515        U=7      $air follower
116  3 -7.8     -500  -515  +516        U=7      $end plug
117  3 -7.8     +500  -502  -511  +516  U=7      $element clad
c    ****0*********0*********0*********0*********0*********0*****
c    Cells 120 - 129 standard triga fuel element
120  1 -1.0     #121  #122  #123
             #124  #125  #126
             #127  #128  #129        U=8      $element clad
121  3 -7.8     -615  -603             U=8      $lower fitting
```

```
122  3 -7.8     -600  -610  +611        U=8      $end closure
123  4 -2.25    -600  -611  +612        U=8      $graphite
124  5 -6.0     -600  -612  +613  +650  U=8      $fuel
125  7 -6.49    -650  -612  +613        U=8      $Zr rod
126  4 -2.25    -600  -613  +614        U=8      $graphite
127  3 -7.8     -600  -614  +615        U=8      $end closure
128  3 -7.8     +610  -604              U=8      $upper fitting
129  3 -7.8     +600  -602  -610  +615  U=8      $element clad
c    ****0*********0*********0*********0*********0*********0*****
c    Cells 130 - 149 fuel follower control rods
c      control rods: reg, shim1 & shim2
130  1 -1.0   #(-507  -520  +531)       U=9      $element clad
131  3 -7.8     -505  -520  +521        U=9      $end plug
132  8 -1.15e-3 -505  -521  +522        U=9      $top space
133  2 -2.7     -505  -522  +523        U=9      $spacer plug
134  8 -1.15e-3 -505  -523  +524        U=9      $void gap
135  6 -2.52    -505  -524  +525        U=9      $absorber
136  2 -2.7     -505  -525  +526        U=9      $spacer plug
137  8 -1.15e-3 -505  -526  +527        U=9      $void gap
138  5 -6.0     -505  -527  +528  +550  U=9      $fuel follower
139  7 -6.49    -550  -527  +528        U=9      $Zr rod
140  2 -2.7     -505  -528  +529        U=9      $spacer plug
141  8 -1.15e-3 -505  -529  +530        U=9      $bot space
142  3 -7.8     -505  -530  +531        U=9      $end plug
143  3 -7.8     +505  -507  -520  +531  U=9      $element clad
```

```
c
c    ****0*********0*********0*********0*********0*********0*********0*****
c    Cells 200 - 999 Modifications and experiment components
c                    Core experiment modifications U = 10 to 50
c    ****0*********0*********0*********0*********0*********0*********0*****
c    Cells 200 - 499 core experiments
c     CT tube
200  1 -1.0     +900                  U=10     $CT cell water
201  2 -2.7     -900  +901  -110       U=10     $Center tube
202  1 -1.0     -901   FILL=20 (0 0 0)  U=10     $CT fill water
205  8 -1.15e-3 -905  -907  +909       U=20     $CT sample void
210  1 -1.0     #205                  U=20     $CT sample void
c    ****0*********0*********0*********0*********0*********0*********0*****
c     PTS system w/o Cd
300  1  -1.0    +910                  U=30     $PTSsystem water
301  2  -2.7    -910  +911  +919  -110  U=30     $PTSsystem outer
302  2  -2.7    -912  +913  +919  -110  U=30     $PTSsystem inner
303  8 -1.15e-3 +912  -914  +916  -110  U=30     $PTS no liner
304  8 -1.15e-3 +912  -914  -916  +919  U=30     $PTS system gap
305  8 -1.15e-3 -911  +914  +919  -110  U=30     $PTS system gap
306  2  -2.7    -913  -917  +918       U=30     $No end shadow
307  8 -1.15e-3 #306  -913  +919  -110  U=30     $PTS system air =2pc
308  2  -2.7    -913  -917  +918       U=30     $Sample capsule
309  2  -2.7    -910  -919  +120       U=30     $end assembly
c     PTS system and Cd
```

```
350  1  -1.0    +910                U=35     $PTSsystem water
351  2  -2.7    -910  +911  +919  -110  U=35     $PTSsystem outer
352  2  -2.7    -912  +913  +919  -110  U=35     $PTSsystem inner
353 10  -8.65   +912  -914  +916  -110  U=35     $PTS Cd liner
354  8 -1.15e-3 +912  -914  -916  +919  U=35     $PTS system gap
355  8 -1.15e-3 -911  +914  +919  -110  U=35     $PTS system gap
356 10  -8.65   -913  -917  +918       U=35     $Cd end shadow
357  8 -1.15e-3 #356  -913  +919  -110  U=35     $PTS system air =2pc
358  2  -2.7    -913  -917  +918       U=35     $sample capsule
359  2  -2.7    -910  -919  +120       U=35     $end assembly
c    ****0*********0*********0*********0*********0*********0*********0*****
c     GD3 system w/o Cd
400  1  -1.0    +920                U=40     $T3system water
401  2  -2.7    -920  +921           U=40     $T3system outer
402  2  -2.7    -922  +923           U=40     $T3system inner
403 11 -11.4    +922  -924           U=40     $T3 Pb liner
404  8 -1.15e-3 -921  +924           U=40     $T3 system gap
405  8 -1.15e-3 -923                U=40
409  8 -1.15e-3 -921 Fill=50 (0 0 0)    U=40     $T3 sample can
410  1  -1.0 -100 fill=40 (+2.17678  +1.0033  0.0) U=41   $D-17
420  1  -1.0 -100 fill=40 ( 0.0      -2.76606 0.0) U=42   $E-22
430  1  -1.0 -100 fill=40 (-2.17678  +1.0033  0.0) U=43   $E-23
450  1  -1.0    +920                U=45     $T3system water
451  2  -2.7    -920  +921           U=45     $T3system outer
452  2  -2.7    -922  +923           U=45     $T3system inner
```

```
453 10  -8.65   +922  -924             U=45     $T3 Cd liner
454  8 -1.15e-3 -921  +924             U=45     $T3 system gap
455  8 -1.15e-3 -923                   U=45
459  8 -1.15e-3 -921 Fill=50 (0 0 0)    U=45     $T3 sample can
460  1  -1.0 -100 fill=45 (+2.17678  +1.0033  0.0) U=46    $D-17
470  1  -1.0 -100 fill=45 ( 0.0      -2.76606 0.0) U=47    $E-22
480  1  -1.0 -100 fill=45 (-2.17678  +1.0033  0.0) U=48    $E-23
490  8 -1.15e-3 #491  #492  #493  #494  U=50     $CT sample can
491  2  -2.7    -922  +923  -950  +955  U=50     $T3 can cylinder
492  2  -2.7    +922  -924  -950  +955  U=50     $T3 can liner
493  2  -2.7    -923  +950  -951       U=50     $T3 can upper
494  2  -2.7    -923  -955  +956       U=50     $T3 can lower
c    ****0*********0*********0*********0*********0*********0*********0*****
c    Cells 500 - 799 beam port experiments
c    Cells 800 - 999 other modifications
c    Core experiment modifications U = 60 to 90
c    ****0*********0*********0*********0*********0*********0*********0*****
c 900  1  -1.0    -150  +160 -165        U=99     $Detector
c 901  1  -1.0 -150 +160 -165  fill=99 (+0.0  +64.0  +0.0) $Detector
999 0          +100: +110: -120       $Non Problem region
c                :(-100  -150)
c                :(-100  -155)
c    ****0*********0*********0*********0*********0*********0*********0*****

c    ****0*********0*********0*********0*********0*********0*********0*****
```

```
c    Problem geometry surfaces.
c    ****0*********0*********0*********0*********0*********0*****
c    Define PROBLEM radial domain:
100     CZ     +150                $Cylinder
c    hexagonal cell lattice surfaces
101     PX      +2.17678            $Fuel lattice hex-prism
102     PX      -2.17678            $Fuel lattice hex-prism
103     P   +1   1.73205  0  +4.35356 $Fuel lattice hex-prism
104     P   +1   1.73205  0  -4.35356 $Fuel lattice hex-prism
105     P   -1   1.73205  0  +4.35356 $Fuel lattice hex-prism
106     P   -1   1.73205  0  -4.35356 $Fuel lattice hex-prism
c    Define PROBLEM axial domain:
110     PZ     +75                 $UPPER BOUND
120     PZ     -75                 $LOWER BOUND
150     CZ     +5.08               $Detector Cylinder
160     PZ     +10                 $Detector Lower
165     PZ     +30                 $Detector Upper
c 150     P    1  +1.732    0  0       $One-sixth plane
c 155     P    1  -1.732    0  0       $One-sixth plane
c    ****0*********0*********0*********0*********0*********0*****
c
c    reactor core grid plate surfaces
200     CZ      1.91135    $Grid plate element holes
201     PZ     +32.3850     $Upper grid plate region
202     PZ     +30.7975     $Upper grid plate region
```

```
203     CZ      27.6225     $Upper grid plate diameter
205     CZ       1.5875     $Grid plate coolant holes
206     PZ     -33.17875    $Lower grid plate region
207     PZ     -36.35375    $Lower grid plate region
c 208     CZ     +27.6225    $Effective core radius
211     PX     +26.1216             $Lower grid plate edge
212     PX     -26.1216             $Lower grid plate edge
213     P   +1   0.57735  0  +29.0240 $Lower grid plate edge
214     P   +1   0.57735  0  -29.0240 $Lower grid plate edge
215     P   -1   0.57735  0  +29.0240 $Lower grid plate edge
216     P   -1   0.57735  0  -29.0240 $Lower grid plate edge
221     PY     +25.1360             $Lower grid plate edge
222     PY     -25.1360             $Lower grid plate edge
223     P   +1   1.73205  0  +52.2432 $Lower grid plate edge
224     P   +1   1.73205  0  -52.2432 $Lower grid plate edge
225     P   -1   1.73205  0  +52.2432 $Lower grid plate edge
226     P   -1   1.73205  0  -52.2432 $Lower grid plate edge
231     PX      +26.6700             $Core shroud inside surface
232     PX      -26.6700             $Core shroud inside surface
233     P   +1   0.57735  0  +29.2100 $Core shroud inside surface
234     P   +1   0.57735  0  -29.2100 $Core shroud inside surface
235     P   -1   0.57735  0  +29.2100 $Core shroud inside surface
236     P   -1   0.57735  0  -29.2100 $Core shroud inside surface
241     PY     +25.4000             $Core shroud inside surface
242     PY     -25.4000             $Core shroud inside surface
```

```
243     P   +1   1.73205  0  +54.9275 $Core shroud inside surface
244     P   +1   1.73205  0  -54.9275 $Core shroud inside surface
245     P   -1   1.73205  0  +54.9275 $Core shroud inside surface
246     P   -1   1.73205  0  -54.9275 $Core shroud inside surface
c    ****0*********0*********0*********0*********0*********0*****
c    core structure surfaces
c    reflector inner shroud
300     CZ      30.083125           $Grid plate alignment ring
301     CZ      29.765625           $Grid plate alignment ring
302     CZ      27.9400             $Grid plate alignment ring
303     PZ     +33.9725             $Grid plate alignment ring
304     PZ     +26.3525             $Grid plate alignment ring
c    shroud load ring
305     CZ      24.7650             $Reflector shroud load ring
306     PZ     -37.30625            $Reflector shroud load ring
307     PZ     -39.52875            $Reflector shroud load ring
c
311     PX     +29.2100             $Reflector shroud support
312     PX     -29.2100             $Reflector shroud support
313     P   +1   0.57735  0  +32.385  $Reflector shroud support
314     P   +1   0.57735  0  -32.385  $Reflector shroud support
315     P   -1   0.57735  0  +32.385  $Reflector shroud support
316     P   -1   0.57735  0  -32.385  $Reflector shroud support
321     PY     +27.9400             $Reflector shroud support
322     PY  -27.9400                $Reflector shroud support
```

```
323     P   +1   1.73205  0  +59.3725 $Reflector shroud support
324     P   +1   1.73205  0  -59.3725 $Reflector shroud support
325     P   -1   1.73205  0  +59.3725 $Reflector shroud support
326     P   -1   1.73205  0  -59.3725 $Reflector shroud support
c
331     PX     +27.3050              $Core shroud plate exterior
332     PX     -27.3050              $Core shroud plate exterior
333     P   +1   0.57735  0  +29.8450 $Core shroud plate exterior
334     P   +1   0.57735  0  -29.8450 $Core shroud plate exterior
335     P   -1   0.57735  0  +29.8450 $Core shroud plate exterior
336     P   -1   0.57735  0  -29.8450 $Core shroud plate exterior
341     PY     +26.0350              $Core shroud plate exterior
342     PY     -26.0350              $Core shroud plate exterior
343     P   +1   1.73205  0  +56.5150 $Core shroud plate exterior
344     P   +1   1.73205  0  -56.5150 $Core shroud plate exterior
345     P   -1   1.73205  0  +56.5150 $Core shroud plate exterior
346     P   -1   1.73205  0  -56.5150 $Core shroud plate exterior
c    reflector outer shroud
350     CZ      54.76875    $Reflector outer shroud
351     CZ      53.49875    $Reflector outer shroud
352     PZ     +28.8925     $Outer shroud upper edge
353     PZ     -32.0675     $Outer shroud lower edge
355     PY      +0.0        $Core shroud section plane
c    reflector beam ports
360     PY     +55.5625                    $Radial penetrating beam port
```

```
361    C/X    -35.2552  -6.985   7.62              $Tangential thru beam port
c
800    RCC    10.16    -35.2552 -7 35.56   0 0 5.40      $outer-canister-steel 0.3302cm
807    RCC    10.55624 -35.2552 -7 32.56   0 0 5.07      $outer-canister-vacuum
801    RCC    10.87374 -35.2552 -8 10.4775 0 0 3.59      $condenser-steel
808    RCC    11.19124 -35.2552 -8 10.16   0 0 3.264     $condenser-vacuum
804    RCC    21.35124 -35.2552 -8  3.3412 0 0 3.81      $copper-fins
814    RCC    24.69244 -35.2552 -8  7.62   0 0 3.175     $copper-helium interface
805    RCC    32.31244 -35.2552 -8 10.8038 0 0 2.86      $end-pipe-steel
815    RCC    45.72    -35.2552 -8 100     0 0 2         $outer-helium transfer line
816    RCC    32.31244 -35.2552 -8 113     0 0 1.25      $inner-helium transfer line
c
c                              **********BP1                              CANISTER
PIPING**********************************************
802    RCC    12.14374  -35.8   -2.75 31.5 0 0  0.635     $1/2inchpipe
803    RCC    13.43374  -34.5   -3    31.5 0 0  0.397     $5/16inchpipe
806    RCC    14        -34.5   -4.2   0 0 1.25 0.397     $5/16inchpipeturn
809    RCC    14        -34.5   -4.2   0 0 1.25 0.367     $5/16inchpipeturnair
810    RCC    13.43374  -34.5   -3    31.5 0 0  0.367     $5/16inchpipeair
811    RCC    12.14374  -35.8   -2.75 31.5 0 0  0.535     $1/2inchpipeair
812    RCC    14     -35.8   -4.2   0 0 1.25 0.55      $1/2inchpipedconnectionair
813    RCC    14     -35.8   -4.2   0 0 1.25 0.65      $1/2inchpipeconnection
c
362    C/X    -35.2552  -6.985   6.9088              $Tangential thru beam port
363    C/Y     0.0     -6.985  10.160                $Radial penetrating beam port
```

```
364     C/Y      0.0     -6.985   9.525                  $Radial penetrating beam port
c
370     CZ       53.3400     $Reflector top shroud
371     CZ       37.4650     $Reflector top shroud
372     PZ      +29.5275     $Reflector top shroud
373     PZ      +28.2575     $Reflector top shroud
374     CZ       52.0700     $Reflector inner shroud base
375     PZ      -27.9400     $Reflector inner shroud base
376     PZ      -29.5275     $Reflector inner shroud base
377     PZ      -36.8300     $Reflector shroud edge ring
c    rsr experiment system
380     CZ       37.1475     $RSR cavity outer ring
381     PZ       +6.9850     $RSR cavity base
382     PZ       +7.3025     $RSR cavity base
c    ****0*********0*********0*********0*********0*********0*****
c    graphite reflector surfaces
400     CZ       53.0225     $Graphite reflector outer radius
401     CZ       37.7825     $Graphite reflector inner radius
402     PZ       27.6225     $Graphite reflector upper section
403     PZ        6.3500     $Graphite reflector section plane
404     PY      -20.32       $Graphite reflector section plane
405     PY      -35.2552     $Beam port penetration
c       C/Y      0.0     -6.985  10.160         $Radial penetrating beam port, bp3
c       C/X    -35.2552  -6.985   7.62          $Tangential thru beam port,  bp1&5
406  2  CY       7.62        $Tangential beam port, bp2
```

```
407  4  CY      7.62        $Radial beam port, bp4
408  2  PY      0.0         $Tangential beam port, bp2
409  4  PY      0.0         $Radial beam port, bp4
411     PX    +27.78125              $Graphite inner surface
412     PX    -27.78125              $Graphite inner surface
413     P   +1  0.57735  0  +31.00875  $Graphite inner surface +1
414     P   +1  0.57735  0  -31.00875  $Graphite inner surface +1
415     P   -1  0.57735  0  +31.00875  $Graphite inner surface +1
416     P   -1  0.57735  0  -31.00875  $Graphite inner surface +1
421     PY    +26.431875             $Graphite inner surface
422     PY    -26.431875             $Graphite inner surface
423     P   +1  1.73205  0  +57.30875  $Graphite inner surface +1
424     P   +1  1.73205  0  -57.30875  $Graphite inner surface +1
425     P   -1  1.73205  0  +57.30875  $Graphite inner surface +1
426     P   -1  1.73205  0  -57.30875  $Graphite inner surface +1
c
430  2  CY      6.9088      $Tangential beam port, bp2
440  4  CY      6.9088      $Radial beam port, bp4
c
450     PX      0.0         $BP1&5 origin
c    beam port tally surfaces bp1&5 and bp3
451     PX     +10.16       $BP1
453     PY     +40.90       $BP3
455     PX    -10.16        $BP5
c    pool structure pipe, bp3
```

```
461    PY    +25.600            $Radial penetrating beam port, bp3
462    PY    +26.235            $Radial penetrating beam port, bp3
463    C/Y    0.0  -6.985  7.62    $Radial penetrating beam port, bp3
464    C/Y    0.0  -6.985  6.9088  $Radial penetrating beam port, bp3
c   ****0*********0*********0*********0*********0*********0*****
c   control element surfaces
500    CZ     1.5113    $Control ELEMENT - absorber surface, radius
c      CZ     1.51638   $Control ELEMENT - clad inner surface
502    CZ     1.5875    $Control ELEMENT - clad outer surface
505    CZ     1.6637    $Control ELEMENT - absorber surface, radius
c      CZ     1.6637    $Control ELEMENT - clad inner surface
507    CZ     1.7145    $Control ELEMENT - clad outer surface
c
510    PZ    +24.765     $Control ELEMENT - element plug, end
511    PZ    +24.13      $Control ELEMENT - magneform plug, upper
512    PZ    +19.05      $Control ELEMENT - absorber surface, length/2
513    PZ    -19.05      $Control ELEMENT - absorber surface, length/2
514    PZ    -21.59      $Control ELEMENT - magneform plug, lower
515    PZ    -70.8025    $Control ELEMENT - air follower section
516    PZ    -72.7075    $Control ELEMENT - element plug, end
c
520    PZ    +34.925     $Control ELEMENT - element plug, end
521    PZ    +31.115     $Control ELEMENT - void gap
522    PZ    +20.6375    $Control ELEMENT - magneform plug, upper
523    PZ    +19.3675    $Control ELEMENT - void gap
```

```
524     PZ     +19.05       $Control ELEMENT - absorber surface, length/2
525     PZ     -19.05       $Control ELEMENT - absorber surface, length/2
526     PZ     -20.32       $Control ELEMENT - magneform plug, lower
527     PZ     -20.955      $Control ELEMENT - void gap
528     PZ     -59.055      $Control ELEMENT - fuel follower section
529     PZ     -61.595      $Control ELEMENT - void gap
530     PZ     -74.93       $Control ELEMENT - magneform plug, bottom
531     PZ     -76.20       $Control ELEMENT - element plug, end
c
550     CZ      0.28575     $Zirconium rod
c
c    ****0*********0*********0*********0*********0*********0*********0*****
c    fuel and moderator element surfaces
600     CZ      1.816       $FUEL ELEMENT - fuel region surface, radius
c       CZ      1.816       $FUEL ELEMENT - clad inner surface
602     CZ      1.867       $FUEL ELEMENT - clad outer surface
603     CZ      1.5306      $FUEL - adapter effective radius, lower
604     CZ      1.9426      $FUEL - adapter effective radius, upper
605     CZ      1.816       $Graphite ELEMENT - element surface, radius
c       CZ      1.816       $Graphite ELEMENT - clad inner surface
607     CZ      1.867       $Graphite ELEMENT - clad outer surface
608     CZ      1.9426      $Graphite - adapter effective radius, upper
609     CZ      1.5306      $Graphite - adapter effective radius, lower
c
610     PZ     +28.5877     $FUEL ELEMENT - element end region, upper
```

```
611     PZ     +27.7368     $FUEL ELEMENT - graphite end region, upper
612     PZ     +19.05       $FUEL ELEMENT - fuel surface, length/2
613     PZ     -19.05       $FUEL ELEMENT - fuel surface, length/2
614     PZ     -27.7368     $FUEL ELEMENT - graphite end region, lower
615     PZ     -28.5877     $FUEL ELEMENT - element end region, lower
c
620     PZ     +28.5877     $Graphite ELEMENT - element end, upper
621     PZ     +27.7368     $Graphite ELEMENT - graphite end, upper
622     PZ     -27.7368     $Graphite ELEMENT - graphite end, lower
623     PZ     -28.5877     $Graphite ELEMENT - element end, lower
c
650     CZ      0.28575          $Zirconium rod
c    ****0*********0*********0*********0*********0*********0*********0*****
c    reactor core modifications, surfaces
c    center tube irradiations
900     CZ      1.905             $ Center tube outer radius
901     CZ      1.69418           $ Center tube inner radius
905     CZ      1.5               $Sample radius
907     PZ     +0.5               $Sample length
909     PZ     -0.5               $Sample length
c    1-element experiment; PTS tube with/out Cd
c    reference to lower grid plate -33.17875
910     CZ     +1.74625           $Al transport tube outer radius
911     CZ     +1.53543           $Al transport tube inner radius
912     CZ     +1.11125           $Al sample tube outer radius
```

```
913     CZ      +0.86995            $Al sample tube inner radius
914     CZ      +1.16205            $Cd two layer liner
c 915     PZ      -2.07645            $PTS sample stop
916     PZ     -18.89125            $Cd absorber end
917     PZ     -21.1264591          $Cd absorber disk, upper edge
918     PZ     -21.17725            $Cd absorber disk, lower edge
919     PZ     -30.32125            $PTS bottom section
c    3-element experiment; tube with Cd or Pb
c    reference to lower grid plate -33.17875
920     CZ      +2.38125            $Al can outer radius
921     CZ      +2.2225             $Al can inner radius
922     CZ      +2.06375            $Al sleeve outer radius
923     CZ      +1.93929            $Al sleeve inner radius
924     CZ      +2.16535            $Cd liner outer radius
c 930     CZ     +0.47625            $Al structure rod
c 940     PZ     -30.xxxx            $Al bearing section
950     PZ      +2.54               $Al upper end cap
951     PZ      +2.5908             $Al upper end cap
955     PZ      -2.54               $Al lower end cap
956     PZ      -2.5908             $Al lower end cap
c    ****0*********0*********0*********0*********0*********0*********0*****


c    ****0*********0*********0*********0*********0*********0*********0*****
c    Append problem data.
c    ****0*********0*********0*********0*********0*********0*********0*****
```

```
c
c    Transformations for beam tube locations:
c
c Thru port, small
  *TR1  0.0      -35.255  -6.985  00  90  90   90  00  90  $BP1
c Tang port, small
  *TR2  +35.255  -06.222  -6.985  30 120  90   60  30  90  $BP2
c Radial port, large
  *TR3  0.0      +25.600  -6.985  00  90  90   90  00  90  $BP3
c Radial port, small
  *TR4  -22.871  +13.216  -6.985  60  30  90  150  60  90  $BP4
c Thru port, large
  *TR5  0.0      -35.255  -6.985  00  90  90   90  00  90  $BP5
c
c    Transformations for control rod positions:
c
  TR6  0  0  00.00     1 0 0  0 1 0    $(000 u) shutdown condition
  TR7  0  0  20.83594  1 0 0  0 1 0    $(525 u) low power critical
  TR8  0  0  27.78125  1 0 0  0 1 0    $(700 u) design high power
  TR9  0  0  38.10     1 0 0  0 1 0    $(960 u) full-out condition
c
c    ****0*********0*********0*********0*********0*********0*****
c    Materials for reactor components
M1    1001.66c     .66667
      8016.66c     .33333             $H2O, coolant & moderator
```

```
MT1   lwtr.01t                  $300K
M2   13027.92c   -0.9685
     26000.50c   -0.0070
     29000.50c   -0.0025
     14000.60c   -0.0060
     12000.66c   -0.0110
     24000.50c   -0.0035
     25055.66c   -0.0015          $AL structure type 6061
c     22000.      -0.0015         $titanium: 0.15
c     30000.      -0.0025         $zinc: 0.25
M3   26000.50c   -0.6785
      6000.66c   -0.0080
     14000.60c   -0.0100
     24000.50c   -0.1800
     28000.50c   -0.0980
     25055.66c   -0.0180
     15031.66c   -0.0045
     16000.66c   -0.0030          $SS structure type 304
M4    6000.66c    1.0            $C graphite
MT4   grph.01t                  $300K
M5   40000.66c   -0.8991045
      1001.66c   -0.0158955
     92238.66c   -0.068170
     92235.66c   -0.0167875        $Fresh U-ZrH Fuel
MT5   zr/h.01t
```

```
     h/zr.01t
M6    5010.66c     .1584            $B4C
     5011.66c     .6416            $B4C
     6000.66c     .2               $carbon
M7   40000.66c    1.0              $Zr Rod
M8    8016.66c   -0.23              $air
     7014.66c   -0.77
M9   29000        1.0              $copper
M10  48000.50c   -1.0               $Cd neutron absorber liner
M11  82000.50c   -1.0               $Pb neutron absorber liner
M12  18036.80c    1.0               $argon-36 **This is at 293.6 K
c    18036.85                      $This is at .1K
c    18000                         $Ar
M13  54000        1.0               $Xe
c    54126.85c                     $Xe @ .1 K
c    54126.80c                     $Xe @ 293.6K
M14  2004.85c     1.0               $He-4 @ .1k **can we find one around 4k?**
c    2000                          $He
c    ****0*********0*********0*********0*********0*********0*****
MODE     N P
phys:p
IMP:N    1         189r      0
IMP:P    1         189r      0
c    Criticality calculation
```

```
kcode   100000     1.0       50    200   $check mcnp6 manual to change number of kcode
iterations
ksrc   3.5      0        0
tmesh
  CMESH3   trans 10          $(this decides how the mesh lies on the grid)
  cora3  0 1i     7.62       $(adds more cylinders, amount of mesh, width of mesh
  corb3  0 10i  100          $(moves the mesh right or left , amount of mesh , length of mesh)
  corc3    10i  360          $(nothing, coarseness of mesh, this defines an angel of the mesh)
endmd
c 0.0     -35.255  -6.985  00  90  90   90  00  90 $BP1 Trans - Original
c *TR10 0 -35 -7.56 90 90 0 90 0 90 0 90 90 1        $Marji - Trans
*TR10   0 -35  -7.56   90 0 0   90 90 0   0 0 90   1
PRDMP 100 100 1
F14:N 801
F24:N 804
F34:N 808
FMESH44:n GEOM=CYL ORIGIN= 0 -35 -7.56
     IMESH= 9   IINTS=50
     JMESH= 150 JINTS=50
     KMESH= 1   KINTS=10
     AXS= 1 0 0 VEC=0 1 0 OUT=IJ
```

Appendix B – SCALE Code

```
=origen
% Activation


solver{
type=CRAM
opt{


order=16 % Order of method (default=16)
% 2-4 substeps results in large accuracy gain with marginal runtime increase (pg 691)
substeps=3 % Number time step divisions (default=1).
}
}
options{
print_xs=no % Output transition matrix x-sections
digits=4 % high-precision with digits=6, 4 is standard
fixed_fission_energy=no % fixed fission energy is 200 MeV/fission
}
bounds{
neutron="origen.rev01.jeff252g" % 252-group structure read from JEFF library used in
COUPLE
alpha = [9I 1e6 2e7] % 10 linearly spaced bins from 1 MeV to 20 MeV
beta = [22I 1 100] % 23 linearly spaced bins from 1 to 100 eV
gamma = [9L 5.0e7 5.0e-5] % 10 logarithmically spaced bins
}


% Start Irradiation Case 1
**********************************************************************
***********
case(irr-2){
title="Irradiation in reactor -- 20 days (8 hr. irradiations each day)"


lib{
file="w17x17.f33"
%"end7dec"
}
mat{
units="GRAMS"
```

```
iso=[
Fe=.65*4173 Cr=0.18*4173 Mn=0.02*4173
Ni=0.08*4173 Si=0.0075*4173 C=0.008*4173
N=0.001*4173 P=0.00045*4173 S=0.0003*4173 %SS 304 composition ~9.2 lbs.
Cu=2358.68 %Copper Condenser ~ 5.2 lbs.
% Ar-36=1.7828 %1 Liter of Argon Gas
% Xe-126=5.8971 %1 Liter of Xenon Gas
% Ar-36=1.7828*3 %3 Liter of Argon Gas
% Xe-126=5.8971*3 %3 Liter of Xenon Gas
Ar-36=1.7828*20 %10 Liter of Argon Gas
Xe-126=5.8971*20 %10 Liter of Xenon Gas
Ni = 1
' Xe-124=0.001
' Xe-132=1
' Xe-130=1
' Ar-40=1
' kr-78=1 kr-84=1
' He-4=40 %Liquid Helium Coolant
]
}
time{
units = HOURS
t = [ 8 16 24 32 40 48 %2 Day increments in 8 hour segments
56 64 72 80 88 96
104 112 120 128 136 144
152 160 168 176 184 192
200 208 216 224 232 240 % 10 Day Mark ***
248 256 264 272 280 288
296 304 312 320 328 336
344 352 360 368 376 384
392 400 408 416 424 432
440 448 456 464 472 480 % 20 Day Mark ***
]%488 496 504 512 520 528
% 536 544 552 560 568 576
% 584 592 600 608 616 624
%632 640 648 656 664 672
%680 688 696 704 712 720 % 30 Day Mark ***


%8760 % 1 year later
%]
}
flux = [2E+12 0 2E+12 0 2E+12 0 %2 Day increments of irradiation and decay
```

```
2E+12 0 2E+12 0 2E+12 0
2E+12 0 2E+12 0 2E+12 0
2E+12 0 2E+12 0 2E+12 0
2E+12 0 2E+12 0 2E+12 0 % 10 Day Mark ***
2E+12 0 2E+12 0 2E+12 0
2E+12 0 2E+12 0 2E+12 0
2E+12 0 2E+12 0 2E+12 0
2E+12 0 2E+12 0 2E+12 0
2E+12 0 2E+12 0 2E+12 0 % 20 Day Mark ***
]%2E+12 0 2E+12 0 2E+12 0
% 2E+12 0 2E+12 0 2E+12 0
% 2E+12 0 2E+12 0 2E+12 0
% 2E+12 0 2E+12 0 2E+12 0
% 2E+12 0 2E+12 0 2E+12 0 % 30 Day Mark ***
%]
% Total flux from Activation -- from excel calcs


print{
nuc{ total=no units=[GRAMS BECQUERELS CURIES] }
cutoffs=[GRAMS=1E-5]
neutron{
summary=yes
spectra=yes
detailed=yes
}
gamma{
summary=yes
spectra=yes
principal_step=LAST % determine principle emitters based on last step
principal_cutoff=2 % cutoff for principle emitters in percent
}
}
save{
file="Irr_2_5-2020.f71"
steps=ALL
}
} % End Irradiation Case 2
**********************************************************************
**********


case(dec-2){
```

```
title="Cool-down -- irradiation 1"


lib{
file="end7dec" % decay library from Origen
}
time ={
units = days
start = 0
t =[40] % Takes a sample a days 3, 6, and 9


}
flux =[1R 0] % 0 flux means decay only, R repeats the number of time iterations


print{
nuc{ total=yes units=[GRAMS BECQUERELS CURIES] }
cutoffs=[ALL=1E-6]
}
save{
file="Irr_2_5-2020.f71"
steps=ALL
time_offset=0
time_units=HOURS
}
neutron=yes % options control the (alpha,n) reaction
alpha=yes % no options. This determines sources of alpha with no slowing down physics
beta=yes % only option: pick sublibs. Like alpha, for source determination (no physics)
gamma=yes % defaults are generally appropriate, with exceptions noted on p731
}
% End Cool-Down Case 2
**********************************************************************
**********
end
```